Deterministic diffusion in smooth periodic potentials

Sol Selene Gil Gallegos

School of Mathematical Sciences

Queen Mary University of London

Submitted in partial fulfilment of the requirements

of the Degree of Doctor of Philosophy

February 2018

I, Sol Selene Gil Gallegos, confirm that the research included within this thesis is my own work or that where it has been carried out in collaboration with, or supported by others, that this is duly acknowledged below and my contribution indicated. Previously published material is also acknowledged below.

I attest that I have exercised reasonable care to ensure that the work is original, and does not to the best of my knowledge break any UK law, infringe any third party's copyright or other Intellectual Property Right, or contain any confidential material.

I accept that the College has the right to use plagiarism detection software to check the electronic version of the thesis.

I confirm that this thesis has not been previously submitted for the award of a degree by this or any other university.

Signature:

Date:

Details of collaboration and publications:

- Main numerical and analytical results of Chapter 3 are currently written up as a short paper, to be submitted to a leading Letter journal:

  R.Klages, S.Gil, J.Solanpää, M. Sarvilahti, E.Räsänen, *Normal and Anomalous Diffusion in Soft Lorentz Gases*.

  The first and the last author designed the research. All authors performed the research, but the second author contributed the majority to it. The computer code (published separately) was provided by the third and the last author. All authors analysed the data. The first author is writing the draft of the paper, supported by all others.

- All detailed numerical and analytical results of Chapter 3 are meant to be published in a long paper, to be submitted to a leading international journal:

  S.Gil, R.Klages, J.Solanpää, M. Sarvilahti, E.Räsänen, *Deterministic diffusion in the soft Lorentz gas as a function of control parameters*.

  The second and the last author designed the research. All authors performed the research, but the first author contributed the majority to it. The computer code (published separately) was provided by the third and the last author. All authors analysed the data. The first author is writing the draft of the paper, supported by all others.

- All detailed numerical and analytical results of Chapter 4 are meant to be published in a long paper:

  S.Gil, R.Klages and E.Räsänen, *Energy dependent diffusion coefficient in soft periodic potentials*.

  The first and the second author designed the research. All authors performed the research, but the first author contributed the majority to it. The computer code (published separately) was provided by the team around the last author. All authors analysed the data, The first author is writing the draft of the paper, supported by all others.

Abstract

Understanding the macroscopic properties of matter, based on the microscopic interactions of the single particles requires to bring together the areas of statistical physics and dynamical systems. For deterministic diffusion one of the most prominent models is the Lorentz gas in which a point particle performs specular reflections with hard disks distributed in the plane. This model generates deterministic chaos and has led to many mathematical results revealing the origin of diffusion starting from chaotic dynamics. For the periodic Lorentz gas on a triangular lattice, it is possible to understand the diffusion coefficient, in the limit of high scatterer densities, in terms of random walk approximations.

The key question addressed in this thesis is: What happens to the diffusion coefficient, as a function of control parameters, if the hard potential walls of the Lorentz gas scatterers are replaced by a soft potential?

In this study we use a repulsive Fermi potential from which the hard limit can be recovered by varying a control parameter. We then performed computer simulations and analytical random walk approximations to understand the functional form of the diffusion coefficient as a function of the following parameters: the minimal distance between two scatters, the softness of the potential and the energy of a moving particle.

Our main results is that the diffusion coefficient is a highly irregular function of each of these control parameters. Under certain assumptions one can construct analytical approximations that describe the coarse shape of the diffusion coefficient when it exists: For high densities of scatterers we develop suitable random walk approximations, in the low density regime we apply a more elaborate argument that tests for memory effects. We find that diffusion in our soft Lorentz gas exhibits different random walk regimes, where either randomization characterizes the evolution of diffusion or spatio-temporal correlations take place. Via Poincaré

surfaces of section we show that the irregularities appearing in the diffusion coefficient, as a function of parameters, which strongly deviate from simple random walk dynamics, come from non-trivial quasi-ballistic trajectories in configuration space.

Contents

List of Figures

Acknowledgement

I would like to thank the academic all the administrative staff at the School of Mathematical Sciences at Queen Mary University of London for their support since the beginning of my studies. Specially to Sarah Coleman and Norman McBreen, their help made the difference through the years.

I thank Franco Vivaldi and Adrian Baule for helpful discussion through my progress in the PhD. Special thanks to Wolfram Just for interesting scientific and philosophical discussions. Also to Shabnam Beheshti, who encouraged me to leave my comfort zone.

I am deeply grateful to Janne Solanpää for assistance in the installation and use of the code BILL2D.

I thank my supervisor, Rainer Klages, for his advice and guidance. He is the live example of discipline and hard work.

I want to thank the Mexican National Council for Science and Technology (CONACyT) for the Scholarship that I received to pursue my PhD.

This research utilised Queen Mary's MidPlus computational facilities, supported by QMUL Research-IT and funded by EPSRC grant EP/K000128/1.

Chapter 1

Introduction

In the quest of understanding the properties of matter two branches of science, statistical mechanics and dynamical systems merge together and give rise to deterministic transport theory. While statistical mechanics deals with the properties of matter via probabilistic averages over all the elements in the system, dynamical systems theory takes into account the detailed microscopic interaction of the elements that form the system.

The process that made these two branches converge was neither straightforward nor instantaneous but can be traced by some key historical events. One of the founders was Poincaré (late 1800 [Poi85]), with his contributions to chaos theory, although the motivation was in the direction of explaining celestial mechanics. A theory that was aimed to understand large scale objects could be conveniently used for other systems too. From the physicist's side, Maxwell, Gibbs and Boltzmann focused on the study of microscopic scattering. The motivation behind their studies was to understand the behaviour of matter at a molecular scale. Then we jump to the modern era of chaos born with Lorenz [Lor63]. He arrived to the conclusion that it was not possible to make long term predictions about the evolution of atmospheric conditions, or in other words the system is chaotic. These lines of research in different branches of science, although unknown to each other, made the building blocks of what is now deterministic theory of transport.

In traditional statistical mechanics, Boltzmann's premise is that in systems such as a gas, the number molecules is so large that motion should be random. Therefore, from this perspective on the physics of matter, stochasticity rules the behaviour of the objects under study on a microscopic scale. If instead, the interactions are treated deterministically then the mathematical theory of dynamical systems can help to infer about the physical features of a given abstract system. At a "microscopic" level the interaction between objects can be tracked using classical mechanics, therefore the dynamics is said to be deterministic. The evolution of an ensemble of particles at a macroscopic level is called a transport process. Such transport processes have to do with the transport of something from regions of high concentration to regions of low concentration. This something can be mass, energy, heat, etc. When we are interested in mass transport, we talk about diffusion and the diffusion coefficient which measures the rate of diffusion of a given abstract or real gas.

1.1 Microscopic chaos and deterministic diffusion

Diffusion is a macroscopic property of matter, product of the evolution of an ensemble of particles moving from regions of high concentration, or density, to regions with lower concentration. In nature, this process occurs whenever the density of particles in discussion is not uniform. The mathematical models that aim to describe this situation are extremely simplified versions of the real world but it is in this way that we can extract information about the physical properties of the system. When diffusion is treated in the framework of dynamical systems we talk about deterministic diffusion.

The term deterministic diffusion comes from the interaction of particles that undergo chaotic motion at a microscopic level, hence microscopic deterministic chaos. Where depending on the laws or rules of the motion, two close initial trajectories diverge exponentially, the rate of separation is called a Lyapunov exponent. This exponent, if positive, is a signature of the chaos at a microscopic

level [Ott02, LL92]. This chaoticity translates into motion that can look random very quickly. Decay of correlations are a physical measure and can be directly related to transport properties like the diffusion coefficient, *e.g.* via the Green Kubo formula [Dor99]; this is why diffusion can be treated deterministically.

Many dynamical systems have been shown to be chaotic [GN90, Gas98, Dor99]. Although there are studies that suggest that real gas systems exhibit chaotic behaviour at a microscopic scale [GBF$^+$99, BGF$^+$01], this is still an open question in the light of other experimental studies that find real systems to be non-chaotic [DC99, GS99].

All these discoveries show the importance of dynamical systems in the understanding of transport processes. In turn, motivated by physical questions, new abstract models are constructed moving forward the boundaries set by mathematical theories.

Take for instance the classic and paradigmatic Lorentz gas aimed to study electrons in a crystal [Lor05]. It has been widely studied from the mathematical point of view as well as from the physical side [BS81, GN90, Dor99, Gas98, Kla07] and turns out to be chaotic. In the Lorentz gas a point particle performs specular reflections with circular scatterers distributed in the plane. If we think of an ensemble of particles evolving in this environment, we can approximate the diffusion coefficient by means of the mean square displacement. Under certain conditions, in a triangular configuration of scatterers, diffusion is known to be normal, that is, the mean square displacement of an ensemble of particles grows linearly with time. In this model, two nearby trajectories move away from each other due to the positive curvature of the scatterers. This instability of initial conditions yields to an overall random behaviour that will induce normal transport.

The Lorentz gas falls into a class of objects called billiard tables, these are models where a point particle, usually travelling in free flight, collides with a hard boundary or a scatterer. Although billiards came up as mathematical idealizations for physical problems, the Lorentz gas and and other simpler models have been studied for their pure mathematical properties, such as chaos, ergodicity and more (see Refs. [BS81, Sin00, Che94, Che97]). But also physical properties, such as

transport coefficients are of interest.

Diffusion in the context of dynamical systems has been studied in several settings, where it is possible to come up with this non-reversible process out of deterministic rules. Examples of such systems are one-dimensional maps (Geisel and Nierwetberg [GN82, GN84], Grossman and Thomae [GT83]), open billiards, and billiards with magnetic fields, just to name a few.

Among the simpler maps we have one dimension piece-wise linear maps even though some can have very simple forms this does not reflect the interesting features observed when studying transport as a function of control parameters in detail. Take for instance the work by Klages and Dorfman [KD95], where diffusion is studied in chaotic linear maps. In this model the diffusion coefficient has a fractal-like shape as a function of the slope of the map. Their finding was outstanding in the field of deterministic diffusion, since it showed an intricate and non trivial dependence of the diffusion coefficient as a function of control parameter. We highlight the importance of their conjecture, that is, that the diffusion coefficient seems to be an irregular function under a control parameter, in low dimension systems with periodic configuration space.

Particularly, in the standard Lorentz gas model the numerically computed diffusion coefficient has shown an intriguing behaviour as a function of a control parameter [KD00]. On a fine scale the diffusion coefficient turned out to be an irregular function under variation of a control parameter. Making a mathematically more precise statement about this is hard, as only numerical simulations are available while exact analytic formulas are not. Numerical simulations can give a good approximation for the diffusion coefficient, but there are other difficulties: one is the limited range where normal diffusion exists and another one is the nature of the results. One has only discrete points on a parameter interval making it difficult to conjecture anything about finer scales. It is still an interesting open question whether the diffusion coefficient in the periodic Lorentz gas presents indeed a fractal structure, respectively to analyse the degree of smoothness of such a curve [Det14, Kla07]. Since it is argued that the irregularities in the diffusion coefficient are due to topological instabilities, more complicated geometries with higher curvature could enhance this fractality. This was achieved with a flower-

shaped billiard, which can be formed starting with the periodic Lorentz gas and adding 'petals' to each scatterer [HKG02]. The flowered-shaped billiard has properties similar to the periodic Lorentz gas [Sin70, BS81, BSC91]: it is hyperbolic and it presents normal diffusion. This billiard showed an even more intricate shape of the diffusion coefficient with respect to the curvature of a petal as a control parameter, in the sense that it exhibits irregularities on a fine scale compared to its precursor, the Lorentz gas. In [HG01] Harayama and Gaspard study the diffusion coefficient as a function of the energy in a one dimensional corrugated floor where a particle experiences a vertical force and collides with arcs positioned horizontally. It is worth noting that their study of the correlation function, which is related to the diffusion coefficient (see Sect. 2.5.3), yields a behaviour similar to the Weiestrass function, a nowhere differentiable function. With this observation they conjectured that the diffusion coefficient is a non differentiable function of the energy as a control parameter (more about this model in Sect. 2.6.1).

In the same line of research other studies support the conjecture of the diffusion coefficient [KD99, GK02, KD97, KK04, GK98], even in more realistic models like billiards, like the already mentioned Lorentz gas [Kla07, KD00], see also Refs. [Gas98] and [CAM+07] for a good miscellaneous of examples. For a detailed description of such systems exhibiting irregular transport coefficient and its origin see [Kla07].

The effect of chaos on the diffusion coefficient has been studied also in more elaborated settings in higher dimensions and incorporating external forces into the dynamics, *e.g.* in the multi baker map [Gas92]. The efforts in this direction had helped in the understanding of transport in terms of the chaotic properties of the systems.

Moreover, billiards in quantum chaos comes into play when trying to understanding quantum mechanics. That is because periodic orbits in classical chaotic systems are key to understand quantum systems (Gutzwiller 2013 [Gut13]). This motivates even further the development of theories behind billiards.

1.2 Billiard systems with smooth potential

We now introduce the dynamics in billiards with smooth potentials or 'soft walls'. Despite the various constructions of billiards with smooth potentials, one usually speaks of a smooth billiard when the hard wall potential at the boundary of the billiard is replaced by a smooth potential which becomes the soft wall. Therefore not only mathematicians and theoretical physicist care about billiards, billiards also play a role in the experimental realm. In view of the features of real systems, like gas molecules, it is necessary to come up with more sophisticated models. In this direction, rigorous mathematical, numerical and experimental studies on Hamiltonian systems with smooth potential have been performed. These play the role of being a softened version of a billiard table or lattice with hard scatterers.

In a very formal and rigorous mathematical approach, Donnay and Liverani [DL91] studied repulsive, attractive and mixing potentials in terms of ergodicity and Lyapunov exponents for constant energy. They claim that there exists potentials, for which the system has positive Lyapunov exponents and the motion is ergodic.

It has been shown theoretically that, when a billiard is perturbed by smoothing the walls, tangential trajectories and homoclinic orbits (Fig. 1.1) induce stability islands in the phase space of the new perturbed system (Turaev and Rom-Kedar, [TRK98, RKT99]); the effect on the system is that this can break ergodicity. This result does not specifically discuss the diffusion coefficient but we will see that in the cases we study here, there are important effects on the diffusion coefficient which could be related to the type of trajectories just mentioned.

Let us recall that the original aim of the Lorentz gas was to study the motion of electrons in metals. The progress of technology allowed to create artificially one and two-dimensional arrays with a periodic potential, which can be adjusted to be steep or shallow. These structures called antidot lattices are analogous to the periodic Lorentz gas model. For instance since the early 90's, experiments in triangular [YTT+91, TKY+91] and square [WRM+91, WLR97] antidot lattices are reported. Graphene, which is a layer of graphite, and has a periodic structure, has become popular. Graphene antidot lattices promise to have better physical

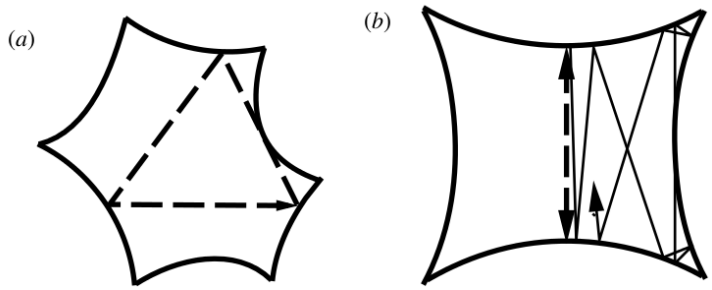

Figure 1.1: This figure illustrates tangent trajectories in a billiard. (a) Singular (tangent) periodic trajectory. (b) Dashed trajectory: Non-singular periodic trajectory. Continuous trajectory: tangent homoclinic trajectory to the periodic trajectory. This figure is taken from Ref. [TRK98].

characteristics than the structures made of GaAs [PRN+16, PFP+08].

Billiards with holes [Det11, KGDK12, DG11a, DG09, DG12, BD05] are also relevant in the light of experiments by realizable atom optical billiards (Kaplan *et.al.* [KFAD01, KFAD04]). It is possible to create two dimensional traps or cavities with a hole at the boundary and soft walls tuned at wish. There is a variety of doable shapes *e.g.* a stadium and a circular shape. The dynamics of atoms interacting with the soft walls inside this artificial billiard yield to stable island in phase space, moreover it has been shown that the size of the islands is very sensitive to the softness as a control parameter [KFAD04].

Billiards are a great laboratory to study transport process as well as mathematical properties. The Lorentz gas has been among the most studied giving successful results in terms of not only its dynamical properties, but also on deterministic diffusion. The question to address is: What would happen if one perturbs the periodic Lorentz gas by smoothing the walls of the potential?

1.3 Overview and structure

In this thesis, we consider a smooth potential periodically located in the plane, which can be viewed as a soft Lorentz gas. In this setting, we explore the diffusion coefficient as a function of control parameters; the separation of the scatters and

the energy of the particles.

In Chapter 2 we give a brief summary on the scientific background and also review relevant concepts of dynamical systems. For a good and pedagogic source of basic information on the topic we recommend Ott 2002 [Ott02]. We discuss the periodic Lorentz gas and explain a random walk approximation for the diffusion coefficient by Machta and Zwanzig. We describe the model that will serve as the soft version of the Lorentz gas. Here we also describe technical details about the simulations of the mean square displacement of an ensemble of particles as well as the numerical extraction of the diffusion coefficient.

In Chapter 3 we analyse the diffusion coefficient as a function of the separation of the scatterers, or the density of scatterers. In Chapter 4 we study the energy-dependent diffusion in the small energy regime and in the high energy regime. There we study two models: one with high density of scatterers and a steep potential and a second one with low density and a more moderate potential.

There is a brief description of the models that we study in each chapter, but the details and technicalities are described in Section 2.7. In both chapters 3 and 4, we develop *ad hoc* random walk approximations to diffusion as a function of control parameters. This with the aim of understanding the diffusion coefficient from microscopic dynamics. We also investigate the phase space via Poincaré surface of section.

We conclude with a summary of the main results and a brief description of possible future work in Chapter 5.

Chapter 2

Preliminaries and Background

In this Chapter we present some basic concepts of dynamical systems theory relevant for our study, starting from dynamical systems, passing trough billiards and the periodic Lorentz gas, and Hamiltonian systems with mixed phase space. For a deeper insight into these topics see Ott 2002 [Ott02], Lichtenberg and Lieberman 1992 [LL92] and Gaspard 1998 [Gas98]. We finish this chapter with the construction of a soft version of a period Lorentz gas, which is the model we use in our analysis in the rest of the thesis. Here we define important concepts related to the soft model along with some technical details. The eager reader might skip the first sections and read through the description of the models in Section 2.7.

2.1 Chaos and Hamiltonian Systems

The main feature of dynamical systems theory is that it focuses on the evolution of a set of initial conditions in the phase space instead of attempting to describe individual orbits. We start with the definition of a dynamical system. A dynamical system is a pair (M, Φ) where $M \subseteq \mathbb{R}^n$ is the phase space (or state space) and Φ a family of maps $\Phi_t : M \to M$ ($t \in \mathbb{R}$ for a continuous system or $t \in \mathbb{Z}$ for discrete a one). The family obeys

1. $\Phi_o(x) = x$ for all $x \in M$

2. $\Phi_s(\Phi_t(x)) = \Phi_{s+t}(x)$ for all $x \in M$.

The index t can be treated as time, in which case we are dealing with a differential equation. Otherwise we deal with discrete iterated maps.

Let $\phi : M \longrightarrow M$, $\phi_{n+1} = \phi(x_n)$ denote a discrete dynamical system on a phase space M. The sequence $x_o,\ x_1 = \phi(x_o),\ x_2 = \phi(x_1), ...$ is called an orbit with initial condition x_o. We call $x_* \in M$ a fixed point if $x_* = \phi(x_*)$. A fixed point is defined to be stable if all sufficiently small perturbations away from it damp out in time; unstable fixed points are those in which disturbances grow in time [Str94]. There are analogous definitions for continuous dynamical systems.

There is not an agreement on the definition of a chaotic system, one way to define it relies on the sensitivity of initial conditions. We follow Ott's 2002 [Ott02] definition: A dynamical system is said to be chaotic if it shows to be exponentially sensitive to initial conditions. A measure of the sensitivity of a system to initial conditions are the so called Lyapunov exponents, see Ref. [Ott02]. This quantity serves as a measure or indicator of the chaoticity of a dynamical system, though it does not say much about its transport properties. A chaotic system is often called hyperbolic, although this term refers to the flow's insensitivity to small perturbations near an equilibrium point of the vector field [Str94]. The dynamic is said to be structurally stable due to the presence of expanding and contracting directions of the derivative of the map in question [HP08, Ott02].

Hamiltonian systems can also be classified regarding their degree of randomness as ergodic, mixing, K-systems, C-systems, and Bernoulli systems; ergodicity being the weakest and with a more physical meaning as we explain next (see Ref. [Dor99, Ott02] for a good revision of these topics). The concept of ergodicity was first expressed by Boltzmann: in some systems, starting in a state x, the orbit eventually explores all of the phase space. This idea is known as the *ergodic hypothesis*. After years of development of mathematical theory, it can now be stated in a more formal way.

Let $\Phi_t : M \to M$ be the flow of a dynamical system, that is, it describes the state of the system at a time t. The map Φ_t is called *measure preserving* if

$\mu(\Phi^{-1}(B)) = \mu(B)$[1] (for any subset $B \subseteq M$ in the σ-algebra).

Now, let $f : M \to \mathbb{R}$ be a function that represents an observable. A measure preserving map $\Phi : M \to M$ is called *ergodic* (with respect to μ) if for any invariant set B, *i.e.* for any set which satisfies $B = \Phi^{-1}(B)$, we have either $\mu(B) = 0$ or $\mu(B) = 1$ [Jus14]. Now that we have defined an ergodic flow, we can state an important result (consequence of Birkhoff's ergodic theorem [Dor99]): *Let $\Phi : M \to M$ be a measure preserving map and ergodic with respect to μ. Then for any given Lebesgue-integrable function $f : M \to \mathbb{R}$, for μ-almost all $x \in M$, the time average*

$$\langle f \rangle(x) = \lim_{T\to\infty} \frac{1}{T} \int_0^T (f(\Phi_t(x))dt$$

exists and equals the space average

$$\bar{f} = \frac{\int_M f(x)d\mu}{\int_M d\mu}.$$

In other words, if a system is said to be ergodic it has to satisfy

$$\langle f \rangle(x) = \bar{f}. \tag{2.1}$$

Note that it is hard or impossible to obtain information on the evolution of Φ at large times whereas the right hand side of Eq. (2.1) could in theory be calculated for some systems. Here lies the relevance of this equation, thus the importance of ergodic systems.

Poincaré Surface of Section

In this section, we describe a very basic but useful tool that helps us understand the complexity of some dynamical systems.

In dynamical systems with two degrees of freedom we have a 4 dimensional

[1] A measure μ is a function that assigns to each set $A \subset M$ (from a special collection: a σ-algebra on M.) a non-negative number $\mu(A) \geq 0$. The function satisfies $\cup\mu(A_i) = \Sigma\mu(A_i)$, for any pairwise disjoint sets A_i and $\mu(\emptyset) = 0$.

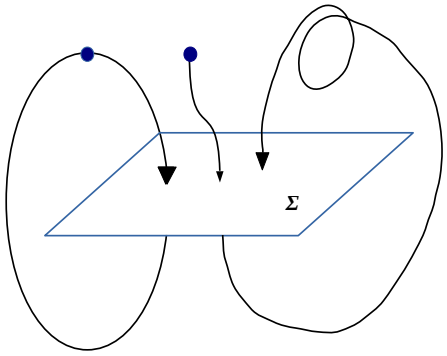

Figure 2.1: Illustration of orbits crossing the surface Σ.

phase space, which is not easy to visualize. Whenever possible, if there is a quantity that is a constant of the motion, the system can be reduced to a 3 dimensional space. We can construct a two dimensional surface, Σ, such that all orbits intersect this surface; this is sometimes called a cross-section. Let us reconsider the notation for a discrete dynamical system. The sequence of subsequent crossing $y_n \longmapsto y_{n+1}$ in the surface defines the Poincaré map $P : \Sigma \longrightarrow \Sigma$. Then, the map P is a discrete time dynamical system that often helps us to visualize the flow, or continuous dynamics, of trajectories. A proper cross-section must be chosen such that all orbits cross it so that no information of the system is lost, see Fig. 2.1. With this construction, if x_* is a fixed point of P, $P(x_*) = x_*$, then x_* belongs to a periodic orbit in the original map; fixed points have Lebesgue measure zero which makes it difficult to locate them in this surface. Higher period orbits, $f^k(x_*) = x_*$ with $k \in \mathbb{Z}$, have also a special signature in the surface Σ.

A periodic orbit is a finite collection of points which are subsequently visited by the orbit of the map; A chaotic orbit is an infinite orbit of the map which has a closure which is not a curve (commonly called chaotic sea); A quasi-periodic orbit is an infinite orbit where the closure is a curve, a topological ellipse.

Periodic orbits are surrounded by quasi-periodic orbits and they partition the phase space in islands. If the phase space has elliptic (periodic) islands and a chaotic sea, it is called mixed phase space. If one observes only the chaotic sea, then there are only unstable (also called irregular) trajectories except for (unstable) fixed points. Recall the case of the Lorentz gas, where the system is known

to be chaotic; there the set of periodic trajectories has measure zero.

Sometimes it is possible to distinguish the islands from the chaotic sea, but we want to point out that finding, or characterizing, exactly the boundaries of the islands in phase space is still an open and very intriguing question. Obtaining information about the averages and observables of a dynamical system is a more realistic task. We will discuss more about the relevance of this topic on transport properties in Sect. 2.6.1.

In most cases it is not possible to come up with an exact formula for the map P. Nevertheless, even if we ignore the explicit form of the map P one can obtain numerically the Poincaré surface of section if we know the evolution of the orbits.

2.2 Mean square displacement and diffusion: normal and anomalous

The diffusion coefficient D measures the rate at which an ensemble of particles disperses or spreads, and can be obtained by the rate of the linear growth of the mean square displacement of the particles as follows:

$$D = \lim_{t\to\infty} \frac{\langle(\mathbf{r}(t) - \mathbf{r}(0))^2\rangle}{4t}, \tag{2.2}$$

where $\mathbf{r}(t)$ is the position of a particle at time t and $\langle(\mathbf{r}(t) - \mathbf{r}(0))^2\rangle$ is called the Mean Square Displacement (MSD) with ensemble average of particles $\langle ...\rangle$. If the limit in Eq. (2.2) exist or equivalently the growth of the MSD is linear with time, then we talk about normal diffusion. The expression is known as Einstein's definition for the diffusion coefficient. If $\langle(\mathbf{r}(t) - \mathbf{r}(0))^2\rangle \sim t^a$ with $a \neq 1$, we say that the diffusion is anomalous, in which case two different scenarios are possible: when $a < 1$, the process is called sub diffusive, and if $a > 1$ the process is called super diffusive [Kla].

Particularly, in the case of the periodic Lorentz gas system, another expression for anomalous diffusion has been determined; this, in the 'infinity horizon regime'

a regime where the mean free path of the particle is unbounded. Here, it happens that Eq. (2.2) diverges [FR84, Bun85]; however, a time dependence of the form $t \ln t$ of the MSD has been observed which yields to a new form of the (super) diffusion coefficientr [Ble92]. We further discuss the infinite horizon and the diffusion coefficient in a periodic Lorentz gas in Sect. 2.5.2.

Even though in this thesis we focus on normal diffusion, sometimes we face regimes where anomalous diffusion takes place, this is regarded as potential future work.

Note that the MSD relates a macroscopic property of matter to the individual evolution of the elements that form it. In Section 2.7.1 we give some examples on how to calculate D from Eq. (2.2).

2.3 Random Walks and the drunken sailor

The simplest version of a random walk is a mathematical model in which a particle moves in steps of equal length at every step without preference of the direction (see *e.g.* [Rei65, Kla]). To illustrate the problem of a random walk, we introduce the classical problem of a not so classy one dimensional drunken sailor. The drunken sailor lacks memory, therefore s/he takes steps to the left or to the right independently of the previous position, that is the steps are uncorrelated. Let p_r the probability of moving to the right and p_l the probability of moving to the left. If there is no bias in the motion then $p_\mathrm{r} = p_\mathrm{l}$. Regardless of the drunkenness of the subject, and for the sake of simplicity, the length l of each step is the same. One can ask: what is the probability $P(x_N, N)$ that the drunken sailor is at the point x_N after N steps (at time $t = N\tau$ with τ the time interval between steps and $x = x_N l$ the distance from the origin) [Pea05].

It can be shown that if $p_\mathrm{r} = p_\mathrm{l}$ then the average net displacement is $\langle x(N) \rangle = 0$ and $\langle x^2(N) \rangle = Nl^2$.

Now, imagine a bunch of drunken sailors, all starting at $x(0)$, performing random walks as described above or speaking in more sober terms, an ensemble of

particles performing a random walk. We can ask how fast the particles spread out from the starting point. This can be answered by the Einstein formula for diffusion Eq. (2.2).

Consider the probability $P(x_N, N)$, if $p_r = p_l$, by taking the continuum limit $\Delta t \to 0$ and $l \to 0$, it is possible to arrive at a spatio-temporal differential equation

$$\frac{\partial P(x,t)}{\partial t} = \frac{l^2}{2\tau}\frac{\partial^2 P(x,t)}{\partial x^2}. \tag{2.3}$$

Letting $D = l^2/2\tau$, the solution to Eq. (2.3) is the Gaussian

$$P(x,t) = \frac{N}{\sqrt{4\pi D t}} \exp\left\{\frac{-x^2}{4Dt}\right\}. \tag{2.4}$$

Taking the second moment of Eq. (2.4) and recalling that $\langle x^2(N)\rangle = Nl^2$ and $D = l^2/2\tau$, we have the relation

$$\langle x^2(t)\rangle = \int P(x,t)x^2 dx = 2Dt. \tag{2.5}$$

We can see a resemblance between Eq. (2.5) and the Einstein relation for diffusion Eq. (2.2). These are not equal but yield the same result for $t \to \infty$.

2.4 Correlation functions and the Green-Kubo formula

There is relation between the diffusion coefficient, D, and the velocity autocorrelation function (VACF) of a particles (see *e.g.* [Dor99]). To establish this relation first we introduce the concept of a time correlation function (CF). CFs are a tool broadly used in problems involving a large number of particles, *e.g.* in molecular dynamics, although it is also possible to define a VACF for one particle. Briefly, a time correlation function carries information about a property (observable) or a function at a certain time, and its relation with another property at a later time (although correlation functions can also be dependent on another variable,

for instance distance, in which case we talk about a spatial CF).

Let us say that we are interested in the velocity of the particle i at time t, call it $v_i(t)$ and its relation with the velocity (of the same particle) in a future time $t' = t + T$; in this case we would be talking of an 'auto-correlation' function. The velocity auto-correlation function (VACF) is defined as follows

$$C_v(t, t') = \frac{1}{N} \sum_i v_i(t) \cdot v_i(t') \tag{2.6}$$

where N is the number of particles. A shorter notation is $C_v(t, t') = \langle v(t) \cdot v(t') \rangle$, where the brackets indicate the average over an ensemble.

If the future velocity $v_i(t+T)$ remains the same as $v_i(t)$, that means that there are no forces on the system or interactions acting on it. Thus, the function $C_v(t, t')$ is a constant with respect to time. This is the case of the ideal gas model without boundaries. Let us say that there are forces acting on the system, for instance, the particles can collide. Every collision would then modify the velocity of the particle, so $v_i(t)$ and $v_i(t + T)$ are different. In the case that every interaction or collision implies a change, the system may 'forget' its initial state. How fast this happens depends on the specific system. In the case of Brownian motion models $C_v(t)$ is expected to decay exponentially in time. When dealing with systems that resemble solids or liquids, the VACF has its own particular signature as well: since collisions allow the particles to bounce back and forward, the velocity can change from positive to negative values. In this case, we expect the VACF to oscillate with time before losing all memory.

The VACF gives an insight of the motion at a microscopic scale of a dynamical system, which in turn can be related to macroscopic transport coefficients. For instance, the diffusion coefficient can be expressed as

$$D = \int_0^\infty \langle v(0) \cdot v(\tau) \rangle d\tau, \tag{2.7}$$

as long as $C(\tau) = \langle v(0) \cdot v(\tau) \rangle$ is an integrable function. The expression in (2.7) is called the Green-Kubo formula for diffusion and can be obtained from the Einstein

relation Eq. (2.2) [Dor99]. Other transport phenomena can also be characterized by a correlation function as a time integral of the ensemble average [EM90].

2.5 Billiards and the periodic Lorentz gas

This section contains an introductory discussion about the theory of billiards. There is a vast compendium of literature in this regard (*e.g.* Refs. [Sza00, Gas98, Det00, Det11] just to name a few). The main purpose of this section is to describe the Lorentz gas model for deterministic diffusion and to elaborate on the random walk approximation for diffusion by Machta and Zwanzig [MZ83].

2.5.1 Billiards

Billiards are a class of Hamiltonian systems where a particle performs elastic collisions with the boundary of a billiard table. The motion of the particle inside the billiard table is dictated by the Hamiltonian

$$H(\mathbf{r}, \mathbf{v}) = \frac{|\mathbf{v}|^2}{2} + V(\mathbf{r}), \tag{2.8}$$

where $V(\mathbf{r}) = 0$, which yields the free flight between collisions. The collision at the boundary is that of a specular reflection, mirror like. The trajectory of the particle is a straight line between collisions, unless some magnetic field is introduced; then the trajectories follow a curvy path. For a more formal definition see Ref. [BDD$^+$00]. These systems are an excellent laboratory for physicists and mathematicians, because their simplicity makes it possible to obtain information that in other more complex systems would be cumbersome. Just by changing the geometry one can get an infinity of billiards. Some representative billiards are the Sinai billiard and the Stadium (see Fig. 2.2). The Sinai billiard (or dispersing billiard [Sin68]) consists of a square box with a circular scatterer in the centre. This system is hyperbolic and ergodic [Sin70]. The Stadium, which is composed of two semicircles connected by straight lines, is also hyperbolic and ergodic [Bun74]. Another, now classical and interesting, example is the mushroom billiard [Bun01].

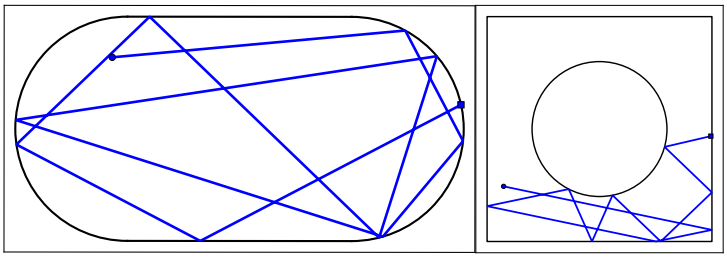

Figure 2.2: Classical billiards: **Left**: Stadium billiard. **Right**: Sinai billiard.

Billiards can be closed, like the examples we just mentioned, or open by removing a fraction of the boundary[Det11, AT09]. The domain can be finite, or by placing scatterers in the plane we get an infinite domain. Billiards with moving walls are also possible. Moreover, billiards in higher dimension can also be defined [Che94].

Sinai started with the mathematical theory of dispersing billiards [Sin70, Sin79]. He proved that a system with two hard disks was ergodic [Sin70]). In Bunimovich 1985 [Bun85] decay of correlations is studied in dispersing billiards and particularly in the periodic Lorentz gas. Young proved an exponential decay of correlations in dispersing billiards [You98]. Then Chernov and Young [CY00] proved it in the particular case of the Lorentz gas and hard balls. This result was extended to billiards in higher dimensions [Che94, Sin00].

More geometrical forms of billiard tables can be used to study transport properties, *e.g.* the mushroom billiard [Bun01, AMK06, DG11a], or a flower shaped billiard [HKG02]. The list of results on billiards, regarding ergodicity, decay of correlations, entropy, periodic orbits, etc. *i. e.* Refs. [BS81, BSC91, Che99, Che97], is wide. For an extensive review on billiards see Chernov and Makarian [CM06] and Sinai [Sin00].

In the next section we focus on a more detailed description of the periodic Lorentz gas, its properties, and important results found in the literature.

2.5.2 The Lorentz gas

Recall that one of the motivations of the study of billiards is that they can represent a simplification of a real system. One example of this simplification is the attempt to model the motion of electrons in a crystal as point particles colliding with solid discs positioned randomly in the plane, the so called Lorentz gas [CM06]. Since Lorentz introduced this model in the early 1900 [Lor05], because of its simplicity and richness, the system's dynamical and physical properties have been studied extensively.

Let us construct a periodic Lorentz gas in a triangular lattice and introduce the concept of a 'trap'. Position circular scatterers of radius r_o at the vertices of a triangular lattice. We call the area inside a triangular region (see Fig. 2.3) a unit cell.

The plane can be covered with copies of unit cells. A particle travels in free flight until it reaches a scatterer, where it performs an elastic collision. The region available, in the unit cell, for the particle in position space is called a trap (see Fig. 2.3). Let us denote by w the closest distance between scatterers as shown in the left of Fig. 2.3. In this way, the length of one side of the lattice is $L = 2r_o + w$. In the following let us set $r_o = 1$.

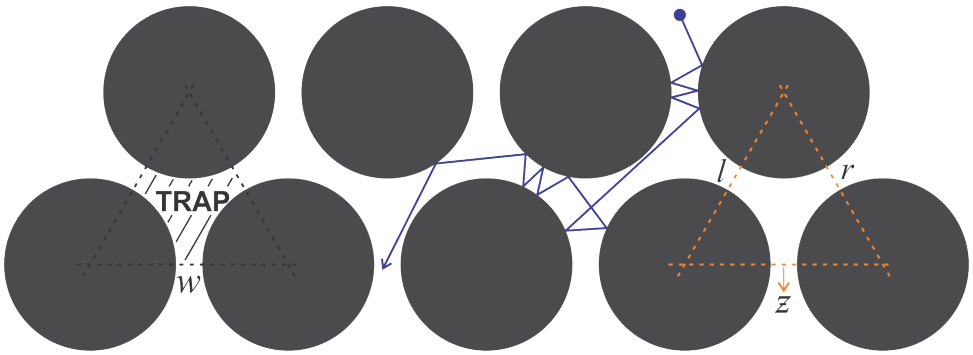

Figure 2.3: Periodic Lorentz gas on a triangular lattice. Blue: A typical trajectory colliding with the scatterers. On the left we illustrated the concept of a unit cell and a trap. The smallest separation between scatterers is denoted w.

These settings describe the triangular periodic Lorentz gas, the original model

Figure 2.4: Different scenarios in the triangular periodic Lorentz gas according to the separation of the scatterers w. **Left**: At $w = 0$ particles can not escape the trap. **Centre**: Particles can travel from one trap to another. **Right** w is such that particles can travel without colliding with any scatterers, this is called the infinite horizone.

placed the scatterers randomly in the plane [Lor05].

How does the diffusion coefficient D depend on the separation of the scatters, w? The separation of the scatterers dictates the behaviour of the diffusion. For instance, if $w = 0$ the gap is closed and the particle can not escape the trap, therefore diffusion does not exist (see Fig. 2.3 left).

In the regime $0 < w < 4/\sqrt{3} - 2 = w_\infty$, the particle can escape from the trap and it travels in free flight until it hits a scatterer and changing its direction (centre of Fig. 2.4), this is called the finite horizon regime.

Regarding transport coefficients Bunimovich and Sinai proved that for the periodic Lorentz gas with finite horizon the displacement of particles $\mathbf{r}(t) - \mathbf{r}(0)$ converges to a Gaussian distribution with the normalization $\sqrt{t}$ [BS81]. In this regime there exist a well defined positive diffusion coefficient [BS80, BSC91]. On the other hand, if $w > 4/\sqrt{3}-2$, the configuration of the scatterers is such that the time between collisions of the particle is unbounded and we talk about an infinite horizon Lorentz gas. In other words, the free path of some particles is unbounded which implies that a normal diffusion process is not possible. This is immediately achieved if the scatterers are placed in a square lattice. In [ZGNR86] it was showed that in a square lattice the VACF decays as t^{-1} and a divergence of the form $t \ln t$ for the MSD. Divergence of the MSD, yielding anomalous diffusion, was also observed in 1-dimensional intermittent maps by Geisel and Thomae [GT84]. In the triangular periodic array an infinite horizon scenarios is also achievable if the scat-

terers are separated enough, as illustrated in the right of Fig. 2.4. In these cases super diffusion takes place. If we attempt to use Eq. (2.2) the diffusion coefficient is infinite [FR84, Bun85]. However, Bleher [Ble92] proposed the normalization $(t \ln t)^{1/2}$ such that $\mathbf{r}(t) - \mathbf{r}(0)$ converges to a Gaussian distribution when time goes to infinity. The conjecture works for any kind of periodic configuration with infinite horizon. With this normalization we have that

$$D = \lim_{t\to\infty} \frac{\langle |\mathbf{r}(t) - \mathbf{r}(0)|^2 \rangle}{2t \ln t} \tag{2.9}$$

is the super diffusion coefficient [Det12]. For more theoretical and numerical results on billiards with infinite horizon see Refs. [SV07, DC09, Det12].

From the branch of dynamics one of the first rigorous results on the triangular periodic Lorentz gas is by Sinai who proved ergodicity and hyperbolicity. Then, Bunimovich and Sinai showed that the Lorentz gas is chaotic. More precisely it is a K-system, following the hierarchy of degree of randomness this means it is mixing and ergodic [BS81, BSC91, Che99]. Then, Young and Chernov [CY00] showed exponential decay of correlations in many types of dispersing billiards, specifically for the Lorentz Gas.

One of the earliest models on diffusion in a Lorentz gas is by Machta and Zwanzig [MZ83]. They studied the diffusion coefficient as a function of the separation of the scatters, assuming a random walk between traps. We shall discuss this model in detail in Sect. 2.5.3.

In the periodic Lorentz gas we can identify unstable periodic orbits. They occupy a set of measure zero in phase space therefore they do not contribute in the calculation of transport properties. For more recent results about the Lorentz gas see [Sza00, BBC+13, Det00, Det11].

2.5.3 Random walk approximation for the diffusion coefficient

Here we explain the random walk approximation by Machta and Zwanzig [MZ83]. Their goal was to come up with an approximation for the diffusion coefficient in the Lorentz gas as a function of the density of the scatters. The main idea behind their approximation is that as collisions occur, the particle loses memory, and therefore its path between 'traps' can be taken as a random walk. For random walks on two dimensional lattices the diffusion coefficient is described by:

$$D = \frac{l^2}{4\tau}, \tag{2.10}$$

where l is the distance travelled in on step and τ is time for a single step in the random walk. Machta and Zwanzig calculated the average rate at which a particle leaves the trap, τ^{-1}, by looking at a fraction of phase space available for the particle for exiting the trap.

The probability to leave the trap is given by the total volume of phase space for a trap and the portion of this space from which a particle escapes the trap in time Δt. This can be expressed in terms of w and the area of the trap, A_{LG} (LG stands for Lorentz Gas). Since the particle is in free motion inside the trap, we consider the case $|\mathbf{v}| = v = 1$. The total phase space is $M = \Omega' \times S'$, where Ω' is the position space available for the particle and S' is the set of velocities of unit magnitude. The total phase space for a particle inside a trap is then $M = A_{\mathrm{LG}} \times 2\pi$. The area A_{LG} is given by the geometry of the billiard and can be expressed in terms of the separation of the scatterers w as:

$$A_{\mathrm{LG}}(w) = \sqrt{3}(2+w)^2/4 - (\pi/2). \tag{2.11}$$

Call M' the portion of the phase space from which a particle escapes from a trap in time Δt. If the particle travels a distance s at a velocity v then $v = s/t$, which implies that in a very short time $v\Delta t = \Delta s$. If $v = 1$ then the amount of particles per unit time with velocity v that escapes from the trap through the exit w is

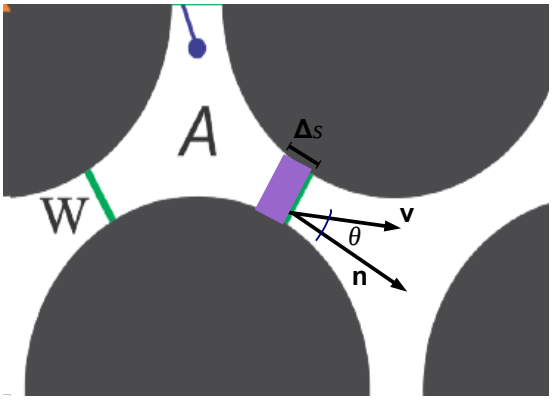

Figure 2.5: Flux of particles with velocity v escaping from the trap of area A_{LG} in time Δt.

given by the flux

$$\int |\mathbf{n}||\mathbf{v}| \cos\theta d\theta = 2, \tag{2.12}$$

where θ is the angle between the velocity vector $\mathbf{v}$ and the normal $\mathbf{n}$ to the segment w. This is represented in Fig. 2.5, the purple area is $v\Delta t \times w$. There are three exits with length w, hence $M' = 2 \times 3w$ and we get:

$$\tau^{-1} = \frac{3w}{\pi A}. \tag{2.13}$$

In the Lorentz gas l is the distance between traps and can be calculated thanks to the geometry of the lattice as

$$l = \frac{(2+w)}{\sqrt{3}}. \tag{2.14}$$

Finally, substituting Eq. (2.11) in Eq. (2.13) and Eqs. (2.13) and (2.14) in Eq. (2.10) we get:

$$D_{\mathrm{MZ}}(w) = \frac{w}{\pi} \frac{(2+w)^2}{(\sqrt{3}(2+w)^2 - 2\pi)}, \tag{2.15}$$

which is an approximation of the diffusion coefficient as a function of w [MZ83]. Since the radius of the scatterers is fixed, varying w is equivalent to vary the density of scatters. Fig. 2.6 shows D_{MZ} as a function of w, and numerical results. $D_{\mathrm{RW}}(w)$ overestimates the diffusion coefficient for large w and underestimate it

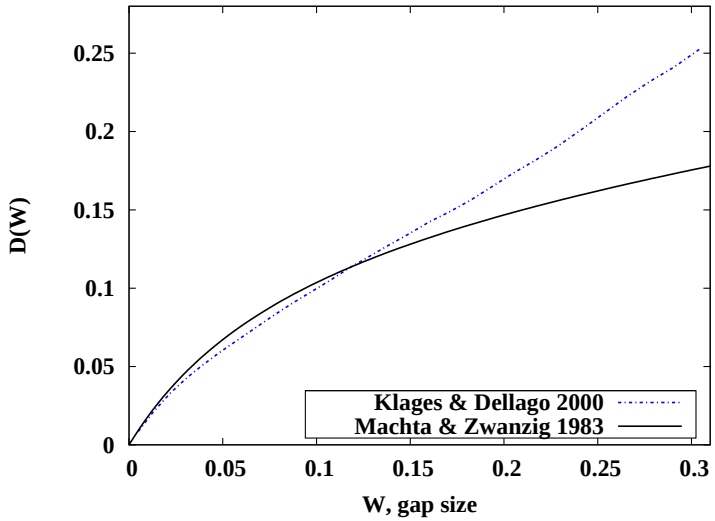

Figure 2.6: Diffusion coefficient D as a function of w from different approaches. Dashed line: Klages, Dellago numerical results [KD00]. Solid line: Machta and Zwanzig approximation, Eq. (2.15) [MZ83].

for smaller w. But it is asymptotically correct when $w \to 0$. Due to the scattering nature of the disks, in every collision the particle loses memory. When $w \to 0$ the particles collide more and lose memory faster, therefore the hypothesis of a random walk is valid in this regime.

2.6 Diffusion in Hamiltonian systems

In the literature we find examples of relatively simple systems that exhibits complex dynamics. This in turn has a non trivial effect of decay of correlations and transport properties. The beauty of all this is that although Hamiltonian systems are reversible systems, it is possible that they can generate non reversible transport processes such as diffusion.

2.6.1 Diffusion in Hamiltonian systems with mixed phase space

In most of the cases Hamiltonian systems present a mixed phase space, that is, the system has at least one chaotic component (chaotic sea), and at least one regular component embedded on it (island of stability). This scenario is accompanied by a phenomenon called stickiness where some trajectories spend a large amount of time in a particular region, close to the island, of phase space (sticky region) before visiting the rest of the phase space as normal. Stickiness phenomena are particularly relevant to transport because they can affect the decay of correlations [CS84] and transport properties [Zas02]. Even in systems where the stickiness is near islands without cantori in the borders, in 'sharply divided' regions, stickiness still has an effect on decay of correlations [AMK06].

Bunimovich and Vela-Arevalo [BVA12] make a distinction of the types of stickiness, here they define internal and external stickiness depending on where it appears. Stickiness present at the boundaries of regular islands and the chaotic sea is called external stickiness, and stickiness that is due to an invariant subset inside the chaotic sea is called internal stickiness. Note that it is not necessary for a system to have a divided phase space in order to exhibit internal stickiness. Moreover, even initial conditions outside the regular component can have an effect on averages of observables as pointed out by Rom-Kedar and Zaslavsky in [RKZ99].

A prototypical example of a Hamiltonian system with a mixed phase phase is the standard map [Chi79]

$$y_{n+1} = y_n + \epsilon \sin(2\pi x_n),\ x_{n+1} = x_n + y_{n+1} \bmod 1,$$

where ϵ is a constant. The map owes its name to the fact that it describes the dynamics of different physical problems, for instance periodically kicked rotors and the motion of charged particles (Refs. [LL92] and [Chi79]). The phase space of this system has regions of chaotic motion and stable islands. In this map, the stickiness phenomenon is also present at the boundaries of the islands and it yields a phenomenon called intermittency. More generally, when varying the control

parameter, there is a transition where regular motion is interrupted by episodes of chaoticity until the system seems completely chaotic. What causes the regular motion is an orbit that seems periodic but, at a critical point, it changes its well behaved nature and shows itself as irregular at different times, these events lead eventually to chaos. In the examples just mentioned, when this process occurs, anomalous diffusion can take place [Chi79, RW80, Leb98].

Harayama and Gaspard [HG01], studied the energy dependent diffusion coefficient, $D(E)$, in a periodically corrugated floor. The system is modelled by a particle subject to a constant vertical acceleration while it interacts with arcs positioned periodically horizontally. In this system it has been found that there are some energies for which islands in phase space exist. The islands induce an algebraic decay in the velocity correlation function, therefore the diffusion coefficient does not exist. When no islands are found, diffusion is normal and the diffusion coefficient has an intricate dependence on the energy. This reminds of the study case by Klages and Dorfman [KD95]. Interestingly, when applying a weak noise, the islands are destroyed and the diffusion coefficient exist in the new system. For diffusion in the presence of noise, the random walk argument as in [KD97] was applied and they found that $D(E)$ grows as a function of the energy, E, as $D(E) \sim g^{-1}(E/m)^{3/2}$, where g is the vertical acceleration and m is the mass of the particle. These studies point to the conjecture that diffusion coefficient has a non trivial, and often fractal-like, dependence of control parameters [KD99, GK98].

2.6.2 On Hamiltonian systems with smooth potential

When it comes to smooth potentials one can distinguish between attractive, repelling and, mixed potentials. These are defined in terms of its derivatives, following Ref. [DL91]. Let $V(r)$ be a radial potential, $r \in \mathbb{R}^+$:

- Potentials $V(r)$ with $V'(r) \geq 0$, $r \in (0, R)$, are called *attractive potentials*.
- *Repelling potentials* are those that satisfy $V(r) \geq 0$, $V'(r) \leq 0$ $r \in (0, R)$.
- We refer to *mixed potentials* to those that exhibit an attractive and a repelling region.

Potentials with singularities of the type $-r^{-1}$ are called Coulomb potentials; for a more formal definition see *e.g.* Knauf 1987 [Kna87].

Consider a point particle with negligible mass (electron) under the influence of a Coulombic type potential periodically distributed in the plane.

The available position coordinates (x, y) for the particle under study is called configuration space, M'. In the following, one of the geometrical properties of the configuration space, the curvature, is considered to study dynamics in the billiard instead of discussing the typical dynamical system given by the Hamiltonian. For a deeper insight of the following concepts see Refs. [Kna87, KK92, Nob95]. The curvature associated to the space M' is defined in terms of a function; this function is the potential V. There is also a metric associated with this potential which we define next. Let q be a point in M' and $h > h_o$ with $h_o = \sup V(q)$ and h finite[2]. The Jacobi metric g' on the configuration space M' is

$$g'(q) = (h - V(q))g(q), \tag{2.16}$$

where g is the Euclidean metric on M'. When h is very large compared to $V(q)$, we have that $V/h << 1$ therefore h is the dominant term in Eq. (2.16). In order to define the curvature associated to a potential V and energy of the particle h we introduce the Gaussian curvature K_E of (M', g') which is given by

$$K_E(q) = \frac{(h - V(q))\Delta V(q) + (\nabla V(q))^2}{(h - V(q))^3}, \tag{2.17}$$

where Δ is the Laplacian and ∇ is the gradient. Let $V : M' \to \mathbb{R}$ be a Coulombic potential and Eq. (2.16) the metric on M' defined by V. If the Gaussian curvature $K_E(q)$ of (M', g') is ≤ 0 and in every maximally extended geodesic on M' there exist points with $K_E(q) \leq 0$, then V is said to be of *negative curvature* at the energy h.

When taking this approach, one does not talk about forces or energies but of the geometry associated to the space M' determined by the potential V. In this context, Knauf (1987) [Kna87] gave conditions for diffusion in terms of the

[2] h has to be finite since it aims to represent a physical situation.

curvature of the attractive potentials. He showed that the motion on the plane with periodic Coulombic potential is diffusive. This formalism was specifically applied to Yukawa potentials, a type of Coulombic potential, where he showed that there exists an energy threshold such that the potential has negative curvature, implying that in this kind of potentials the motion in the plane is diffusive.

Following these lines, Nobbe (1995) [Nob95] calculated the energy threshold for diffusion in an square lattice of Coulombic potentials type, especifically a Yukawa potential. Next, we will discuss the energy dependent diffusion coefficient $D(E)$ in systems ruled by this kind of potential.

Example: Yukawa potential

The so called Yukawa potentials are of the form

$$V^{\mathrm{Y}}(q) = -\frac{\exp(-|q|)}{|q|}.$$

Based on Knauf's results, Nobbe 1993 [Nob93] calculated analytically a threshold for diffusion in a finite square lattice with a Yukawa potential. He calls the motion in a crystal to be diffusive if a finite and positive $\lim_{E\to\infty} D(E)$ exist. His proposition applies to Coulombic potentials and reads as follows: *Let* $V : M \to \mathbb{R}$ *be a potential and* $h = 5.17$. *For all electrons with* $E > h$ *one has that* $K_E(q) < 0$, *where* K_E *is the Gaussian curvature* Eq. (2.17).

The threshold h is obtain by solving $K_E(q) < 0$ in terms of the energy. It is possible to calculated numerically a more accurate threshold of the energy with the same arguments. Unfortunately, this method is not applicable in the presence of potentials with positive curvatures, which is the case we study here, the Fermi potential.

In 1995 Nobbe writes a paper, which is related to his thesis results [Nob95], where he describes an approximation for the dependence of diffusion on the energy that goes like: $D(E) \sim const \cdot E^{3/2}$ as $E \to \infty$. In the deduction of this law, the mean free path length of a particle (electron) is considered. Here it is argued that "the increase of the diffusion constant $D(E)$ with the energy follows from a rise of the mean free path length...".

The works cited above state that the curvature determines the dynamics of the system; an attractive potential with negative curvature implies diffusivity in the plane. However, Donnay and Liverani [DL91] proposed conditions for ergodicity in a varied class of potentials, some with positive curvature. They proved that the motion of a particle on the torus exhibits a positive Lyapunov exponent and is ergodic for three types of potentials (repelling, attracting, and mixed). Though it should be mention that the construction of the potential is different from those studied by Knauf [Kna87] and Nobbe [Nob95]. In [DL91], the type of scatterer that was considered is a symmetric potential of finite range (compound potential). The motion of a particle inside a disc D of radius R is under the influence of $V(r)$ and outside the disk is that of a free flight, this means that at set of parallel trajectories leaving the disk will stay parallel. To proof positive Lyapunov exponents and ergodicity they studied the flow of the phase space and used the so called invariant cone-field technique [Woj85]. It is also worth noting that smoothness does not imply ergodicity, they showed that there are smooth systems without singularities with positive Lyapunov exponent which are not ergodic. Moreover, conditions for non-ergodicity in Leonard-Jones potential have also been found [Don99].

In the same spirit, Bálint and Tóth (2004) [BT04] studied mathematical properties of billiards made of radially symmetric potentials, that is the particles are allowed to enter the scatterers and travel in free flight outside the range of the potential. The configuration of the scatterers is periodic. For this type of system, they conclude that for all cases where the system was ergodic the correlation decay is exponential, see also [Bal88].

A similar model is studied by Aguer *et. al.* [ADB10] where a 'soft inelastic' periodic Lorentz gas is proposed. In order to model the obstacles, they used time dependent flat circular scatterers, where the particle changes its momentum depending on the time of the arrival to the centre of a scatterer. Next, it travels with this new moment until it reaches another scatterer. The model is such that there is a finite horizon for the particles. In this model, they claim that after a long time the motion of the particle gets randomized and use this argument to construct a random walk for the motion of the particles which yields to a diffusion coefficient that grows as a function of the momentum of the particle

p like $D(p) \sim p^5$. Numerical simulations are also performed which match their analytical random walk.

Bagchi, Zwanzig and Marchetti (1985) [BZCM85] inspired by Machta and Zwanzig's work [MZ83] analysed diffusion in a triangular lattice with a smooth potential as a function of the energy. The system they considered is modelled with

$$V(x, y) = \cos(x + y\sqrt{3}) + \cos(x - y/\sqrt{3}) + \cos(2y/\sqrt{3}).$$

This is an analogous case to a softened version of a periodic Lorentz gas in the sense that it yields a triangular lattice and it has saddle points in the middle of the exits, maxima in the lattice points and minima in the centre of triangular traps. In this study, Bagchi *et. al.*, conjectured that the diffusion coefficient exists for all values above some critical energy, and below some maximum value of the energy.

Another example that shows interesting features on transport when varying the energy of the particle, E, is by Geisel, Zacherl and Radons (1987) [GZR87]. The study is on the motion of a classical particle in a two dimensional square lattice with an egg-crate like potential

$$V(x, y) = A + B(\cos x + \cos y) + C \cos x \cos y. \tag{2.18}$$

Two cases were considered. In one case it is observed that diffusion is normal in the range of $5 < E < 6$ and anomalous for smaller energies $2 < E < 4.6$. In another setting where the valleys coincide with the saddle points, they only found normal diffusion up to energies smaller than the maximum of the potential. They state that saddle points and potential wells focus the trajectories in long free paths.

Later, Geisel *et. al.* in [GWNO90] and [WGNO92] studied diffusion as a function of the energy in two dimensional square lattice but including a magnetic field. They found regions of normal and anomalous diffusion and claim that increasing energy yield a decreased in the diffusion coefficient. The anomalous diffusion in this case is caused by orbits trapped in a specific region of the phase space.

The model discussed in Geisel *et.al.* serves as a model of the motion of electrons in lateral super lattice conductors [WKP89]. With the progress of technology, *e.g.* in lithography techniques, it is possible to create a planar array with scatterers tuned by a periodic steep potential where the motion of the electrons can be artificially controlled. The settings in these structures yield a motion of the electrons in a classical regime. These realizations are called anti-dot lattices and can be used to study transport in solids [PWSB89, WLR97, WRM+91, LKP91a, YTT+91, TKY+91]). It has been observed repeatedly that when measuring magnetoresistance in a square antidot lattice there are oscillations associated with the magnetic field [WLR97, WRM+91, LKP91b]. The oscillations are attributed to the interplay of the lattice period and the cyclotron radius. The observed magneto-transport features were explained with classical equations of motion in a magnetic field, where localized classical orbits of the electrons account for a maximum observed in the magnetoresistance [FGK92, LKP91b].

Artificial billiards are also helpful in the study of the chaotic behaviour at a quantum level [DG11b]. Nano scale billiards can be constructed by creating semi conductors quantum dots, that is, structures with steep potentials (see *e. g.* Refs. [NH04, FLH+01, JBS90]). Also models of billiards with holes can be constructed via atomic-optic billiards with soft walls. In this line of research Kaplan *et. al.* [KFAD04, KFAD01, FKCD01] studied the dynamical effects of the Bunimovich stadium, which happens to be chaotic and ergodic. They provided numerically and experimentally evidence of the formation of stability islands in the stadium billiard with soft walls. In agreement with Rom-Kedar and Turaev's theory [TRK98, RKT99], they found that islands form in phase space near tangential trajectories (see Fig. 1.1) in the non perturbed billiard. In these realizations of billiards it is also possible to measure the decay in the number of atoms inside the billiard which can be compared directly with numerical simulations [KFAD04].

2.7 The model: Soft Lorentz Gas

Having made clear the need to explore a soft version of the Lorentz gas, in this section we will construct a soft version of the Lorentz gas which shall be used in Chapter 3 and 4. The idea of the model is to keep the triangular configuration of the Lorentz gas by replacing the hard scatterers by a smooth potential. For this we introduce the Fermi potential which is given by

$$V_{\mathrm{F}}(\mathbf{r}) = \frac{1}{1 + \exp\left(\frac{|\mathbf{r}| - r_o}{s_o}\right)}, \tag{2.19}$$

where s_o is the softness of the potential and r_o is the radius of the potential. This is a repelling potential where the softness parameter can be adjusted to create a steep potential similar to an antidot lattice which is an experimental realization of a billiard (Weiss *el. al.* [WLR97, WRM+91] and Lorke, Kottaauss and Ploog [LKP91a]). Let us consider the motion of a particle in a triangular periodic array as illustrated in Fig. 2.7 with a Fermi potential at each point of the lattice given by Eq. 2.19; the potential field is then

$$V(\mathbf{r}) = \sum_n V_{\mathrm{F}}(\mathbf{r} - \mathbf{r}_n), \tag{2.20}$$

where $\mathbf{r}_n$ is the position vector to the n-th point of the lattice in the plane.

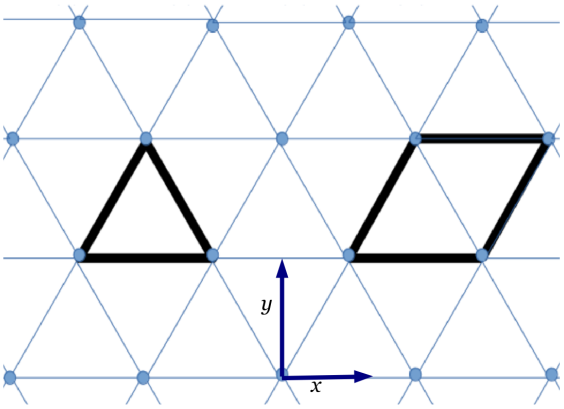

Figure 2.7: Examples of unit cells in a triangular lattice.

In the triangular periodic array depicted in Fig. 2.7 we can define a unit cell. Broadly speaking, a unit cell is a geometric structure in position space, at a microscopic scale, that can cover the whole plane with copies of it. For instance, the area inside a triangle formed by the vertices of the lattice is a unit cell, another unit cell is a diamond formed by two triangles, see Fig. 2.7. In what follows, we will consider the triangle as a unit cell.

Now let us look at the lattice with the Fermi potential in the plane Eq.(2.20). Note that maxima occur at the vertices of the triangles, minima at the centre of the triangles, and saddle points in the midpoints of the edges of the triangles as illustrated in Fig. 2.8.

We call a "trap" the region that is available for the particle in position space inside the unit cell, in congruence with the trap in the hard Lorentz gas (see Section 2.5.3). In this setting, the so called scatterers are the hills of the potential field. Our selection of the unit cell yields three exits from the trap; the width of the exit or gap between scatterers is shown in Fig. 2.8 and we shall denote it by w.

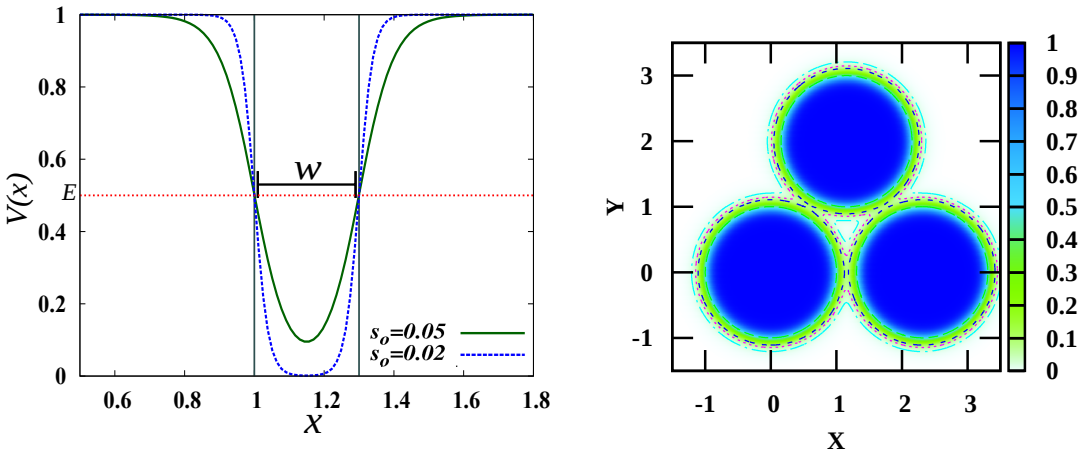

Figure 2.8: Left: Solid vertical lines indicate the hard walls in the Lorentz gas, dashed lines indicate V_{F} with a different smoothness parameter. **Right**: Triangular array of Fermi potentials in the plane with equipotential lines.

Although we consider the motion of the particle in the plane, in what follows, for the purposes of defining the separation of the scatters analytically, we look at one potential, Eq. (2.19), and two neighbouring potentials. First, let us consider the contribution of two adjacent scatterers at the corners of a triangle in the lattice at the points $(0,0)$ and at $(L,0)$ with $L = 2r_o + w$ in the $x-y$ plane indicated in Fig. 2.7.

We would like to define the separation between scatterers, w, such that for two adjacent potentials at the points (0,0) and $(L,0)$ and for $\mathbf{r}_1 = (r_o, 0)$ and $\mathbf{r}_2 = (r_o + w, 0)$ we have that

$$V_F(\mathbf{r}_1) = 1/2 \,\text{and}\, V_F(\mathbf{r}_2 - \mathbf{r}_L) = 1/2, \tag{2.21}$$

where $\mathbf{r}_L$ is the position vector of the potential centred at $(L,0)$.

It is important to mention that the relation in Eq. (2.21) is not satisfied for Eq. (2.20) due to the nature of the overlapping potential. We always have that $V(\mathbf{r}_1) > V_F(\mathbf{r}_1)$, and the difference between $V_F(\mathbf{r}_1)$ and $V(\mathbf{r}_1)$ increases as the separation between scatterers gets smaller. In the overlapping case, if we want the separation between scatters to satisfy $V(\mathbf{r}_1) = 1/2$ one needs to define the gap separation from $L = 2r_o + 2\epsilon + w'$ and taking $\mathbf{r}'_1 = (r_o + \epsilon, 0)$ and $\mathbf{r}'_2 = (r_o + \epsilon + w', 0)$ such that

$$V(\mathbf{r}'_1) = 1/2 = V(\mathbf{r}'_2). \tag{2.22}$$

This in order to be able to compare the soft Lorentz gas directly with the hard Lorentz gas results, where the energy of the particle was chosen to be $E = 1/2$. Note that $w' < w$ and for large w we have that $\epsilon \to 0$ and $w' \to w$; therefore, in this soft systems there are two parameters related to the separation of the scatterers. In the following for the sake of simplicity we will consider w, defined by Eq. 2.21, as a control parameter.

We look at the contribution of two adjacent potentials along the x-axis at the line $y = 0$. Then the potential is shown in the left panel of Fig. 2.8. Note that in the limit when s_o approaches zero, we recover the periodic hard Lorentz gas. Therefore, we can think of this model as smoothing the walls of the potential in

the periodic Lorentz gas.

The state of the system can be described by the position and velocity vectors $\mathbf{r} = (x, y)$ and $\mathbf{v} = (v_x, v_y)$ of the particle or by points in the phase space, Ω, which consists of all possible (x, y, v_x, v_y). The evolution of a classical particle, of unit mass $m = 1$, is fully determined by the Hamiltonian (Eq. 2.8). Conservation of energy allows to reduce the number of degrees of freedom by expressing v_x in terms of v_y so we can describe the system with (x, y, v_x). Alternately we can use the triplet (x, y, θ), where θ is the angle between the velocity vector and the normal to the x-axis. The motion of the particle is such that the velocity is given by the potential field. If its energy is higher than some energy threshold, E_h, then the particle can escape from the so called trap, and move to another one, otherwise the particle is confined in a trap.

An ensemble of particles is uniformly distributed in the phase space associated to a rhomboid unit cell (see Fig. 2.7): only valid combinations of (x, y, v_x, v_y) are allowed. In a purely chaotic system the selection of initial conditions is not important, since correlations decay fast. However, for the system we are concerned with, we want to make sure that the selection of initial conditions will not produce any artificial dynamical correlation.

If the energy of the system is less than the threshold energy, then the particle gets trapped indefinitely in some region of the configuration space and the diffusion coefficient is zero. If the particles can escape the trap then we have two possible scenarios depending on the growth of the MSD over an ensemble of particles; the system can exhibit normal diffusion or super diffusion. We give some examples of the MSD in this system in the next section.

In the next chapters we always refer to the lattice sides as $L = 2r_o + w$ with $r_o = 1$. In Chapter 3, which features the analysis of the diffusion coefficient as a function of the separation of scatters, we choose the the smoothness parameter $s_o = 0.05$ and total energy $E = 1/2$. If $E = 1/2$ and considering the Fermi potential in Eq. (2.8), an approximation for the threshold for diffusion is given by

$$w_* = 2\ln(3)s_o \text{ or } s_{o*} = w/2\ln(3). \tag{2.23}$$

The selection of s_o allows the system to be smooth and the selection of E and r_o allow us to make a direct comparison with the Lorentz gas presented in Section 2.5.3. When discussing the parameter w, we call the high density regime regions where $w \to w*$ and the low density regime where $w \to 1$. In Chapter 4 we shall vary the energy parameter and study two models with combinations of w and softness s_o that yield a high density of scatterers with steep potential and another one with a softer potential and a low density of scatterers.

Some technical details about numerical computations

We perform simulations of the MSD (introduced in Section 2.2) with the code BILL2D [SLR16]. The code implements the velocity Verlet algorithm to solve the equations of motion, for more about this method see Appendix A.1. We usually adopt a time step $\Delta t \times 10^{-3}$ unless specified otherwise. These computations were performed with the cluster Apocrita-QMUL (MidPlus).

We limit the numerical computations to the superposition of the four neighbouring Fermi potentials Eq. (2.19) located at the four vertices in the rhomboid unit cell (Fig. 2.7). The particle is thus exposed to the force generated by the resulting overlapping Fermi potential in the respective unit cell where it is located. Since we are adding continuous potentials, the sum is also a continuous one. The summation is truncated at the boundaries of the unit cell, supplemented by periodic boundary conditions. This truncation and the structure of the unit cell yield a non-smooth potential at the boundary. Let us say that a particle is about to cross a unit cell from top to bottom: before crossing, the potential to consider is the summation of the four corners of that rhomboid in the top $V_u(x, y)$ then, just after crossing, the potential is due to the summation of the corners of the rhomboid in the bottom $V_l(x, y)$. At any point, exactly in the boundary, both potentials should be equal but because of the asymmetry of the unit cell, there is a discrepancy[3]. This discrepancy gets bigger as the potential gets smoother. In Fig. 2.9 we show the difference $V_u(x, 0) - V_l(x, 0)$ for a system with smoothness

[3]In a square lattice this problem is absent even with a truncated potential because of the symmetry of the lattice in both horizontal and vertical directions.

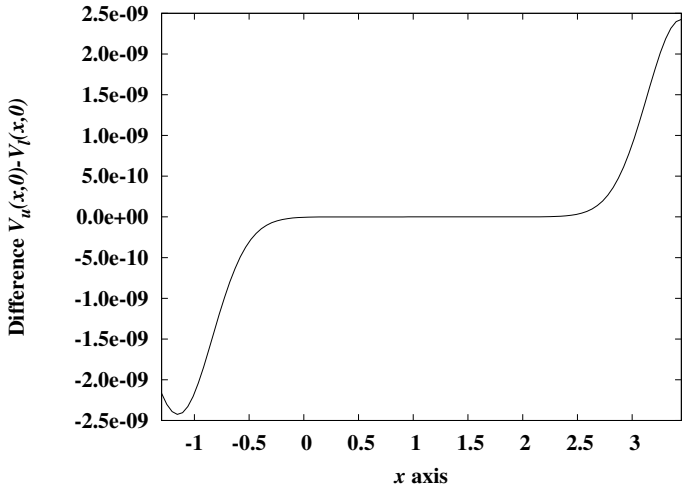

Figure 2.9: We take the difference $V_u(x,0) - V_l(x,0)$, if the potentials have the same value the difference should be exactly zero. We test the potential with parameters $r_o = 1$, $w = 0.3$ and $s_o = 0.05$.

parameter $s_o = 0.05$. We see that the difference is very small in the order of $3e^{-9}$. By summing up all the potentials across the whole plane, the problem should vanish, however, this is not possible computationally. Regarding the effect on the outcome of the simulations, preliminary tests showed that adding contributions from more points on the lattice does not change the quality of the results. Moreover, due to the numerous summations, it would be a cumbersome task to follow the trajectory at every single point with exact precision.

2.7.1 Mean Square Displacement and the diffusion coefficient

The diffusion coefficient is approximated by taking the slope from a linear fit to the MSD as a function of time. It is crucial that the MSD presents a linear growth with time, otherwise the diffusion coefficient can be erroneously calculated or it can also be the case that normal diffusion might not even exist for the given parameters. For more details on how the diffusion coefficient, D, is defined see Sect. 2.2.

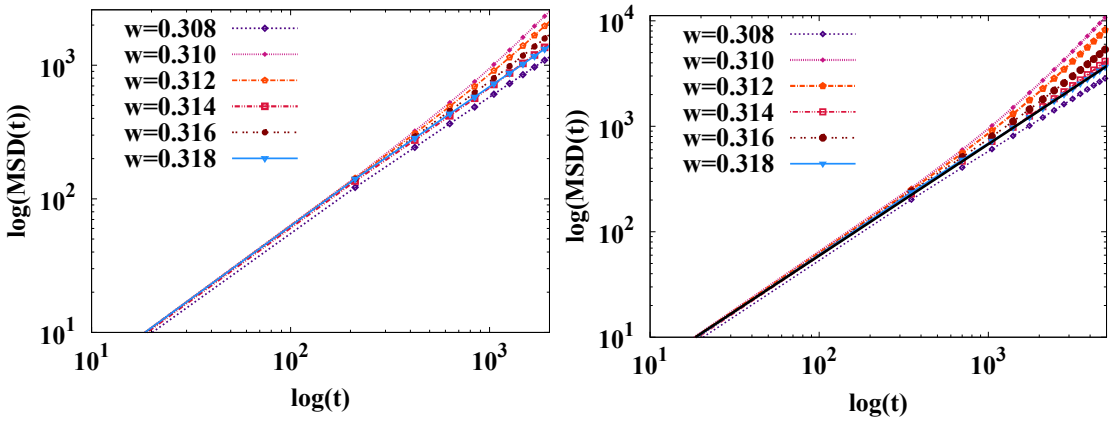

Figure 2.10: Left: Log-Log plot of the MSD(t) for different values of w ($t = 2000$). **Right**: Same as Fig. in Left for longer times ($t = 5000$). The black line indicates slope $m = 1$.

First we will compute the MSD with different values of w. For this test, the input parameters are: ensemble size 100000, energy 0.5, time step 1×10^{-3}, $r_o = 1$, $s_o = 0.05$ and iteration time $t = 2000$. The output is shown in the left panel of Fig. 2.10. In this graph we see that the MSD behaves "nicely" in the sense that it grows linearly in time for some values of w; for instance at $w = 0.308$. However, at the values $w = 0.310$ and $w = 0.312$ the MSD seems to grow faster than linearly with time. The MSD at $w = 0.314$, $w = 0.316$ and $w = 0.318$ looks to grows linearly in time. There are two possible explanations for the unexpected behaviour of the MSD at $w = 0.310$; either the linear regime has not been reached and the system is in a transient state or there is no normal diffusion for this combination of parameters. The diffusion coefficient should be calculated from a fit of the MSD once the linear regime has been reached in time. If we iterate for longer times ($t = 5000$), see the right panel of Fig. 2.10, the MSD at $w = 0.310$ keeps growing faster than linearly in time, the same for $w = 0.312$. It becomes clear that the MSD at $w = 0.308$ and 0.318 is linear with respect to time. There is an unsolved case at $w = 0.314$ where the MSD seems to grow slightly faster than linear.

In the next subsection we shall introduce a convergence analysis of the MSD, which will help to clarify this situation.

2.7.2 Testing the convergence of the MSD

A more reliable conclusion about the linearity of the MSD, can be made if we test its convergence to some specific value of the diffusion coefficient. One way to test this is by looking at the slope of the MSD over intervals of time. We use as input parameters the ones in Sect. 2.10 and vary the iteration time. Start by partitioning the total time in small intervals: the first interval is the whole interval from 1 to 5 000 then from 1000 to 5000 and so on, until the interval 4000 to 5000. Then, take the slope α in each interval so that we have $\alpha(t(1, 5000))$, $\alpha(t(1000, 5000)), ..., \alpha(t(4000, 5000))$. In order to get an estimation for the diffusion coefficient, we just simply divided by 4 (see Eq. 2.2). If the slope has been taken such that there is a linear regime, we should see that the $\alpha's$ converge to some value instead of fluctuating. The slope from the first interval, $(1, 1000)$, might carry an error due to the systems transient; taking the diffusion coefficient from this interval is therefore not ideal. As we move to intervals at longer times, we should get a more accurate value of D.

In Fig. 2.11 we plot $\alpha/4$ as a function of w for different intervals. From the figure, around $w = 0.310$, if we go for longer times and then take the slope α of the linear fit to the MSD as explained, we see a systematic increment on $\alpha/4$. strictly speaking, this is not the diffusion coefficient since the MSD in Eq. 2.2 has not reached a linear regime. The scenario at $w = 0.314$ is subtle, there is a small increment in $\alpha/4$ on each time interval and although the increment is not as notorious as the previous case this might be a transition to a regime between MSD$\sim t$ and MSD$\sim t^a$, with $a > 1$.

The lines in Fig. 2.11 could also overlap; which would indicate that the linear regime has been reached.

In the numerical experiments that we present in Chapter 3 for instance, the slope of the MSD was extracted in the time interval (4000,5000); there we generally see a systematic convergence towards a value for the diffusion coefficient. In these computations an ensemble of 100 000 particles was used. If a smaller ensemble is chosen we get qualitatively the same shape of $\alpha/4(w)$ but increasing the number of particles yields a faster convergence to the diffusion coefficient all the while

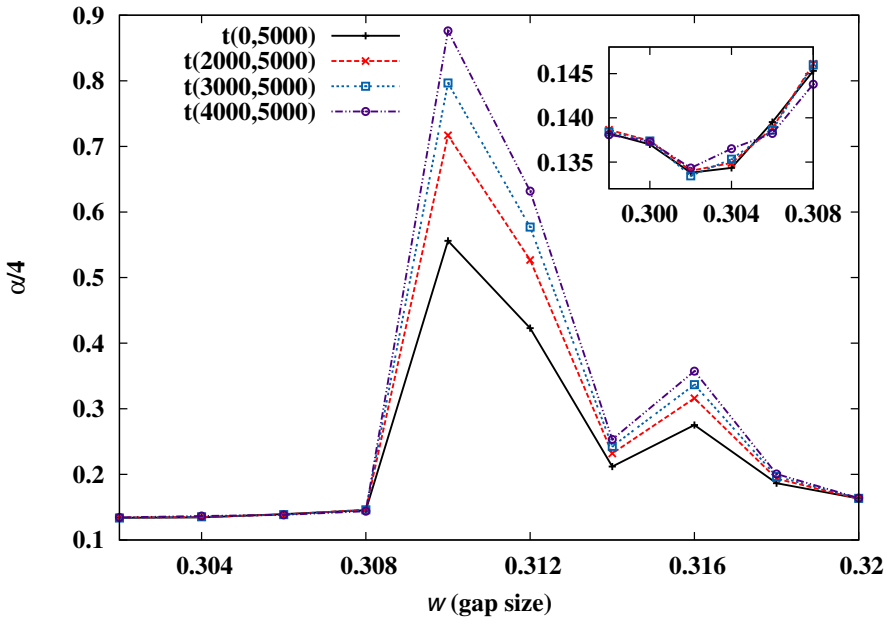

Figure 2.11: Convergence of $\alpha/4$ as a function of w: the slope α taken from linear fits of the MSD over different time intervals.

being more accurately. For the study of the diffusion coefficient as a function of the energy, in Chapter 4, the iteration time is of the same magnitude whereas for high energy it needs to be longer since the system takes longer to get randomized.

2.7.3 Construction of the Poincaré Surface of Section

For the particular case of a soft billiard that we address here, let us consider the rhomboid unit cell (see Fig. 2.7), and consider the motion of the particle when it crosses the boundary of the unit cell, *i.e.* we restrict to $y = 0$. The Poincaré surface of section (PSoS), Σ, that we will use is going to be given by the position of the particle at the moment of crossing the boundary of the unit cell (x-axis) and the sin of the angle between its velocity vector and the normal to the boundary of the unit cell ($\sin\theta$) (see Fig. 2.12). Since the phase space of the system is described by (x, y, v_x), the surface of section that we just constructed (as the plane with coordinates $(x, \sin\theta)$) captures completely the nature of orbits in phase space. Studying the motion of the particle in the unit cell is equivalent

to study the motion of the particle in a Torus, then periodic trajectories in the configuration space, of any period, should look like periodic orbits, with the same or higher period on Σ.

We will use this PSoS to study the phase space of the system described earlier in Chapter 3 and Chapter 4.

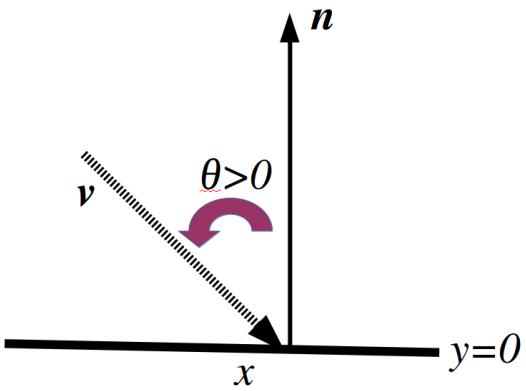

Figure 2.12: Construction of cross section in the soft billiard system: We take the position coordinate x and the sin of the angle θ between the velocity vector and the normal to the boundary of the rhomboid unit cell at the moment of crossing.

Chapter 3

Density dependent diffusion coefficient in a softened periodic Lorentz gas

In previous chapters we have discussed the importance of the Lorentz gas model as a paradigmatic tool for understanding the fundamental laws of thermodynamics. Its simplicity allows us to explore macroscopic transport properties of a given system in terms of the effects of interactions at a microscopic level. If the aim is to predict diffusion in the real world, a more realistic model is desirable. Since physical particle, *e.g.* molecules, interactions are more complicated than elastic collisions, a more realistic model is needed. The required characteristic can be acquired by replacing the hard walls of a billiard by a smooth potential. The study of these soft models for diffusion is already well established; several studies in this direction point to a change in the dynamics when softening the walls of the scatterers.

In this chapter we study the diffusion coefficient as a function of a spatial control parameter in Hamiltonian systems with smooth potential. The softness of the billiard is achieved by replacing the hard scatterers by a Fermi potentials as described in Section 2.7. Due to the form of the potential in the model that we study here, one has to make assumptions to simplify the problem and to be able

to come up with an analytical approximation for the diffusion coefficient.

3.1 Introduction and Motivation

Theoretical studies on the dynamics of Hamiltonian billiards mainly by Turaev and Rom-Kedar [TRK98, RKT99] showed that when perturbing billiards that contain a special class of periodic trajectories, island of stability appear and ergodicity breaks up. They proved that the presence of tangent periodic trajectories and homoclinic orbits in the original billiard (Fig. 1.1 illustrates this scenario) creates islands of stability in the phase space of the perturbed system. Another important contribution in the field of Hamiltonian billiards is by Liverani and Donnay's [DL91] on attractive and repelling potentials. They proved that under certain conditions, Hamiltonian systems where a particle interacts with a compound potential have a positive Lyapunov exponent and are ergodic.

All of these features are linked to transport properties, e.g. transport by diffusion, via the decay of correlations, that is why one is interested in such mathematical concepts.

Knauf [Kna87] proved that the motion of a particle in a periodic Coulombic potential is a diffusive process. Unfortunately, the theory by Knauf can not be applied directly to the repulsive system that we construct as the softened version of the Lorentz gas. However we could explore how much we can extrapolate the diffusive properties of the chaotic Lorentz gas model to a more realistic system of particles. Our task in this chapter is to elaborate on the question: How do the diffusive properties of a system from the Hard wall limit case change to the soft wall potential case? We shall perturb the periodic Lorentz gas by softening the walls and investigate its effect on transport properties. Specifically, we consider the diffusion coefficient as a function of control parameters: the smoothness of the potential and the separation of the vertices of the lattice. The latter serves as a direct comparison with the Lorentz gas if the symmetry of the configuration of the scatterers is conserved.

Several studies have considered a smooth potential focusing on the energy as a

control parameter. We will study this aspect in the next chapter. Here, we focus on the diffusion coefficient as a function of the separation of the scatterers and the smoothness of the potential by keeping the energy constant.

The chapter is organized as follows: In Section 3.2 we present numerical results for the diffusion coefficient as a function of separation of scatters, $D(w)$. In Section 3.3 we elaborate on semi-analytical random walk approximations to the diffusion coefficient as a function of a control parameter and compare them against numerical results. The first idea is to extend Machta and Zwanzig's [MZ83] random walk model (explained in Sect. 2.5.3) in the Lorentz gas to the soft system. We construct a second approximation based on a collision-less flight argument and a third one that includes memory effects in the jumping process. In Section 3.4 we briefly study the diffusion coefficient as a function of the smoothness of the potential. In Section 3.5 we explain the behaviour of $D(w)$ as a consequence of stability islands in special regions of the phase space. To understand the behaviour of the diffusion on a fine parameter scale we analyse the Poincaré surface of sections and its evolution as the density parameter is varied, in addition to analysing the probabilities of jumping to different parts of the configuration space. Finally, in Section 3.6 we summarise the results and conclude.

3.2 Numerical results for diffusion as a function of the separation of the scatterers

Recall that the model we use here consists of Fermi potentials in a triangular lattice. The general settings of the model were described in Section 2.7. We will use these settings, and vary the separation of the scatterers w only. The physical parameters that we keep fixed are: the softness of the potential $s_o = 0.05$ and the radius of the potential $r_o = 1$ in Eq. (2.19). Taking w as a control parameter in this setting we have that the onset for diffusion is $w_* = 0.109$ (see Eq. (2.23)).

We will approximate the Diffusion coefficient, D, from simulations by comput-

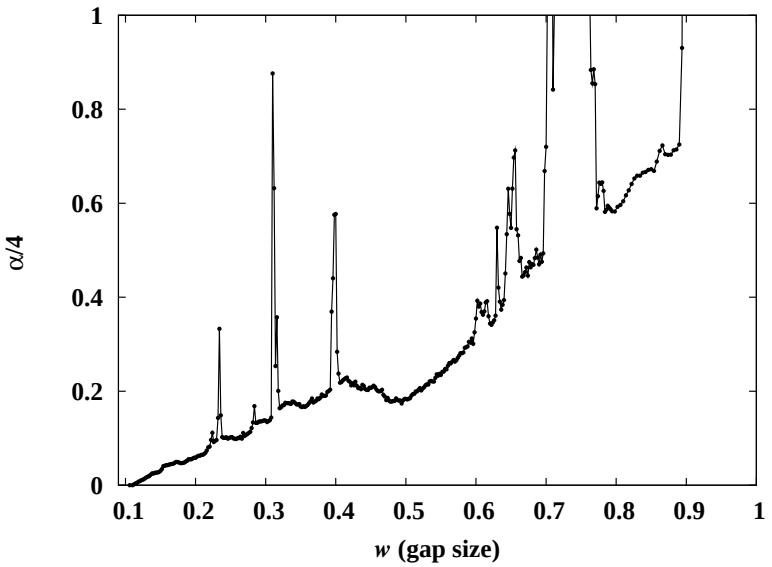

Figure 3.1: Numerical results $\alpha(w)/4$, where α is the slope of the linear fit taken from time interval (4000-5000). Input parameters: softness of the potential $s_o = 0.05$, radius of the potential $r_o = 1$, and energy of the particle $E = 0.5$.

ing the MSD over an ensemble of particles. Our selection of numerical parameters are the ensemble size of particles, which consists of 100 000 non-interacting particles, and the iteration time $t = 5000$.

We take the slope, α, of a linear fit of the MSD in the time interval $(4000-5000)$ and plot $\alpha/4$. We can take as a first approximation $D = \alpha/4$. Next in Sect 3.3 we take only those values where some convergence has been reached, as illustrated in Fig. 2.11 (for details see Subsection 2.7.1 and 2.7.2). The numerical results for the diffusion coefficient are shown in Fig. 3.1. We see that $D(w)$ is an irregular function of w, with zones of normal diffusion and in small regions, peaks, where the linear regime in the MSD was not reached, leaving an open question about the dynamics at these parameters; this occurs even for small w, where we expect normal diffusion in the hard Lorentz gas. In general the diffusion coefficient tends to grow as w increases but it presents some interesting features. Compare this graph to the curve that one gets when studying the Lorentz gas as a function of the separation of the scatters (see Fig. 2.6): In the soft system we notice that there is normal diffusion even for higher values after the critical w_∞ in the hard

Lorentz gas. We can distinguish two regions in the graph $D(w)$ separated by a local minimum around $w = 0.5$.

We show results up to $w = 1$, close to what appears to be a situation similar to the infinite horizon regime in the hard Lorentz gas (see Fig. 2.4). In Appendix A.4 we will discuss the system's dynamics of special trajectories that appear in this regime.

We found in the literature, systems that present a similar behaviour in terms of irregularities of the diffusion coefficient. For instance, for 1-d chaotic maps, it has been found that there is a fractal-like dependence on the diffusion coefficient as a function of the slope [KD95]. Moreover, Klages and Dellago (2000) [KD00] had conjectured that, on a small scale, the diffusion coefficient is a non-trivial function of the control parameter: the separation of scatterers in the hard Lorentz gas. A related example is the non-linear climbing sine map which exhibits normal and anomalous diffusion on a self similar structure on a fine scale (Korabel and Klages 2002, 2004 [KK02b, KK04]). This phenomenon is also observed in a system with a corrugated floor (Harayma and Gaspard 2001 [HG01]), except that there the parameter under consideration is the energy.

3.3 Semi-analytical approximations

In this section we try to approximate the coarse shape of $D(w)$ in the high and low density regimes by various methods. For the high density regime, we adapt the Machta and Zwanzig formalism of a random walk based on a phase space argument to approximate D. In this regime we also elaborate on an approximation based on a collision-less flight argument. In the low density regime we adapt a third approach that includes memory effects in the approximation. In the following, when comparing numerical results with the approximations we will discard the values of w with 'peaks' in $\alpha/4$, *i.e.* those points with no clear convergence in $\alpha/4$, as this behaviour means that the diffusion coefficient might no exist. The criteria for convergence is illustrated in Fig. 2.11.

Before proceeding to the approximations, we work out estimations for the ve-

locity of the particle at the moment of its exit from a trap[1].

1. One way to do this is to assume that the particle has a maximum constant velocity at the moment of exiting the trap. That is, the velocity vector at $y = 0$ along the x-axis between two scatterers, see Fig. 2.8.

   Recall that a potential Fermi pole is given by Eq. (2.19) at each point of the lattice. Consider the base of a triangle in the array as the x-axis and let us take into account the contributions of two close adjacent potentials, V_1 and V_2, as shown on the left of Fig. 2.8. If we consider the contribution of the potential from two adjacent points in the plane, namely at the points $(0, 0)$ and $(L, 0)$, the joint potential reads

   $$V_1(\mathbf{r}) + V_2(\mathbf{r}) = \frac{1}{1 + \exp((|\mathbf{r}| - r_o)/s_o)} + \frac{1}{1 + \exp((|\mathbf{r} - \mathbf{r_L}| - r_o)/s_o)}, \quad (3.1)$$

   where $\mathbf{r_L} = (L, 0)$. For simplicity we continue our analysis only considering the contribution of the potential in the x-axis and denote it as

   $$V_1(x) + V_2(x) = \frac{1}{1 + \exp((|x| - r_o)/s_o)} + \frac{1}{1 + \exp(|x - L| - r_o)/s_o)}. \quad (3.2)$$

   This expression is equivalent to Eq. (3.1). If we look at Fig. 2.8, due to symmetry the minimum of the potential along the x-axis when $y = 0$ occurs in the middle of the gap $x_{\min} = r_o + (w/2)$ and we have that:

   $$V_1(x_{\min}) + V_2(x_{\min}) = V\left(\frac{2r_o + w}{2}\right) = \frac{2}{1 + \exp\left(\frac{w}{2s_o}\right)}. \quad (3.3)$$

   Conservation of energy yields

   $$v = \sqrt{2(E - V(x))}, \quad (3.4)$$

   where $v = |\mathbf{v}|$. We can combine it with Eq. (3.3), $V_{\min}(x) = V_1(x_{\min}) + V_2(x_{\min})$, so that we can express the maximum velocity at the moment of

[1] The concept of a trap in the soft version of the Lorentz gas is explained in section 2.7.

the exit of the trap just in terms of w and s_o as:

$$v_{\max}(w) = \sqrt{2\left(E - \frac{2}{1+\exp(w/2s_o)}\right)}. \tag{3.5}$$

2. Another way to obtain an explicit form for the velocity is to assume an average potential, V_{ave}, over the exit of the trap. Then we need to calculate:

$$V_{\text{ave}}(x, w) = \frac{1}{w}\int_{r_o}^{r_o+w} V(x)dx.$$

This integral can be calculated analytically, and we get a function that depends on w only as:

$$V_{\text{ave}}(w) = 2\left(1 + \frac{s_o}{w}\ln\left(\frac{2}{1+\exp(w/s_o)}\right)\right). \tag{3.6}$$

This way, the velocity can be expressed as

$$v_{\text{ave}}(w) = \sqrt{2(E - V_{\text{ave}}(w))} \tag{3.7}$$

3. A third definition is to calculate the *true* average velocity. Here we would have to compute the following integral:

$$v_{\text{num}} = \frac{2}{w'}\int_{r_o+\epsilon}^{r_o+w/2} \sqrt{2(E - V(x))}dx. \tag{3.8}$$

with $V(x)$ as in Eq. (3.1) and the average being over the gap size w' defined in Eq. (2.22). This velocity is a function of the exact size of the gap w', the separation of the scatterers w, and the position of the particle r. The integral is not solvable analytically but we can make an approximation numerically. We choose points in the domain of w and compute the integral to get a function with discrete points (w, v_{num}). One can fit this data and get a velocity function, v_{num}, that depends on the variables w' and w.

3.3.1 Diffusion based on random walk in a high density regime

In order to approximate the diffusion coefficient D in the soft system, we can try to use the same phase space argument by Machta and Zwanzig for the Lorentz gas [MZ83]. We make the same assumption of a particle following a random walk from trap to trap, and use the expression for diffusion $D = l^2/4\tau$, where l is the distance between centres of traps and is given in terms of w just as in the hard Lorentz gas and τ is the escape time from the trap. We need to express τ in terms of w, however, given that in this case the potential is different from zero, the velocity of the particle is not constant. The flux of particles that leaves the trap, which depends on the velocity at the moment of the exit, can not be solved analytically as in Eq. (2.12), so we can not apply the same argument directly.

For fixed w, the distance between the scatters remains constant and the expression for so D as a function of w and v is

$$D_{\mathrm{MZ}} = \frac{l^2(w)}{4\tau(w', v)}. \tag{3.9}$$

Let us suppose that the velocity of the particle is constant at the moment of exiting the trap. Then Eq. (2.12) yields

$$\int |\mathbf{n}||\mathbf{v}| \cos\theta v d\theta = 2v^2,$$

where $|\mathbf{v}| = v$ needs to be determined. Note that if $|\mathbf{v}| = 1$ we recover the result obtained for the hard potential case. Then by the Machta and Zwanzig phase space argument, τ will depend on the velocity v as follows

$$\tau^{-1}(w', v) = \frac{3w' \times 2v^2}{2\pi v \times A_{\mathrm{trap}}} \tag{3.10}$$

where A_{trap} is the area of the trap which can be assumed to be equal to the area $A(w)$ in the original Lorentz gas as in Eq. (2.11). Strictly speaking $A_{\mathrm{trap}} < A_{\mathrm{LG}}(w)$, $A_{\mathrm{LG}}(w)$ is given in Eq (2.11). This difference is enhanced for small w or

large s_o because of the overlapping of the potential.

Substituting Eqs. (2.14), (2.11) and (3.10) in Eq. (3.9) we get:

$$D_{\mathrm{MZ}}(v, w', w) = \frac{(2+w)^2}{4A_{\mathrm{LG}}(w)\pi} \times w' v(w'). \tag{3.11}$$

Now, we use the three approximations for the velocity defined previously. By substituting $v_{\max}(w)$ in Eq. (3.11), we get an estimation of the diffusion coefficient as:

$$D_{\mathrm{MZ}}(v_{\max}, w', w) = \frac{(2+w)^2}{4A_{\mathrm{LG}}(w)\pi} \times w' v_{\max}(w). \tag{3.12}$$

Next, substituting Eq. (3.7) into Eq. (3.11) we get an approximation for diffusion that depends only on w and w':

$$D_{\mathrm{MZ}}(v_{\mathrm{ave}}, w, w') = \frac{(2+w)^2}{4A(w)\pi} \times w' v_{\mathrm{ave}}(w). \tag{3.13}$$

For the third approximation, we take the numerically calculated velocity in Eq. (3.8),

$$D_{\mathrm{MZ}}(v_{\mathrm{num}}, w, w') = \frac{(2+w)^2}{4A(w)\pi} \times w' v_{\mathrm{num}}(w, w'). \tag{3.14}$$

In Fig. 3.2, we plot these three approximations, Eqs. (3.12), (3.13) and (3.14). The approximation based on a maximum velocity, $D_{\mathrm{MZ}}(v_{\max})$, matches the threshold because of how the velocity was formulated.

The $v_{\max}$, Eq. (3.5), is a function of E and w, it was constructed with Eq. (3.3) where we used the minimum of the potential. Therefore, we should get that $v \to 0$ as the gap closes $w \to w_*$.

Unsurprisingly, assuming a maximum velocity for the particles when they cross the exit yields overestimates diffusion in almost whole range up to $w \approx 0.4$. On the other hand, $D_{\mathrm{MZ}}(v_{\mathrm{ave}})$, assuming an average potential, misses the threshold but is qualitatively a better approximation than $D_{\mathrm{MZ}}(v_{\max})$ in the high density regime. The third approximation, $D_{\mathrm{MZ}}(v_{\mathrm{num}}, w, w')$, preserves the threshold and captures the essence of $D_{\mathrm{MZ}}(v_{\mathrm{ave}})$ for higher w. For larger w, $D_{\mathrm{MZ}}(v_{\max})$ coincides with the

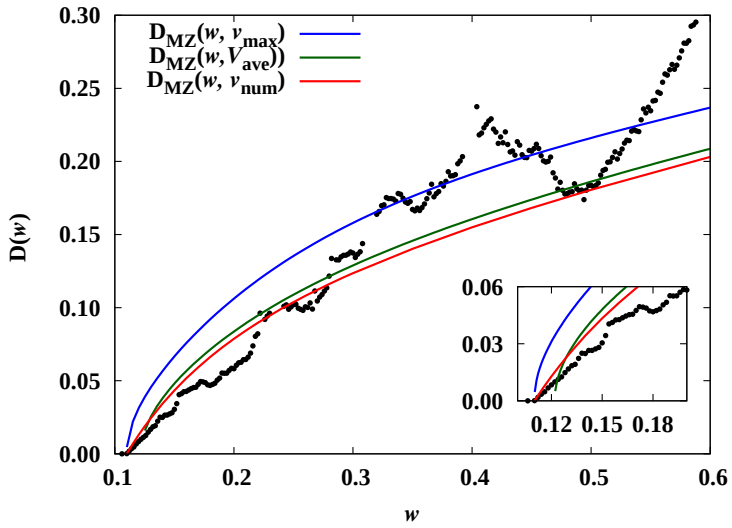

Figure 3.2: Approximations $D_{\mathrm{MZ}}(v, w', w)$ based on random walk between traps. Blue: assuming maximum velocity Eq. (3.12); green: assuming velocity from an average potential Eq. (3.13); red: assuming numerical average velocity Eq. (3.14). Black dots: Numerical simulations as in Fig. 3.1 minus those points where the diffusion coefficient does not exist according to the convergence criteria (Sect. 2.7.2).

local minimum around $w = 0.5$. One may wonder whether this coincidence or is there a trapping mechanism behind.

3.3.2 Diffusion based on a collision-less flight argument

Another way to approximate diffusion is by considering a collision-free time, that is, the time the particle travels without collisions. This approach is motivated by [KD00].

In a soft system, collisions do not occur; instead, the particle always interacts with the potential and changes its trajectory. We proceed to this analysis bearing in mind that in the limit when the smoothness parameter, s_o, approaches zero we recover the hard system where collisions actually take place.

The expression for diffusion in Eq. (2.10), expressed in terms of collisions, reads

$$D_{\mathrm{B}} = \frac{l_c^2}{4\tau_c}, \tag{3.15}$$

where l_c stands for the collision length or the mean free path and τ_c for mean free time between collisions. In the hard Lorentz gas, τ_c can be calculated using an analogous phase space argument [MZ83] where the flux of particles to consider is to the walls or hard disks in the trap. If we consider a collision-less flight argument we should get τ_c

$$\tau_c^{-1} = \frac{3L \times 2v^2}{2\pi v \times A_{\text{trap}}}, \tag{3.16}$$

where L is the length of the walls in the trap where the particle can "collide" before escaping and is taken to be a sixth of the circumference of a disk with radius r_o, v being some average velocity and A_{trap} the area available in the phase space.

If we assume that particles travel with the same constant velocity as used in Eq. (3.16) we can say that:

$$v = l_c/\tau_c \text{ or } l_c = \tau_c v,$$

and substitute these two last equations into Eq. (3.15) to get the relation:

$$D_{\text{B}}(v, w', w) = \frac{A_{\text{LG}}(w)}{4} \times v(w') = \frac{\sqrt{3}/4(2+w)^2 - \pi/2}{4} \times v(w'). \tag{3.17}$$

For the velocity, we consider the average velocities obtained previously: a maximum velocity v_{max}, a velocity given by an average potential v_{ave} in the gap and the average velocity obtained numerically v_{num} and substitute these into $D_{\text{B}}(v, w', w)$.

These approximations $D_{\text{B}}(v_{\text{max}})$, $D_{\text{B}}(v_{\text{ave}})$ and $D_{\text{B}}(v_{\text{num}})$ are shown in Fig 3.3. In the inset of the figure, we can see that the approximation $D_{\text{B}}(w, v_{\text{ave}})$ with an average potential misses the threshold, whereas $D_{\text{B}}(w, v_{\text{num}})$ has the correct form as it approaches the threshold.

On the positive side, both approximations $D_{\text{B}}(w)$ reproduce qualitatively the shape of $D(w)$ up to $w \approx 0.4$; nevertheless, they missed the second regime where the approximations deviate from the numerical results.

After removing the peaks, we observe that there are irregularities on $D(w)$. This irregularity resembles the results found in other systems when studying dif-

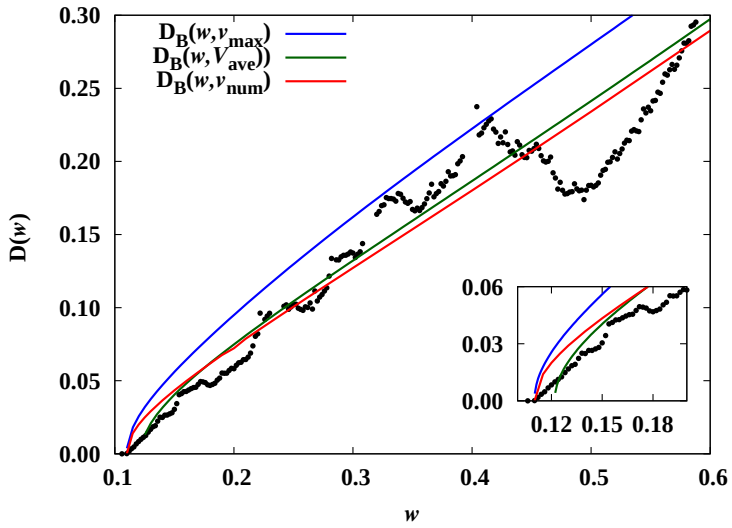

Figure 3.3: Approximations $D_{\mathrm{B}}(v, w', w)$, Eq. (3.17), based on collision-less flights. Blue: assuming maximum velocity, green: assuming velocity from an average potential then red: assuming numerical average velocity. Black dots: Numerical simulations as in Fig. 3.2.

fusion as a function of a control parameter namely Harayama, Klages and Gaspard [HKG02], Harayama and Gaspard [HG01], Gaspard and Klages [GK98], and Klages and Dellago [KD00].

If we ignore the irregularities and focus on the general shape of $D(w)$, can we differentiate the random walk and collision-less flight regimes? Fig. 3.4 shows a direct comparison between the two approximations D_{MZ} and D_{B}, Eqs. (3.11) and (3.17), with the numerically computed average velocity $v(v_{\mathrm{num}})$ *i.e.* Eq. (3.8). In the high density regime, D_{MZ} is asymptotically correct for $w \to w_*$. Whereas D_{B} has the wrong asymptotic form; this can be understood in the light of the fact that the collision-less time τ_c is defined even for $w < w_*$ or *i.e.* when the exits of the trap are closed. But due to the construction of the velocity v_{num}, $D_{\mathrm{B}}(v_{\mathrm{num}})$ will go to zero as $w \to w_*$ despite the wrong asymptotic.

By looking at the graph we can say that D_B is in general a better approximation because after $w \approx 0.3$ the approximation keeps consistently matching the numerical data on a coarse scale. On the other hand, D_{MZ} matches the data at $w = 0.5$; this either means that the system gets randomized again or there is

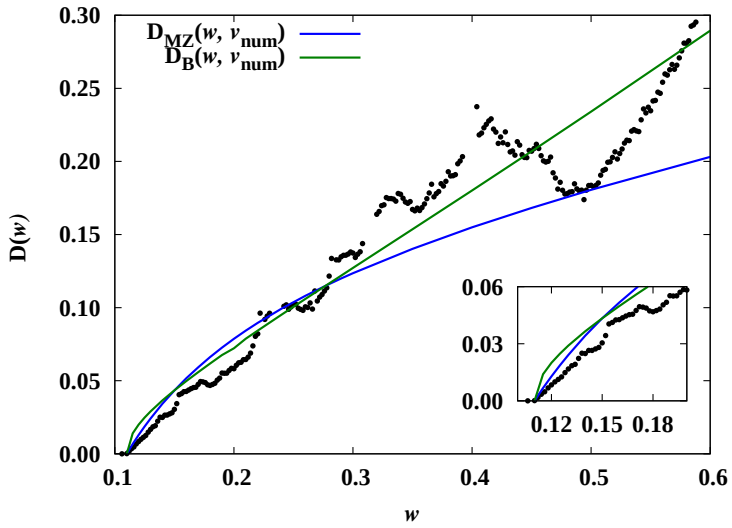

Figure 3.4: Direct comparison between different approximations: $D_{\mathrm{MZ}}(v_{\mathrm{num}}, w, w')$ (Eq. (3.14)) and $D_{\mathrm{B}}(v_{\mathrm{num}}, w', w)$ (Eq. (3.17)). Black dots: Numerical simulations as in Fig. 3.2.

some mechanism that inhibits diffusion, *e. g.* localized motion of particles. This motivates the application of the method in the next subsection where higher order correlations are taken into account to approximate the diffusion coefficient. And later in Section 3.5 we explore the phase space looking for special trajectories.

In the high density regime one expects more close interactions within the trap before escaping producing loss of memory, which is what happens in the Lorentz gas via collisions (see Klages and Dellago [KD00]).

Now, let us look again at the big picture in Fig. 3.1. There is an interval where the approximation D_{MZ} matches the data, around $w \approx 0.5$. Here, $D(w)$ has a local minima, the matching could be a consequence of a randomization of the system or a trapping mechanism. There is a second regime (large w) where diffusion grows faster, here maybe governed by the distance between scatterers, where close interactions are not important. Something worth mentioning here is that the potential suffers a transition around $w = 0.5$. As the gap opens, the flux of particles leaving the trap depends on w and the velocities given by the potential. After a critical point, the opening in the gap yields no major change in the minimal of the potential. At $w = 0.5$ the scatterers are separated such that the

minimum of the potential in the middle of the gap does not change dramatically as a function of w, *i.e.* the derivative of the function $V_{\min}(w)$ is almost a constant.

3.3.3 Low density regime, an analysis in terms of probabilities

Now, we will consider dynamical correlations in the jumps between traps, or memory effects, following the formalism by Klages and Korabel (2002) [KK02a]; the idea there was to include higher order correlations to better approximate the diffusion coefficient. They applied the theory to a unit interval map and to the Lorentz gas. Their results showed that including dynamical correlations enhances the quality of the basic Machta and Zwanzig approximation. The same method was also applied in a flower shape billiard by Harayama, Klages, Gaspard (2002) [HKG02] where the conclusion was that incorporating memory effects to the simple random walk yields a more accurate approximation of the diffusion coefficient. Gilbert and Sanders (2009) [GS09] developed a slightly modified approach in the Lorentz gas also using the basic idea of including correlations; this was done using persistent random walks which means that the state at a time k, depends on the state at time $k-1$.

We will adapt Klages and Korabel's method to approximate the Diffusion coefficient in the soft system. For that we need to know the probability that a particle exits a trap from the same gap where it entered, we call this backscattering.

We can calculate numerically the probability of backscattering, p_{bs} or $p(z)$, in the soft system by shooting particles uniformly distributed at the entrance of the trap and tracking their evolution in time. If the particle escapes from the same gap it entered we use the symbol z, if the particle leaves the trap through the right exit we assign the symbol r and if it leaves through the left exit we assign the symbol l. We denote by $p(z)$ the probability of escaping through the same entrance, $p(r)$ the probability of exiting through the right and $p(l)$ the probability of exiting through the left, see Fig. 3.5. Calculating probabilities in the regime of very small w is numerically complicated since particles stay for very long times in

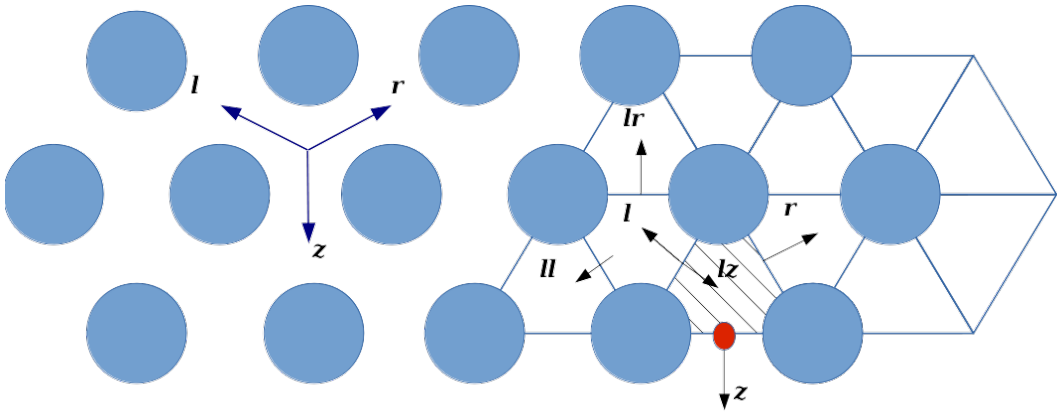

Figure 3.5: When entering the trap indicated by a dashed area, the particle has 3 options: it can leave the trap through the left exit, the right exit, or it can leave the trap from the same entrance. We assign a letter to each exit and describe the path of the particle in terms of sequence of symbols. The sequence lr, means that the particle enter a trap then it went to the left exit and then it took the right exit. In the left we have indicated the lattice vectors $\mathbf{l}_z$, $\mathbf{l}_r$, and $\mathbf{l}_l$. Note that the lattice vectors form an hexagonal lattice.

the trap making it hard to get a reliable statistic. We present results that were obtained with enough samples of trajectories to get convergence when calculating the probabilities.

Starting with the Einstein relation (2.2), Klages and Korabel derived a Green-Kubo formula for an ensemble of particles:

$$D(w) = \frac{1}{2\tau} \sum c_k \langle \mathbf{j}(\mathbf{x}_0) \cdot \mathbf{j}(\mathbf{x}_k) \rangle.$$

The coefficient c_k is defined as follows: if $k = 1$ $c_k = 0$ and $c_k = 1/2$ if $k = 1, 2, ..,$ the term $\mathbf{j}(\mathbf{x}_k)$ defines velocity-jumps at the k-time step, in terms of the lattice vectors $\mathbf{l}$ (illustrated on the left of Fig. 3.5), and τ is the average residence or escape time from the trap.

Under this scheme, the description of the position of the particles is on a hexagonal lattice. One way to interpret this expression is that in the long time limit what is relevant for D is the unit cell in which the particle is and not really its exact position in it. In this approach, one is interested in the direction in which a

particle travels when it leaves the trap; this means that we need to consider if the particle goes through the left exit, the exit on the right or if it goes back from the same gap where it first came.

Then the previous expression can be written in terms of the lattice vectors and the probabilities of particles following specific paths: escaping through the back, right, or left exit as:

$$D_n(w) = \frac{l^2}{4\tau} + \frac{1}{2\tau}\sum_{\alpha\beta\ldots} p(\alpha\beta\ldots)\mathbf{l}\cdot\mathbf{l}(\alpha\beta\ldots), \tag{3.18}$$

where $\alpha\beta\ldots$ is the symbol sequence representing the path of the particle in terms of the exits it went through. This is the nth-order approximation to the Green-Kubo formula [KK02a].

The 0-order approximation is the first term, D_0, and turns out to be the case of the random walk approximation (jump to the next trap) $D_0 = D_{\mathrm{MZ}}(w)$. Recall that for our case of study $D_0 = D_{\mathrm{MZ}}(w', v)$, where v is an average velocity (discussed in previous sections).

The first order approximation, D_1, takes into account the probability of performing backscattering, $p(z)$, and takes the form

$$D_1(w, p(z)) = D_0(w) + D_0(w)(1 - 3p(z)). \tag{3.19}$$

Note that if the system is purely random then $p(z) = p(r) = p(l) = 1/3$ and Eq. (3.19) becomes D_0, where the assumption was random walk between traps, *i.e.*, no preferences or equal probabilities.

The second order approximation, D_2, takes into account two jumping events, meaning the probability of double backscattering, $p(zz)$, $p(lr)$, etc., and is given by

$$D_2(w, p(zz)) = D_1(w) + Do(w)(2p(zz) + 4p(lr) - 2p(ll) - 4p(lz)). \tag{3.20}$$

In Fig. 3.6, the approximations in Eq. (3.19) and Eq. (3.20), as well as the very

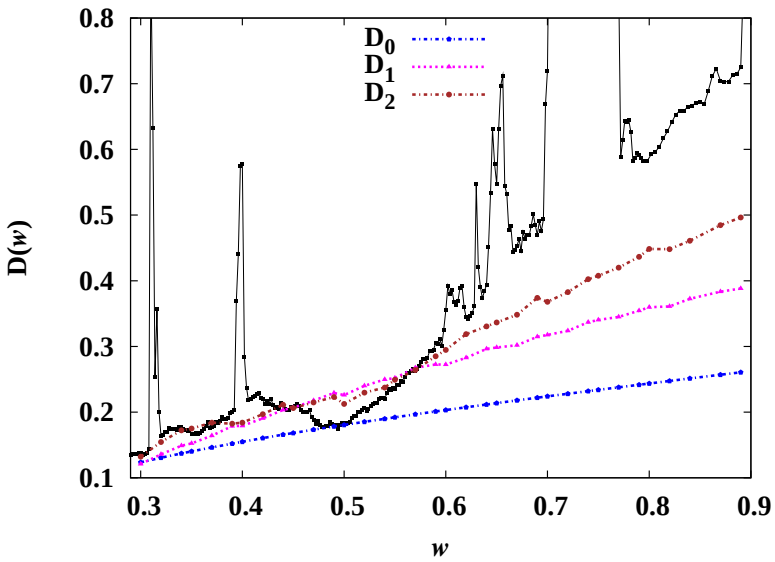

Figure 3.6: Diffusion coefficient as a function of the separation of scatterers: focus on low density (large w). Approximations $D_0(w)$, $D_1(w)$, and $D_2(w)$ from Eq. (3.18). Black dots: Numerical simulations as in Fig. 3.1.

first approximation D_0, are plotted for a larger range of w than before. In the three approximations: D_0, D_1 and D_2 we use data from numerical average velocities.

As observed before, the first approximation, D_0 should be the same as D_{MZ}, it matches the numerical data only for small w. From this comparison, we can see that taking into account higher order probabilities the functional form of the approximation converges towards the exact numerical results. This also indicates that the system is not random and the particles have a preference for special paths in configuration space. We elaborate further about this observation in Section 3.5.

For large w, the particles can escape through the gaps with higher kinetic energy than for small w, therefore long flights are more likely to occur. Thus, higher symbol probabilities are required to follow the path of the particle. Our numerical approximations of the probabilities stopped at 2-symbol probabilities, that is why the approximation D_2 is not enough to capture the dynamics of the particles at large w (Fig. 3.6).

In order to obtain accurate higher-order memory approximations, we need re-

liable symbol probabilities. If one wants accurate probabilities at higher order memory approximations, we need a larger number of test particles as the number of symbol sequences to consider increases. We have that the convergence to the numerical result is faster at small w ($w \approx 0.3$) than at large w if the number of test particles is kept fixed.

Calculating the next approximation is desirable, but computing 3-symbol probabilities gets computationally expensive: the computation is time-consuming and it is hard to obtain reliable probabilities. Instead, in Section 3.5.3 we will explore the relation between some 3 and 4-symbol probabilities with specific trajectories.

3.4 Smoothness parameter

In the previous section, we found an irregular shape of the diffusion coefficient as a function of the separation of the scatterers. Now, we want to explore briefly the behaviour of the diffusion coefficient as a function of the smoothness parameter. For the energy of the particle we will use the same energy $E = 0.5$ and the same iteration time 5000 as in the previous model. Since we are interested in the broad shape of $D(s_o)$ we will keep the the ensemble size to $n = 10000$, which also gives reliable estimations of the diffusion coefficient, according to the convergence of the MSD, and it is faster to compute. Now that we consider the smoothness parameter, s_o, let the rest of parameters be fixed and vary s_o.

Numerical results for two different fixed w are shown in Fig. 3.7. We have chosen $w = 0.235$ and $w = 0.31$. Both graphs of $D(s_o)$ show an irregular structure as observed in $D(w)$ (see Fig. 3.1).

We can try to apply the approximation based on the random walk between traps and the phase space argument to $D(s_o)$. The expression for the approximation of $D_{\mathrm{MZ}}(s_o)$ with fixed w turns out to be as in Eq. (3.9) with the assumption of a constant velocity:

$$D_{\mathrm{MZ}}(s_o, v) = \frac{l^2(w)}{4\tau(s_o, v)}, \tag{3.21}$$

where w is fixed. Although the approximations for the diffusion coefficient were

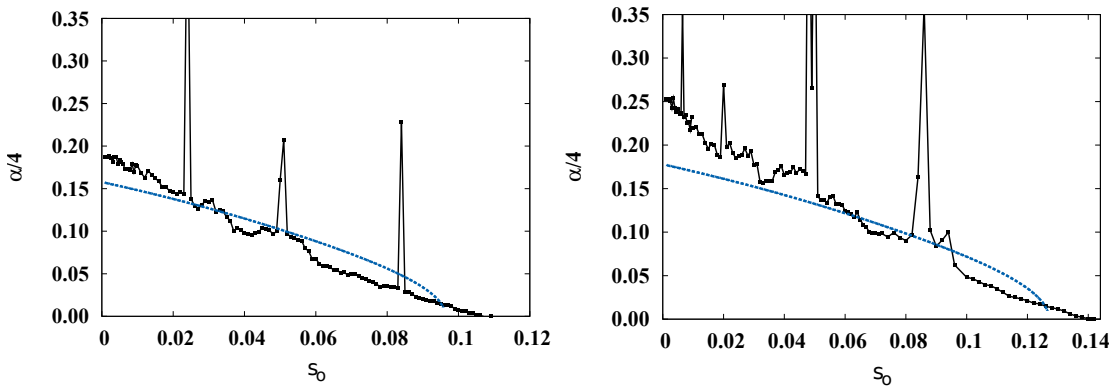

Figure 3.7: Black dotted line: Numerical results $\alpha/4$, where α is the slope of the MSD, as a function of the smoothness parameter s_o, see text for information about the input parameters. Blue dashed line: Random walk approximation $D_{\mathrm{MZ}}(s_o, v_{\mathrm{ave}})$ Eq. (3.21). **Left:** $D(s_o, w = 0.235)$. **Right:** $D(s_o, w = 0.310)$.

deduced varying w as a control parameter (Eq. (3.11) and Eq. (3.17)), it is straightforward to apply them to $D(s_o)$. Just as in the previous sections, we can choose a constant average velocity. In Fig. 3.7, we compare the numerical simulations with two different values of w and its respective approximations based on the random walk $D_{\mathrm{MZ}}(s_o, v_{\mathrm{ave}})$.

Since we chose an average velocity, the threshold does not match. As we can see, $D(s_o, w = 0.235)$ reproduces qualitatively the shape of $D(s_o)$ in the domain. On the other hand, $D(s_o, w = 0.31)$ fails to follow the shape of $D(s_o)$ for small s_o and for high s_o it matches the data qualitatively. For high values of w, we do not expect a good match since we already know that D_{MZ} fails for the regime $w > 0.1$ since the random walk approximation is known to perform better if there is loss of memory which is more likely to happen in small w, or high density.

We present two examples of $D(s_o)$ with fixed w and we found similar peaks to those we also found in $D(w)$. Are the peaks in $D(s_o)$ for the two different parameters of w related? Are they universal? Should these irregularities be consistent when varying the parameter s_o?

In Fig. 3.8 we present numerical results of $D(w)$ for different smoothness parameters, including the results of Sect. 3.2. In the figure, we can follow the general form of $D(w)$ when varying s_o and we can see the appearance of the peaks is

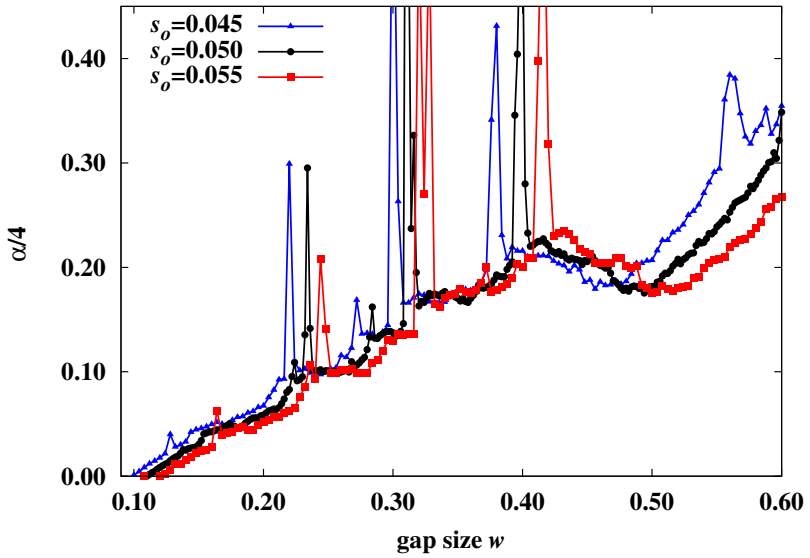

Figure 3.8: Numerical results of $\alpha(w)/4$ with different smoothness parameters $s_o = 0.055, 0.050, 0.045$. In this simulations we used: Number of particles 100000 and iteration time 5000.

consistent and somehow ordered with respect to the variation of s_o.

In the next section, we will explore the phase space of the system and will study how the softness of the potential, s_o, and the separation of the scatterers w determine the behaviour of the diffusion coefficient.

3.5 Stability islands and bifurcations in phase space

In this section we explore the dynamics of the system by looking at its phase space via Poincaré surface of Sections (PSoS). As explained in Chap. 2 this description of the system comes very helpful for the understanding of the structure of the phase space, therefore for the understanding of the dynamics.

We described the PSoS in Section 2.7.3. To understand the irregular structure of $D(w)$ we explore the Poincaré surface of section and its evolution in regions of

the parameter w for which convergence of $\alpha/4$ was not reached (peaks in Fig. 3.1), as well as for the local minimum at $w = 0.455$. Then, in the next subsections, we consider symbol sequence probabilities on association with specific trajectories in configuration space. This section ends with a global picture of the diffusion coefficient based on objects that appear in the phase space.

Now we proceed to explore the evolution in phase space of orbits in an interval of w with irregularities in $D(w)$, which correspond to special trajectories in configuration space. We will discuss the scenarios of two different kinds of trajectories, one that exhibits localized motion and one with the characteristic that propagates in one direction only.

3.5.1 Bifurcation scenario of localized trajectories

We start with $w \approx 0.225$, where we find stable islands in phase space. These correspond to localized trajectories in position space. The PSoS, islands and its respective trajectories are shown in Fig. 3.9. At $w = 0.220$ the shape of the trajectory resembles a needle (3.9-c) (*c. f.* with one of the characteristic localised trajectories in the hard Lorentz gas). In the hard Lorentz gas, this trajectory is unstable and its corresponding PSoS will present only one fixed point surrounded by the chaotic sea. In the first column of Fig. 3.9, we can see that the stable island is surrounded by the chaotic sea, in the magnification (18% of the total of the PSoS), we see clearly the stable island. As we move in parameter w to $w = 0.225$, the island splits into two stable islands. The original vertical trajectory deforms and bends, it does not cross at the middle of the gap, but it crosses near the centre and when it returns it crosses through the other half side symmetrically. In $w = 0.230$, we can see how the islands have separated further and even though they shrink in size, stickiness phenomenon is still present. Despite the stickiness, these kind of trajectories do not suppress diffusion, normal diffusion is observed for sufficient long times. This is because diffusion is still dominated by the contribution to the MSD of the particles that travel longer flights.

Another example of a localized trajectory is the hexagon, this trajectory exists around $w = 0.455$, where there is a local minima in $D(w)$, see Fig. 3.10. In the soft

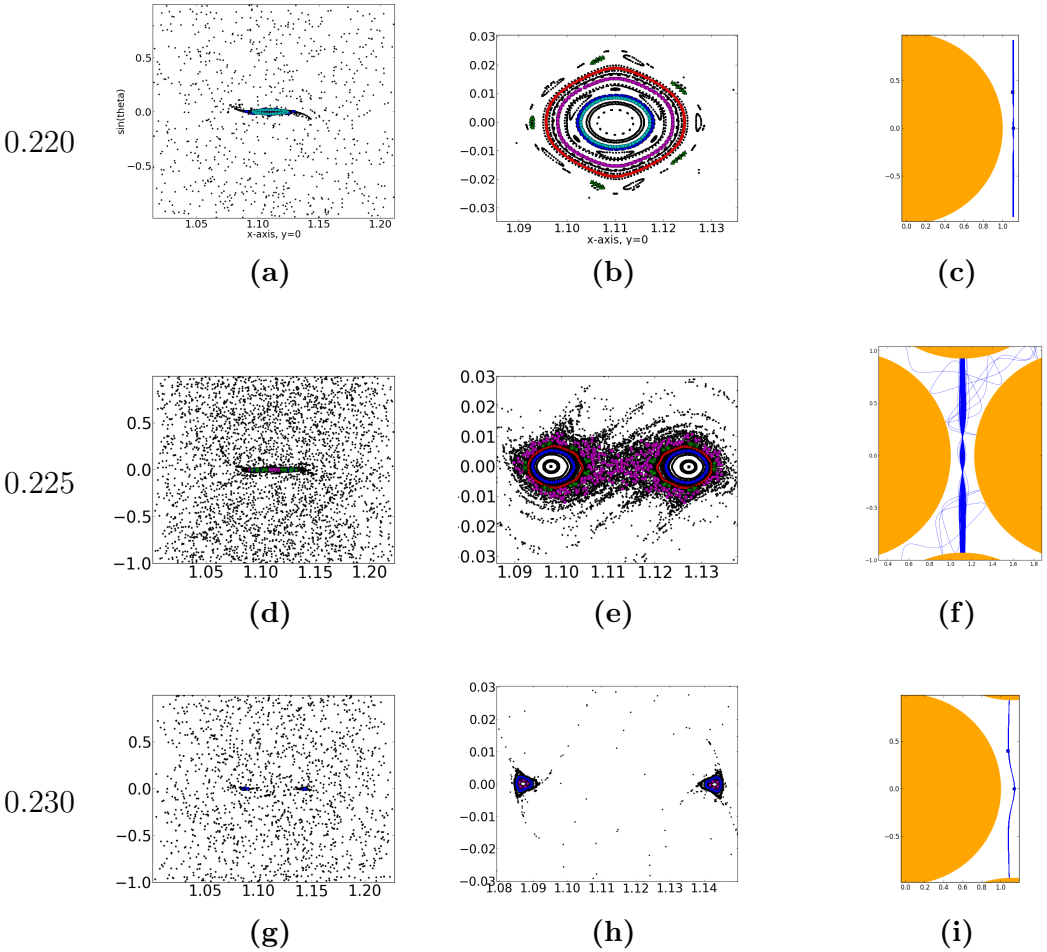

Figure 3.9: Bifurcation scenario of localized trajectory around $w = 0.225$. **Left**: PSoS as described in Subsec. 2.7.3. **Centre**: magnification of PSoS in the first column. **Right**: Trajectory in position space. The yellow circles have radius r_o centred at lattice points and are drawn here to locate the trajectory configuration space.

system the hexagonal trajectory emerges around $w = 0.45$. Its evolution on phase space is shown in Fig. 3.11. We can follow the island for a relatively long interval and see how it bifurcates. First, at $w = 0.450$ the geometry allows the particle to bounce with the scatterers and return to the same initial position and only one island is observed in the PSoS. Then, the shape of the island changes showing more stickiness. Finally it bifurcates into two stable islands until they gradually disappear. Note that the new islands are bigger in size than the original one. Also note that this bifurcation is in the $sin(\theta)$ parameter, whereas the bifurcation in the previous example was along the position axis. While major changes can occur during this process we want to emphasise that the islands are surrounded by stickiness.

The analogues of these trajectories in the Lorentz gas have no effect on the diffusion coefficient. Here, these hexagonal trajectories are stable and are accompanied by sticky trajectories this has an effect on the convergence of the diffusion coefficient but still normal diffusion is observed.

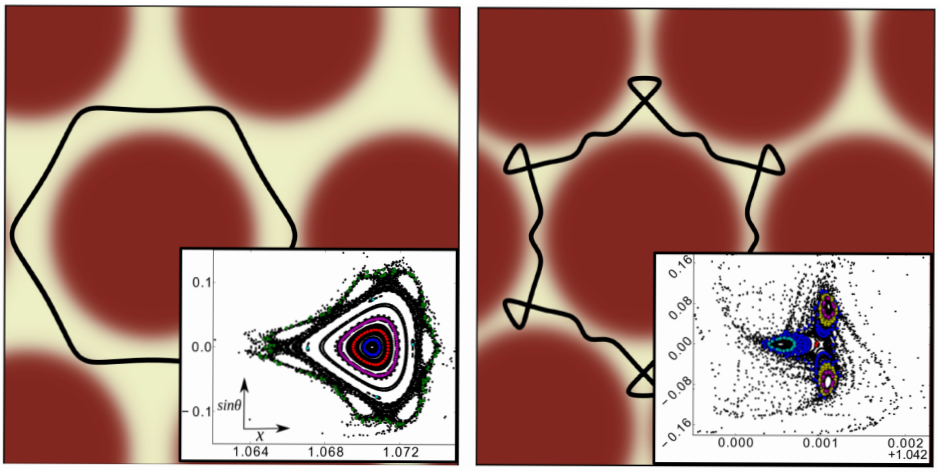

Figure 3.10: Examples of localised periodic trajectories in position space and their corresponding islands in PSoS. **Left:** Hexagonal localized trajectory at $w = 0.455$. **Right:** Localised trajectories at $w = 0.180$.

3.5.2 Bifurcation scenario of a quasi-ballistic trajectory

We will study a trajectory that propagates quasi ballistically on one direction. We focus on one of the peaks around $w = 0.235$. A PSoS in this parameter shows an stable island surrounded by the chaotic sea 3.12.

The stable islands corresponds to a quasi-ballistic (q-b) trajectory (top of Fig. 3.12). Sticky orbits make their appearance in the picture, as we see from the evolution of the island, these orbits stay around the island for some time and eventually leave to the chaotic sea. Its effect can be seen in the growth of the MSD (peak in Fig. 3.1).

As we move slightly to higher values of w the island evolves and starts to bifurcate. In Fig. 3.12 we can see the evolution of the stable island and its surroundings. The evolution in the PSoS resembles a Pitchfork bifurcation. We found this parameter particularly interesting since in its counterpart, in the hard Lorentz gas, at this parameter trajectories that travel in the same direction for a long time are suppressed due to strong scattering.

Other studies in periodic lattice with Lennard-Jones potential found similar q-b trajectories in the direction of the system's main symmetry axes [YZ10]. In the model we study here, we found q-b trajectories that follow non trivial paths in other channels not only in the main symmetry axes, see for instance the trajectory on the right of Fig. 3.15. Symmetric and periodic configuration of the scatters allows the particle to travel in the same direction in quasi-free flight.

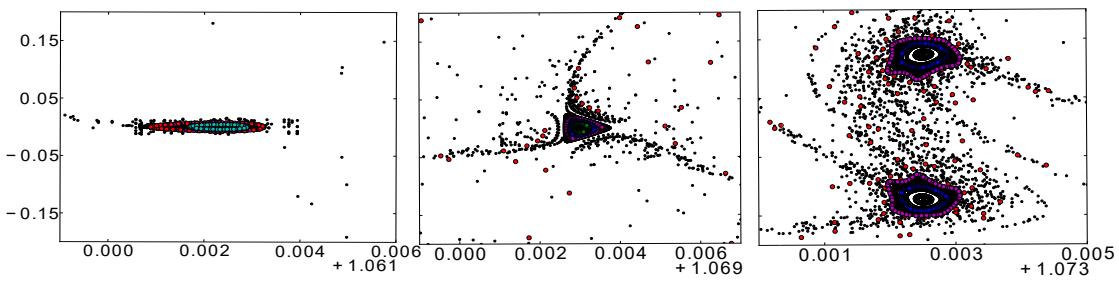

Figure 3.11: Bifurcation scenario of the hexagonal trajectory at $w \approx 0.458$, the axis are the same as in Fig. 3.10. Hexagonal trajectory is shown in Fig. 3.10.

The evolution of the islands in phase space can suffer drastic changes in a small δw. For the examples described earlier this is not observed because we are interested more in the overall behaviour. A more detailed example of a bifurcation is presented in Appendix A.2.

A finer analysis along the parameter w helps to understand the irregular structure of $D(w)$. Let us focus on q-b islands that cross the gap through the middle. We can capture periodic orbits as we move in w. Similarly for the irregular zones discussed earlier, we found a zoo of periodic trajectories, localised and quasi ballistic (q-b). In Fig. 3.13 we plot the position in the parameter w and the value of the angle of the velocity vector when the particle crosses the gap. The points with $sin(\theta) = 0$ correspond to localized trajectories (needle). The very last set of points to the right corresponds to q-b trajectories that start to resemble that of free flight in the Lorentz gas. For a closer look see Appendix A.4.

Let us compare $D(w)$ in Fig. 3.1 with this plot. Note that those regimes

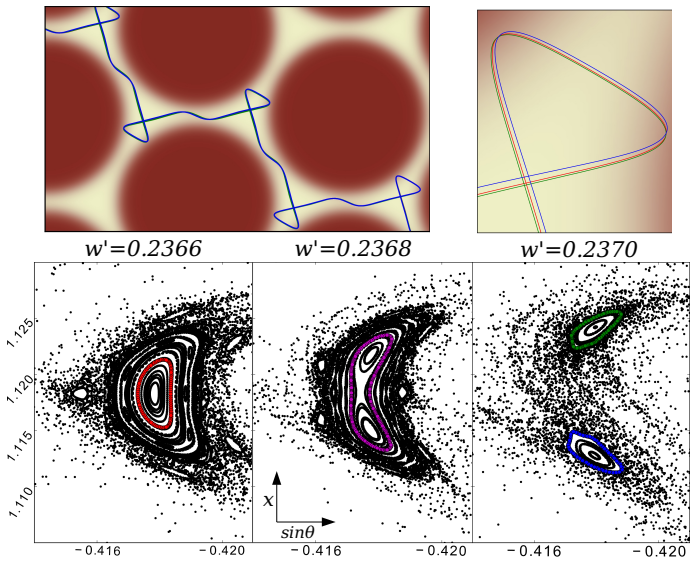

Figure 3.12: Quasi ballistic trajectory and PSoS at $w = 0.235$. **Top:** Trajectory in position space and magnification showing two nearby initial conditions. **Bottom:** Bifurcation scenario in PSoS, different colours indicate different orbits: the trajectory in colour blue corresponds to the orbit it the same colour in the PSoS.

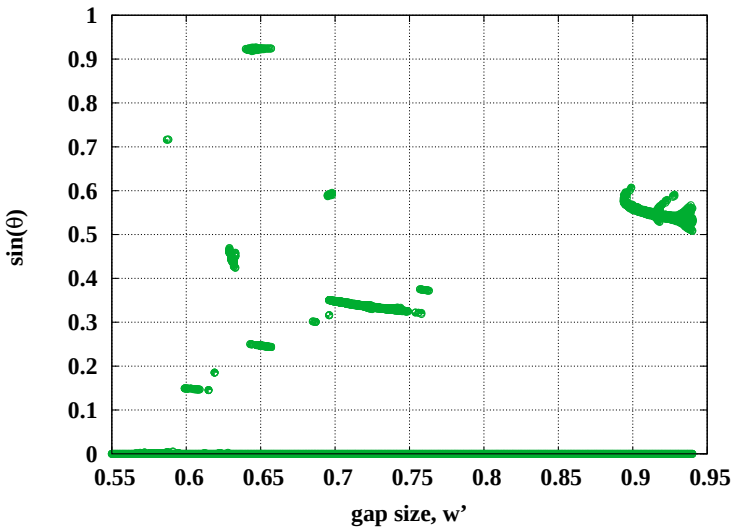

Figure 3.13: Periodic orbits that cross the middle of the gap generating islands in phase space. The figure shows where there is an island along w and the angle of the velocity vector of the particle when it crosses the trap (see Fig. 2.1).

where there are q-b islands match with the peaks in $D(w)$, and the regimes with no islands match to those regimes with normal diffusion. The q-b islands and the sticky orbits are responsible for the peaks. These contribute anomalously to the MSD. In the case of localized orbits, the size of the island and the stickiness around can have an effect on the growth of the MSD and therefore on the diffusion coefficient, but do not generate sub-diffusion.

There are two mechanisms that can destroy the islands: one is the evolution from a stable island into a bifurcation that splits the island producing two new islands accompanied by sticky orbits. The process of bifurcation can be complex, but eventually the periodic orbit disappears. The other mechanism is geometry, sometimes the configuration does not allow any more the existence of some islands, they get smaller and this disappear without bifurcating. The bifurcation scenario is complicated, a more detailed example is explained in the appendix where we show the evolution in phase space of a stable island due to a q-b trajectory.

Other systems exhibit this kind of phenomenon, where periodic orbits affect the nature of the diffusion coefficient. Like the chaotic pendulum by Blackburn and Gronbech-Jensen(1996) [BGJ96].

3.5.3 Co-existence of islands and probabilities of symbol sequence

Now, we come back to the probabilities analysis. Recall that in Subsection 3.3.3 we assigned a sequence of symbols to a path in configuration space. The sequence of symbols is given by letters that represent the exit from which a particle jumps to the next trap. We will discuss the relation of the sequence of symbols probabilities of special trajectories in position space and its relation with $D(w)$. The reasoning is the following. The occurrence of a periodic orbit in phase space, with stickiness, should contribute to a higher probability of a particular sequence of symbols.

As explained in previous sections we can compute numerically the probability that a particle leave the trap through any given exit. And also calculate higher order symbol probabilities: three and four symbol probabilities.

It is not possible to exactly distinguish the fraction of phase space that is chaotic and the one that exhibits regular or stable motion due to a periodic trajectory, but looking at the symbol sequence probabilities we can see how strong its effect is as we observe the change in correlations through w.

In Fig. 3.14 (Left) we plot some 3-symbol probabilities $p(zzz)$, $p(lrl)$, $p(rlr)$, etc., as function of w. And in Fig. 3.14 (Right) some key 4-symbol probabilities $p(llrr)$, $p(rrll)$, $p(rlrl)$ and $p(lrlr)$. From the figures, it is clear that there are correlations as we move along w, otherwise we should have that

$$p(lll) = p(llr) = p(lrz) = ... = p(lrr) = p(rrr)$$

for all w.

For the 3 symbol sequences we see that $p(lrl)$ and $p(rlr)$ behave similarly which is consistent with the symmetric configuration of the scatters. The same for $p(rrr)$ and $p(lll)$ as they follow the same pattern.

We can relate these probabilities with the occurrence of particular trajectories in configuration space, for instance, the sequence zzz is related to path of the needle trajectory: goes back and forth normal to the x-axis in the middle of the

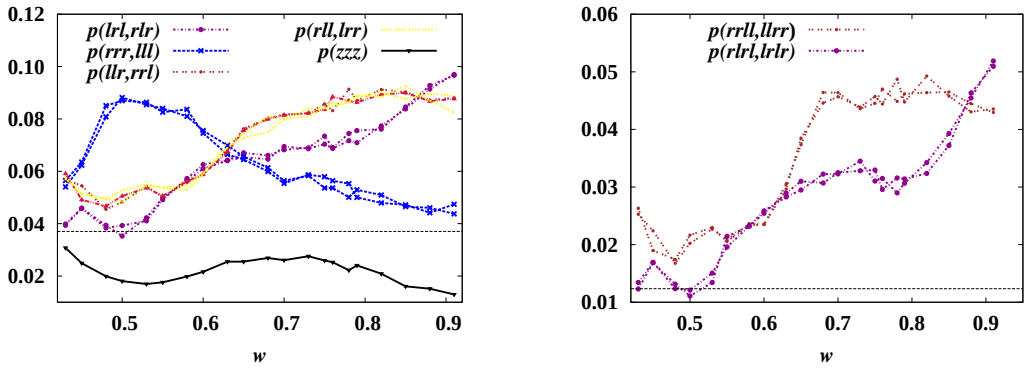

Figure 3.14: Left: Some 3 symbol probabilities, the dashed line indicates the value for equal probabilities 1/27. **Right:** Some 4 symbol probabilities, the dashed line indicates the value for equal probabilities 1/81.

gap.

The sequences lll and rrr resemble the path of the hexagonal trajectory. From Fig. 3.14 we can see that $p(rrr)$ and $p(lll)$ have a maximum around $w = 0.5$ which coincides with the minimum in $D(w)$ (see Fig. 3.1). One can argue that this minimum in diffusion is related to the hexagonal orbit and the effects of stickiness (Fig. 3.11).

The symbol sequences rlr and $plrl$ can be related to a q-b trajectory in Fig. 3.15-left, the same can be argued for the 4 symbol sequences $rlrl$ and $lrlr$ which follow the same path.

Note that $p(rrll)$ and $p(llrr)$ increase drastically with respect to $p(rlrl)$ after $w = 0.6$, the former symbol sequence relates to the path of trajectories of the type shown in Fig. 3.15. If we look again to Fig. 3.13 where we have indicated islands along the parameter w, we see that around $w = 0.6$ there are islands and they correspond to the same type of trajectories.

The probability $p(rlrl)$ and $p(lrlr)$ increases noticeable after $w = 0.8$. If we look at Fig. 3.13, there are islands close to $w = 0.9$. This matches with the appearance of an infinite horizon type island which follows the same symbol sequence $rlrl$ or $lrlr$.

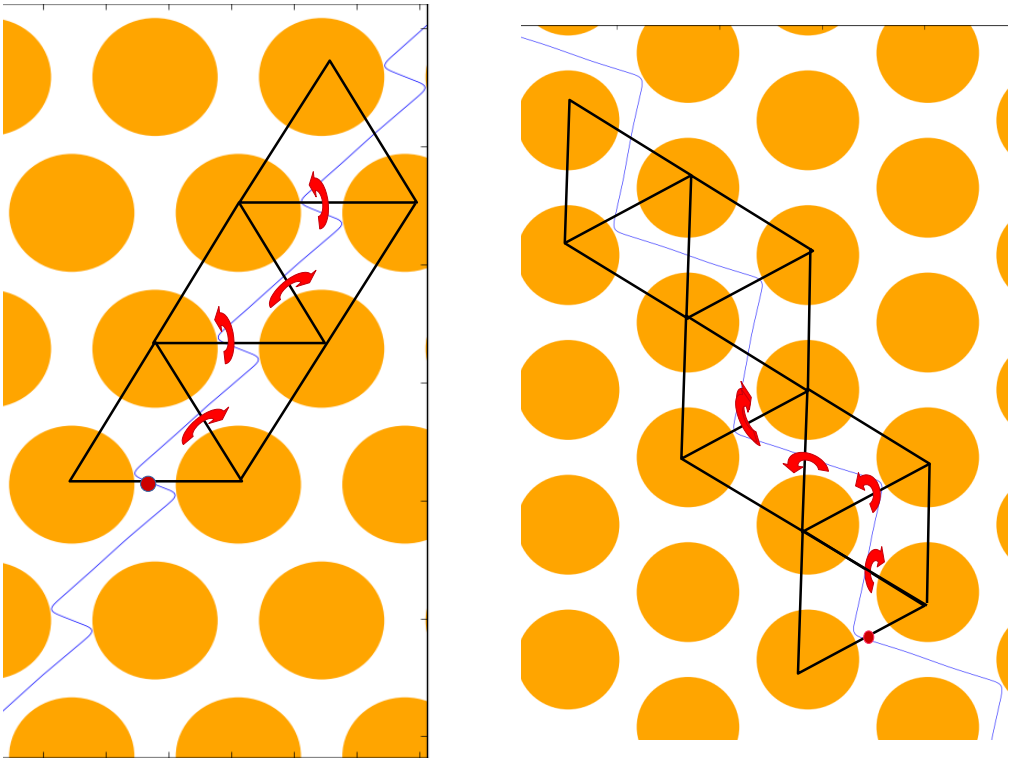

Figure 3.15: Quasi ballistic trajectories and jumps through traps. The yellow circles have radius 1 and are artificially located at the vertices of the triangular array. **Left:** The occurrence of this trajectory contributes to $p(lrlr)$ and $p(rlrl)$. **Right:** The occurrence of this trajectory contributes to $p(llrr)$ and $p(rrll)$.

3.5.4 Phase diagram

In previous sections we analysed the system when the separation of the scatters changes. As well as, a variation in the smoothness of the potential and we observed that the diffusion coefficient is an irregular function in both cases. Meaning that if all parameters are fixed and vary s_o or w the diffusion is an irregular function with some regions where normal diffusion does not exist followed by regimes with normal diffusion.

Existence of stable islands in soft billiards is explained by Turaev and Rom-Kedar [TRK98, RKT99]. They proved that when a billiard is perturbed, by softening the boundaries, stability islands in phase space appear from periodic tangential trajectories and homoclinic orbits. Tangential trajectories mean, tangential to the

walls of the billiard (see Fig. 1.1). A clear example when this occurs in the hard Lorentz gas is at $w = \sqrt{3}/4 - 2 \approx 0.309$ which is the starting point of the infinite horizon regime due to the appearance of a free flight trajectory (see right of Fig. 2.4). This trajectory is tangent to the scatters. We expect Turaev and Rom-Kedar conclusion to work here. By softening the potential walls, stability islands appear and break ergodicity. But, when or where do the islands exactly appear? Is hard to predict analytically where diffusion is normal in terms of w and s_o. Moreover, as seen in Sec. 3.5 the evolution of island in phase space is complicated. Islands due to q-b trajectories enhance the growth of the MSD, therefore affecting the diffusion coefficient. That is why we would like to have a global picture of the situation showing islands of stability appear as function of the control parameters w and s_o.

The combination of parameters between s_o and w generating islands is represented in a phase diagram shown in Fig 3.16.

Here, every point represents the existence of q-b island in phase space. Based on changes in s_o and w, island move accordingly in phase space (this figure rep-

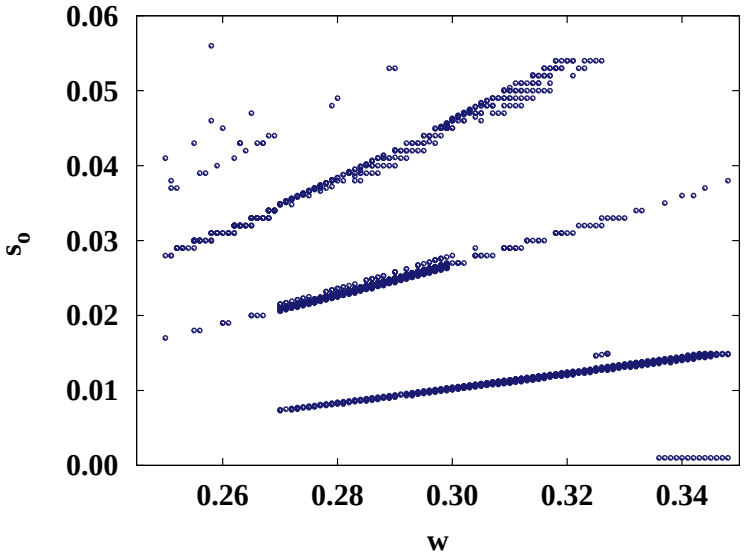

Figure 3.16: Phase diagram of softened periodic Lorentz gas. Every dot in the diagram w-s_o indicates an island in phase space.

resents a fragment of the whole set of tongues, see Appendix A.3). We are not disregarding the existence of islands in between the branches, these might contain very small islands that escape from our methods of detection. On the other hand this presentation of results unveils an ordered structure of the phase space and the dynamics of the system in terms of the parameters w and s_o. Instead of looking at irregularities of the diffusion coefficient along parameters, this pictures enable to see the evolution of the islands as a result interplay of the control parameters.

According to Turaev and Rom-Kedar's theory [TRK98, RKT99] stability islands appear for any arbitrary small perturbation on the smoothness of the billiard. If this is the case, we must see this branches of islands getting closer and closer for small s_o whenever there is tangential periodic trajectory in the unperturbed billiard. Then, in our diagram every branch should go from right to left and eventually go to $s_o = s_{o*}$ and $w = w_*$.

3.6 Conclusions

In this chapter we have studied the diffusion coefficient in the periodic array with Fermi potential as a function of the separation of the scatters, w, and the softness of the potential, s_o. Numerical results show that the diffusion coefficient is an irregular function of w and s_o. As one of the parameters is varied there are zones that exhibits normal diffusion and in between there are regimes where the diffusion coefficient does not exist. At large scale there is some degree of structure as we observe in Fig. 3.2. Whether there is fractality in this model on a fine scale is hard to conclude since the islands (peaks) opaque the real shape of $D(w)$. Also, our numerical results are constrained by computational resources.

While in the Lorentz gas the interactions of the particles with the scatterers have a defocusing character, in the softened version the walls of the potential play the role of focusing the trajectories. As the w parameter increases the particles can travel to further traps more easily, because the gap between traps gets bigger. At the same time, for some combination parameters, focusing of trajectories induces motion in a particular channel and enhances long travels.

These results suggest that the system exhibits normal and anomalous diffusion, in agreement with the conjecture by Klages *et.al.* [KD95]. This phenomena is also present in the study by Gaspard and Harayama [HG01], they study a 1-d system formed by particle interacting with a periodically corrugated floor and conclude that localized orbits are responsible for the algebraic decay of autocorrelation functions.

In order to describe the coarse shape of the diffusion coefficient we have calculated semi-analytical approximations, based on a random walk and a phase space argument, for high densities this gives a good match to the diffusion coefficient as a function of the separation of the scatterers. And, based on a collision less flight approach which qualitatively reproduces the shape of the coefficient for lower density, or large w. This indicates that the system can be regarded into two regimes, one where random walk motion dictates the behaviour of the diffusion coefficient and a second one where long flights dominate. A third approach takes into account correlations between traps jumps, such inclusion improved the basic random walk approximation to the diffusion coefficient. But still higher order probabilities are needed.

We also perform numerical simulations along the softness parameter to calculate $D(s_o)$, where we found a similar scenario as $D(w)$. The diffusion coefficient as a function of the smoothness parameter shows zones with normal diffusion and intervals with anomalous growth of the MSD.

Those regimes where diffusion is anomalous are due to quasi-ballistic trajectories which in turn come from stability islands in phase space. If we follow Turaev and Rom-Kedar's theory, stable islands in phase space should appear because of tangential periodic orbits in the corresponding hard system.

This analysis showed a complicated structure of the phase space, and a non-trivial series of bifurcations along the parameter w. These factor make complicated a theory that describes fully the behaviour of the diffusion coefficient. Some stability islands evolves and disappear by bifurcating, accompanied by sticky trajectories that enhances the growth of the MSD. Another mechanism responsible for birth and destruction of island is the geometry, geometry destroys abruptly

stable islands.

A diagram with the stability islands in $w - s_o$ shows a well behaved form as we move along parameters which at the same time gives the irregular shape of $D(w)$. It is pending task to see if the branches get arbitrarily close to $s_o = s_{o*}$ as predicted by Turaev and Rom-Kedar's theory, although this task might be restricted to computational capacity.

We finish this chapter with visual summary of how the dynamics of the trajectories affect the overall behaviour of the diffusion coefficient as the separation of the scatterers, w, is varied. In Fig. 3.17 we put together all the pieces of the puzzle, the plot shows the diffusion coefficient as a function of the parameter w, and indicates the shape of some of the periodic trajectories. Each periodic trajectory is associated with a stable island in phase space.

This chapter dealt with diffusion coefficient as a function of two control parameter; one spatial parameter and a smoothness parameter. We investigate in next chapter the energy dependent diffusion coefficient.

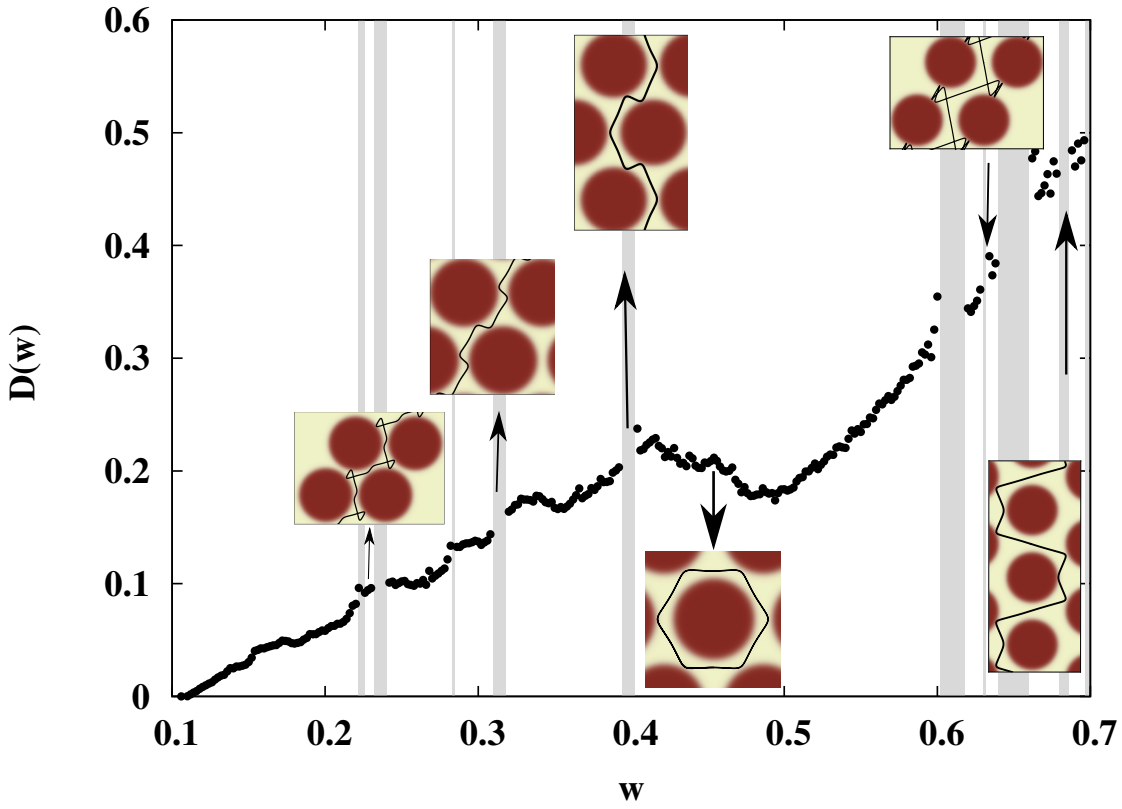

Figure 3.17: Diffusion coefficient as a function of the separation of the scatterers. The grey zones indicate that the diffusion coefficient does not exist there. Some periodic trajectories are indicated to emphasize that their appearance affects the nature of the diffusion coefficient.

Chapter 4

Energy dependent diffusion coefficient

In the Lorentz gas the energy plays only a scaling role in the diffusion coefficient since the velocity is constant, but when smoothing the walls of the potential the scenario changes drastically. This chapter concentrates on the study of the diffusion coefficient as a function of energy as a control parameter. The dynamics is in a 2-d periodic triangular lattice with Fermi potentials, qualitatively equal to the system described in Chapter 3.

We will see that including a smooth potential in the system enriches the dynamics of the system yielding a non trivial dependence of the diffusion coefficient as a function of the energy as control parameter. For fixed smoothness and separation of scatterers the chance of a particle exiting some region in position space is now a function of the energy. This is because a particle with low energy will be more likely to be trapped in a region with small potential energy for a longer time before climbing the potential and crossing to another region, and a high energy particle would have a better chance to escape quickly from a trap since it can easily climb the potential.

In section 4.1 we briefly discuss the laws for $D(E)$ as $E \to \infty$ that we found in the literature. This serves as a motivation for our analysis in section 4.2, where we

develop random walk approximations based on the phase space argument of the type of Machta and Zwanzig [MZ83] (explained in Sect. 2.5.3) as well as collisionless flight approach for the small energy regime. The arguments used for these approximations are similar to the ones used in Chapter 3, but the goal here is to express the elements in terms of the energy E. We have studied in detail two different models: in the first one in Section 4.3, we focus on normal diffusion in high energy regimes; in the second one in section 4.4 we focus on normal diffusion and emphasize the complicated structure of the phase space and the appearance of islands as energy increases. For the sake of consistency we explore both models as follows: firstly the small energy regime, $E_* < E < V_{\max}$; secondly the regime $1 < E < 2$ which we call intermediate regime; and lastly the high energy regime $E > 2$. We also study a transition phase around $E = V_{\max}$ where a new mechanism dictates the dynamics of the system. Here a new random walk based on traps of slow motion is developed, we compare this analysis to numerical simulations. Also, in both models we study the possibility of characterize the asymptotic form of the diffusion coefficient for high enough energy which we denote by $E \to \infty$. In Sect. 4.5 we give an illustrative model where islands appear for very small energies. Finally, in Sect. 4.6 we make some observations, state open questions and conclusions.

4.1 Energy dependent diffusion coefficient in the high energy regime

As a function of the energy as a control parameter diffusion might still exist for energies higher than the maximum of the potential used. The existence of normal diffusion will depend on the selection of the potential and parameters. We find some contrasting conjectures in the literature. Nobbe [Nob95] conjectures that in systems with repulsive potentials the energy dependent diffusion coefficient $D(E)$ grows as $E^{3/2}$ for sufficiently high energies. On the other hand, Aguer *et. al.* [ADB10] conclude that $D(p) \sim p^5$, where p is the momentum of the particle, yielding to $D(E) \sim E^{5/2}$. Although it is worth mention that both have

studied qualitatively different billiard models. In [ADB10] the configuration of the scatterers is that of a Lorentz made of compound potentials. Aguer's model for diffusion is based on a series of assumptions on the asymptotic behaviour of the path of the particle. Assuming that the motion is randomized for sufficiently long time, they claim that the motion is that of a random walk, from which they deduce the asymptotic behaviour for the diffusion coefficient for sufficiently large energies.

A numerical study by Yang and Zhao [YZ10] deals with a Lennard-Jones potential, which is repulsive and attractive potential, in a hexagonal lattice where they observe intervals of superdiffusion and normal diffusion when increasing the energy E. They claim this is due to the extinction of islands in phase space.

Finally, it is known that in Coulombic type potentials in periodic array is diffusive (see Ref. [Kna87]. In contrast, in Asch and Knauf [AK98] proved that the motion in smooth potentials is ballistic for high enough energies.

The questions are

- What is the onset for diffusion? In the case that it exists and, if it exists, how is this dependence of diffusion as a function of the energy as control parameter?
- Following Aguer's assumption for large energies; Is it valid to assume that the dynamics for small energies can be thought as a random walk?
- Another important regime to be explored is the transition when particles fly over the potential, or $E = V_{\max}$. Some studies conclude that for $E > V_{\max}$ only anomalous diffusion is observed [BZCM85].
- We also want to explore the long time limit for large enough energies where diffusion could appear after a long transient. What is the asymptotic behaviour of D for high energies?

We investigate the validity of Aguer's and Nobbe's approximations for high energy regimes. Later, in section 4.3, we will compare in detail these models with our numerical results.

In the next section we describe the concepts necessary to construct the random walks approximation in terms of the energy for the small energy regime or $E < 1$.

4.2 Analytical random walk approximations for small energies

The model that we use next is briefly explained here, for more details see Section 2.7. For small energies, $E < V_{\max} = 1$, we will approximate the diffusion coefficient as a function of the total energy, first using Machta and Zwanzig's phase space argument [MZ83], and secondly using a collision less flight or Boltzmann approach. The method is qualitatively similar to the method we used to construct $D_{\mathrm{MZ}}(w)$ and $D_{\mathrm{B}}(w)$, Eqs. (3.11) and (3.17) in the previous chapter, but adapted to the energy as a control parameter.

If we want to calculate an approximation for D as a function of the energy we need to find the escape time, τ, as a function of the energy, but first let us introduce concepts necessary for us to construct the approximations.

In our model, in general, if a particle has total energy $E > E_*$ then it can escape from the trap through the available space between r and $r + W(E)$, with length $W(E)$, where r should be also stated as a function of the energy.

As a function of the energy, constrained to the Fermi potential, the gap through which a particle can escape from a trap is approximately given by

$$W(E) = L - 2r, \tag{4.1}$$

where L is fixed and r is the radius that can be computed as follows.

The exact radius should be computed considering the contribution of all V_i located at each point of the lattice. If we consider the contribution of two adjacent potentials as in Eq. (3.1), to find the radius r it would be necessary to solve for $r(x)$ and $r(x - L)$ when $V_1(x) + V_2(x) = E$. Alternatively, considering only $V_1(x)$, we can obtain an analytical expression for the radius. The radius in terms of the

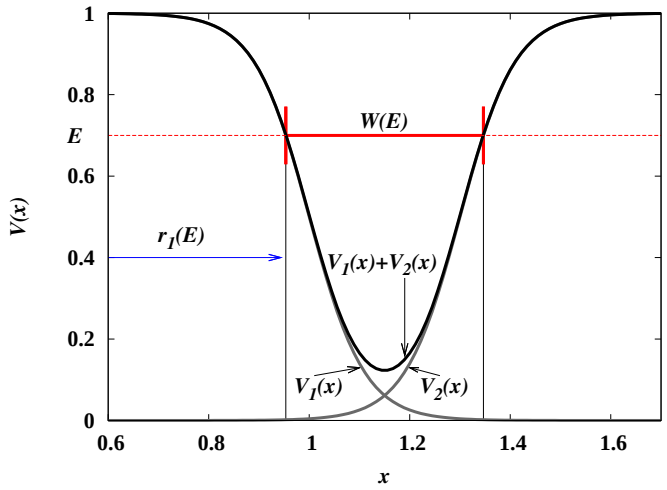

Figure 4.1: Gap size $W(E)$ and radius $r_1(E)$ defined by the energy E, see Eqs. (4.1) and (4.2).

energy is obtained by solving $V_1(x) = E$ for $r(x)$. For simplicity we will label this new radius with r_1 and is given by

$$r_1(E) = s_o \ln(1/E - 1) + r_o. \tag{4.2}$$

Note that due to the overlapping potential the radius r_1 is and under estimation of the real radius r in Eq. (4.1) since r_1 has been computed considering only one potential. Since the real gap size $W(E)$ given by Eq. (4.1) using this r_1 here as the radius, yields an overestimation. This effect is enhanced when $E \to E_*$ because the difference $r - r_1$ is bigger. As we move to higher energies $E \to 1$, the difference tends to zero, as illustrated in Fig. 4.1, so we have that $W(r_1(E)) \to W(r(E))$. Finally, note that $w \neq W(E)$ but these two quantities are related by

$$L = 2r_o + w = 2r(E) + W(E).$$

In our approximation we will use the radius from Eq. (4.2) always bearing in mind that there is a greater error the closer E is to threshold E_*.

Next, we will calculate approximations for $v(E)$ in a similar way as in sec-

tions 3.3.1 and 3.3.2, but here the energy plays a major role determining the gap size. Therefore, any estimation we make about the velocities will also be affected.

From energy conservation we have that the expression for the velocity in terms of the energy is

$$v(E) = \sqrt{2(E - V(r))},$$

where $V(r)$ is the potential energy. Recall that the minimum of the potential gives the energy threshold, E_*; this occurs in the middle of the gap:

$$E_* = V_1(r_o + w/2) + V_2(r_o + w/2) = 2/(1 + \exp(w/(2s_o))),$$

1. If we choose a maximum velocity $v_{\max}$ in the exit of the trap then:

$$v_{\max}(E, w) = \sqrt{2(E - V(r_o + w/2))}.$$

   This velocity, $v_{\max}$, is a function of the energy and independent of the gap size of the gap $W(E)$.

2. We can also choose an average potential in the gap with size $W(E)$, as calculated before. Due to symmetry, we can calculate the integral of the potential $V_1(r)+V_2(r)$ in the first half of the region and average over $W(E)/2$,

$$V_{\text{ave}}(W(E)) = \frac{2}{W(E)} \int_{r(E)}^{r(E)+W(E)/2} V_1(r) + V_2(r) dr.$$

   Alternatively, if we choose to integrate from $r(E)$ to the middle of the gap,

$$V_{\text{ave}}(W(E)) = \frac{2}{W(E)} \int_{r(E)}^{r_o+w/2} V_1(r) + V_2(r) dr,$$

   we get the same result. The average potential considering V_1 and V_2 reads:

$$V_{\text{ave}}(E, W(E)) = 2 + \frac{2s_o}{W(E)} \ln \left[\frac{1 + \exp(r(E) - r_0)/s_o)}{1 + \exp((L - r(E) - r_o)/s_o)} \right]. \tag{4.3}$$

   From Fig. 4.1 we can see that the contribution of V_2 to the integral is very

small when $E \to 1$.

Therefore, the velocity is a function of the energy and the average potential V_{ave} in the exit of the trap with width $W(E)$:

$$v_{\text{ave}}(E, W(E)) = \sqrt{2(E - V_{\text{ave}}(W(E))}.$$

3. Now, let us try to approximate an average velocity in the gap of size $W(E)$

$$v = \frac{2}{W(E)} \int_{r(E)}^{r(E)+W(E)/2} \sqrt{2(E - V(r))} dr,$$

where $V(r) = V_1(x) + V_2(x)$ is as in Eq. (3.1). This integral is not solvable analytically, but we can solve it numerically. We choose points in the domain of E and compute the integral and we get a function with discrete points $E, v_{\text{num}}(E)$.

Now that we have expressions for the velocity in terms of the energy, we proceed to construct random walk approximations in terms of the energy; here these expressions for the velocity will be used.

4.2.1 Machta and Zwanzig random walk and phase space argument

Recall that the argument in the Machta and Zwanzig approximation, as explained in sect 2.5.3, is that the process by which particles travel from trap to trap is assumed to be a random walk and therefore we use $D = l^2/4\tau$. The escape time τ has now to be expressed in term of the energy so that we can deduce an expression for diffusion as a function of the energy of the form

$$D_{\text{MZ}}(E) = \frac{l^2}{4\tau(E)}, \tag{4.4}$$

where the distance between two adjacent traps, l, remains a constant since we are not including a variation of the lattice. For a smooth potential and some energy

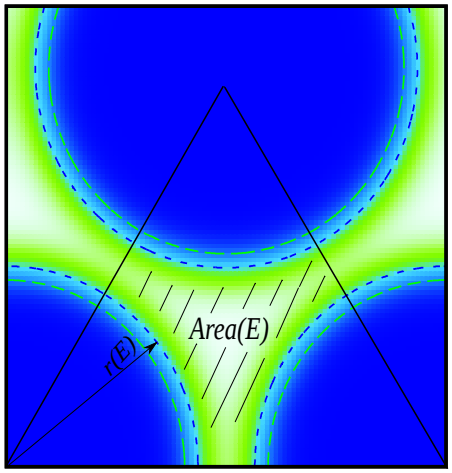

Figure 4.2: Definition of Area in terms of energy: $A(E)$ is the area inside the unit cell enclosed by the equipotential lines with radius $r_1(E)$ such that $E = V_1(r_1)$.

E, by the phase space argument we have that the escape time is given by the quotient of the total phase space Ω and the flux of particles that escape form the gap in some time δt, ω, as

$$\tau = \Omega/\omega. \tag{4.5}$$

The velocity space is $2\pi v(E)$ and, again, we assume $v(E)$ to be constant. Then, the total volume of phase space is

$$\Omega = A_{\text{trap}} \times 2\pi v(E), \tag{4.6}$$

where A_{trap} is the area available in position space which is also a function of the energy $A_{\text{trap}} = A(W(E))$. This area, as depicted in Fig 4.2, depends on the radius $r_1(E)$ as expressed in Eq. (4.2).

We can calculate the available area for the particles in position space by geometrical means in analogy to the Lorentz gas. We need to compute the area with borders given by the equipotential lines with $V_1(r) = E$ and the three exits of the trap. We take the area of the unite cell and extract the 3 times the area formed by the semicircle with radius, $r_1(E)$, as in Eq. (4.2).

Then we get that $A(W(E))$ or $A(E)$ is given by the expression

$$A(E) = \sqrt{3}(2r_o + w/2)^2 - \frac{\pi}{2}(s_o \ln(1/E - 1) + r_o)^2.$$

Strictly speaking, the function $A(E)$ has a more complicated dependence on E, due to the overlapping of the potential. Where scatterers are closest to each other, the radius suffers the same problem illustrated in Fig. 4.1. This is especially a problem for small energies but we shall use $A(E)$ as a first approximation.

For the flux of particles leaving the trap, we have that there are 3 exits of size $W(E)$, so $\omega = 3W(E) \times 2v^2(E)$.

It remains to substitute these quantities in Eq. (4.5). Then τ reads

$$\tau(E) = \frac{A(W(E))2\pi v(E)}{3W(E) \times 2v(E)^2}. \tag{4.7}$$

Finally we can substitute $\tau(E)$ in the expression for the diffusion coefficient Eq. (4.4)

$$D_{\mathrm{MZ}}(E) = \frac{3l^2 W(E)}{4\pi A(W(E))} v(E). \tag{4.8}$$

4.2.2 Random walk approximation based on collision less flights

Remember that this approximation is based on collision less flights, so

$$D_{\mathrm{B}} = \frac{l_c^2}{4\tau_c}, \tag{4.9}$$

where τ_c stands for the mean free time between collisions, and l_c is the mean free path between collisions. In chapter 3 we made the observation that in systems with smooth potentials collisions are not defined, but we proceed with our analysis with the understanding that in the limit when $s_o \to 0$ the potential is that of a hard wall where collisions are well defined.

Now we will calculate τ_c from a phase space argument.

Recall that in the Lorentz gas, in order to calculate τ_c, instead of considering the length of the exits or gaps, we need to calculate the length of the walls inside the trap. We will use the arc length that originates from the angle $\pi/3$ and a radius $r(E)$ in the equipotential line determined by $V(r) = E$. There are three arcs so $l = 3 \times \text{length(arc)} = \pi r(E)$ and

$$\omega = r(E) \times 2v^2(E)$$

The total volume of phase space Ω is the same as in Eq. 4.6. If an average constant velocity v is assumed as before, then

$$\tau_c = \frac{A(W(E))}{r(E)v}. \tag{4.10}$$

Consider an average velocity given by $v_{\text{ave}} = l_c/\tau_c$, and substitute $l_c = \tau_c v_{\text{ave}}$ in Eq. (4.9) and we get

$$D_{\text{B}} = (\tau_c v_{\text{ave}})^2/4\tau_c = v_{\text{ave}}^2 \tau_c/4$$

and substitute τ_c to get

$$D_{\text{B}}(E) = \frac{A(W(E))}{4r(E)} v_{\text{ave}}(E). \tag{4.11}$$

Ideally, we would like the term $W(E)$ to converge to L , and $A(E)$ to A_T according to the geometry of the problem. According to the formulation these terms depend on r_E, which diverges as $E \to 1$, so does $A(E)$ and $W(E)$. On the other hand, the expressions for the velocity we constructed converge to a finite value when $E \to 1$.

Observe that in Eq. (4.8) the term $A(E)$ is in the denominator, contrary to the situation in D_{B}; the numerator and denominator in Eq. (4.11) both diverge but the numerator is faster, therefore $D_{\text{B}} \to \infty$ as $E \to 1$.

Next, we will compare our random walk approximations $D_{\text{MZ}}(E)$ and $D_{\text{B}}(E)$ against numerical simulations of two different models, meaning different parameters w and s_o.

4.3 Diffusion in a steep potential and high density of scatterers

Here we focus on the normal diffusive regime for small and high energies as well as on a transition zone where we develop a new random walk model. For our first goal, we need to find a combination of parameters such that normal diffusion is observed in a relatively long interval of energies. Making a smoother potential yields a shallow potential (see Fig. 4.3), in which particles travel in the same direction very easily. The combination of all parameters will determine the type of dynamics and the diffusion coefficient of the gas particles. The separation of the scatterers, dictated by w, should be such that there is enough space to make the gap large enough to allow particles to escape to the next unit cell. And, as we will see, the diffusion coefficient is also sensitive to the smoothness parameter, as we change this parameter. The smoothness parameter should be such that the depth in the potential at the exits is large enough to allow particles to exit, avoiding scenarios like the one on the left of Fig. 4.3.

Here we work with the parameters $w = 0.05$ and $s_o = 0.01$, these parameters yield a steep potential in the gap between scatterers as illustrated in the right of Fig. 4.3. In the simulations of the MSD we use the following input parameters.

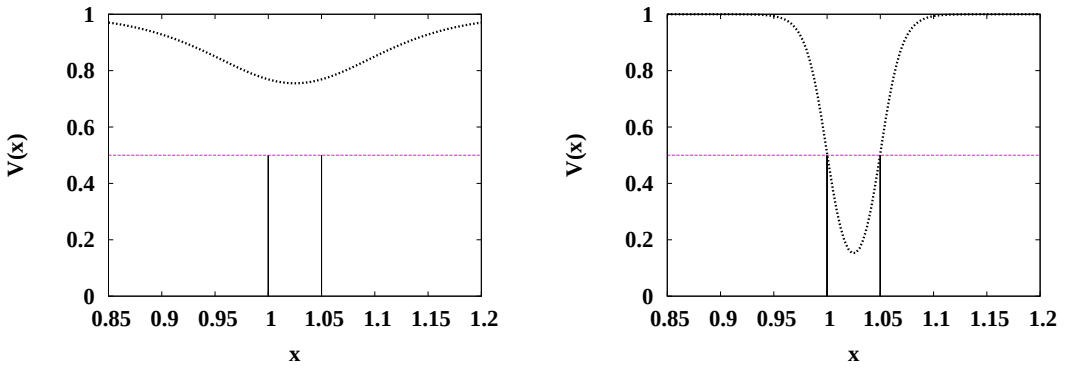

Figure 4.3: Potential V(r) with separation between scatterers $w = 0.05$, the horizontal line corresponds to $E = 1/2$ and the vertical lines indicate $x = r_o$ and $x = r_o + w$. **Left**: Softness $s_o = 0.05$, avoid this kind of scenarios where the potential is too shallow. **Right**: $s_o = 0.01$, in this section we use this setting to study $D(E)$.

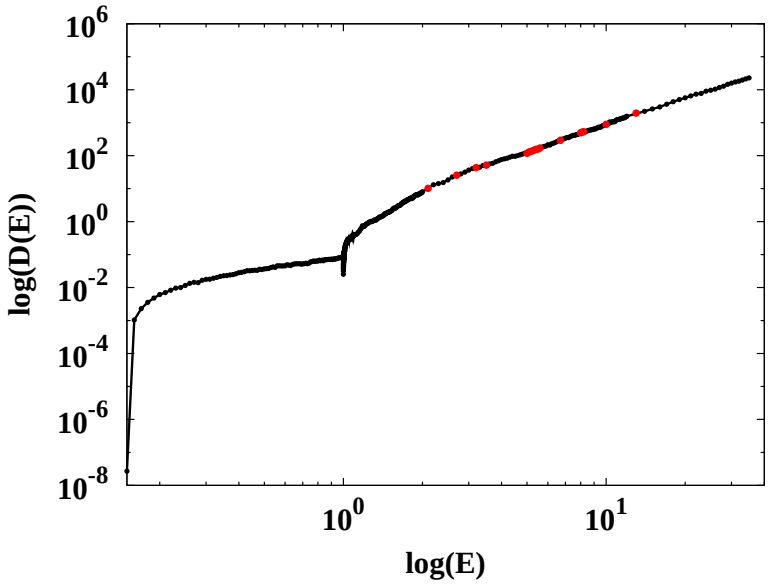

Figure 4.4: Log-log graph: Numerical diffusion coefficient D as a function of energy E in a model with high density of scatterers. Input parameters: $w = 0.05$ and $s_o = 0.01$, see text for the rest of paramters.

In the small and transition energy regime, $E < 2$, the iteration time is $t = 5000$ and the ensemble size of $n = 20000$. For energies $E > 2$ we set the ensemble size $n = 40000$ and iteration time $t = 40000$. With this choice of parameters the system exhibits normal diffusion for a broad range of energies. In Fig. 4.4 we show the diffusion coefficient calculated numerically. We can distinguish different regimes along the energy parameter where the diffusion coefficient behaves differently in small and high energy regimes. Also we observe a transition point around $E = V_{\max} = 1$.

Next we will explore the different regimes. In the small energy regime, $E < 1$, we apply the random walks Machta and Zwanzig and Boltzmann approximations and to compare to $D(E)$, including a third one with τ_e computed numerically. At $E = V_{\max}$ we found a transition regime, $1 < E < 2$. We will carefully analyse it and develop an appropriate random walk. Then we will focus on finding a law $D(E) \propto E^m$ for high energies; for this we will study the MSD and the $PSoS$ as we change the energy, we will also calculate an error estimate for the diffusion coefficient.

4.3.1 Small energy regime, $E < 1$, and random walk model

Here we put to the test the random walk approximations obtained earlier in Sect. 4.2. Also, we compute from simulations the escape time τ to incorporate into $D = l^2/4\tau$ so that we get a third approximation, $D(\tau_{\text{num}})$, half numeric half analytic random walk.

Random walk approximation

First we remark that in the Lorentz gas with the analogue parameter $w = 0.05$, D_{MZ} slightly overestimates the diffusion coefficient, but is in the random walk regime (see Fig. 2.6), therefore here we are not expecting an exact match between $D_{\text{MZ}}(E)$ and the computed $D(E)$ but we take our arguments to construct a qualitative approximation.

Based on the random walk argument, we obtained an expression for diffusion D_{MZ} in Eq. (4.8). The graph of the approximations D_{MZ} with three different velocities and the numerical data are shown in the left of Fig. 4.5. As expected, D_{MZ} with average velocity misses the threshold and D_{MZ} that uses a maximum velocity recovers the threshold.

The approximation D_{MZ} with maximum velocity does not give a good match indicating that not many particles travel with maximum velocity but with some average velocity instead.

If we look at the inset, we observe that $D_{\text{MZ}}(E, v_{\text{num}})$ captures the threshold and gives the correct asymptotic when $E \to E_*$.

Collision less flight: Boltzmann approximation

We also compare $D_{\text{B}}(E)$ Eq. (4.11) with the data in this model. The graphs of D_{B} with three different velocities are shown in the right of Fig. 4.5.

D_{B} with average velocity matches the data for large energies $E \to 1$. In this system we use $s_o = 0.01$ which is very close to the hard Lorentz gas. Since the

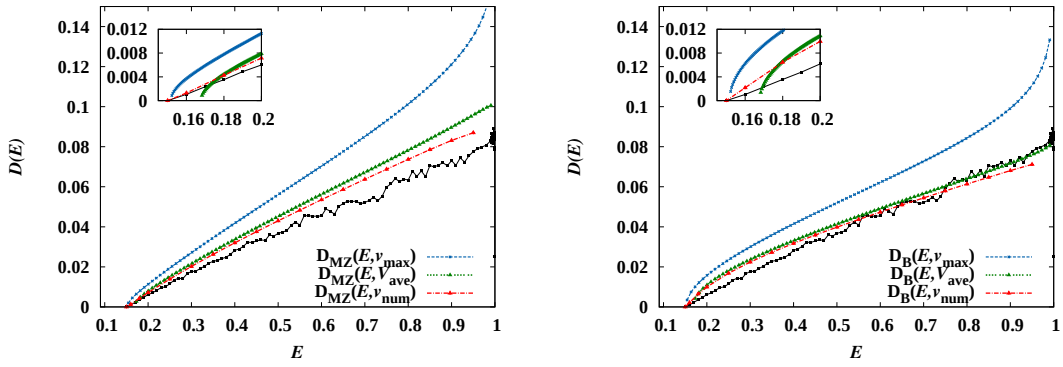

Figure 4.5: Diffusion coefficient as a function of the energy in the small energy regime with a high density of scatterers. Black line: Numerical simulations with input parameters as in Fig 4.4. Random walk approximations: **Left** Machta and Zwanzig approximation $D_{\mathrm{MZ}}(E)$ Eq. (4.8). **Right** Boltzmann approximation $D_{\mathrm{B}}(E)$ Eq. (4.11). Green lines indicate that an average velocity has been used and blue lines a maximum velocity. Red lines indicate a numerical computed average velocity.

smoothness parameters makes the potential very steep, particles are more likely to travel as free flight before getting close to a scatterer. This can explain why D_{B} is a better approximation than D_{MZ} although it fails as energy approaches the threshold. This approximation is based on collision less flight and it turns out that τ_c is defined even when $E < E_*$. D_{B} still manages to go to the threshold, because of the construction of the velocity, but it does with the wrong shape.

Escape time (τ from numerics)

To the best of our knowledge, in this system it is not possible to compute the escape time analytically. However, one can make approximations and assumptions just like the phase space argument. Numerically, it is a straightforward calculation, the limitations we face here are finite computing time and computer capacity.

In order to get a curve $\tau_{\mathrm{num}}(E)$, we must check for convergence in time and in the number of particles. For relatively large values of energy, particles escape fast from a trap, but as the energy gets smaller, particles get trapped for longer times. As a consequence one needs to iterate for long times in order to allow particles to escape. Our estimation of τ_{num} is affected by this problem, hence our curve $\tau(E)$

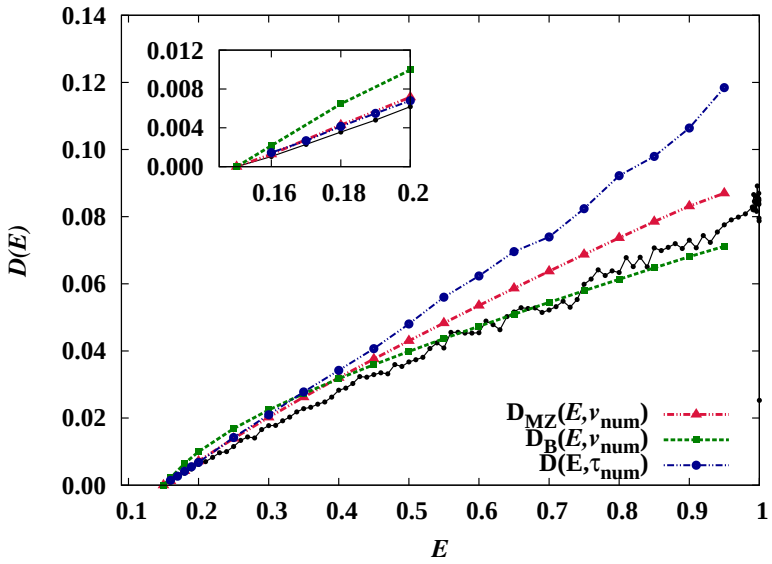

Figure 4.6: Direct comparison between different approximations in the small energy regime. Black line: Numerical simulations as in Fig. 4.5. Red line: $D_{\mathrm{MZ}}(E, v_{\mathrm{num}})$ and green line: $D_{\mathrm{B}}(E, v_{\mathrm{num}})$. Blue dotted line $D(E, \tau_{\mathrm{num}})$, see Eq. (4.12), based on escape time and from phase space argument. The crossing point between the approximations separates the random walk regime and the free flight regime.

is an upper bound for the exact one, for which one would need infinite time. Now we can compute

$$D(E, \tau_{\mathrm{num}}) = \frac{l^2}{4\tau_{\mathrm{num}}(E)}, \tag{4.12}$$

where the distance between centres of traps l is kept constant and τ_{num} is the time escape calculated numerically.

Fig. 4.6 shows the data compared to $D_{\mathrm{MZ}}(E, v_{\mathrm{num}})$ and $D_{\mathrm{B}}(E, v_{\mathrm{num}})$, with numerical average velocity, and $D(E, \tau_{\mathrm{num}})$. The numerical τ gives a correct prediction at the origin of diffusion. As stated before, this is an upper bound since it is very hard to calculate numerically the real τ as we go to smaller energies.

The approximation based on the random walk overestimates the diffusion coefficient. In the regime of $E > 0.5$, by definition, the exits of the trap get bigger, therefore it is clear that more particles escape faster without scattering. The random walk assumption is not valid in this regime. From the Fig. we can see clearly where the different mechanisms dominate in the figure, this is given by the cross-

ing point of the two graphs. It is not coincidence that $D_{\mathrm{MZ}}(\tau_{\mathrm{num}})$ cuts D_B where D_{MZ} does. After all, they are based on the same argument. From the inset we see that, even tough D_{B} is in general a better approximation, it is asymptotically incorrect when $E \to E_*$ whereas D_{MZ} reproduces the shape of $D(E)$.

4.3.2 Transition regime and a random walk motivated by slow motion

In this section we will explore the region $1 < E < 2$; If we look at Fig. 4.4 we see an interesting feature in $D(E)$. There seems to be steep jump at $E = 1$. A different mechanism appears near this values that inhibits the diffusion coefficient exactly after $E = 1$.

The potential $V(r)$ plays a dominant role here. Before $E = 1$, particles can not pass the potential hills but are restricted to a certain area in configuration space. Trivially, this area covers the traps and the channel that connect them. Diffusion is enhanced by movement of particles trough the exits of the traps and suppressed by normal scattering inside the traps. When approaching $E = 1$ from the right, the particle has enough energy to cross the scatterers, in this process it actually crosses the scatter conversely to what happened in the cases with $E < 1$.

We will elaborate on the following points:

- Study the transition region for D(E) closely around $E = 1$, look carefully at $MSD(t)$; is there an indication of suppression of diffusion?
- Does even $D(E) \to 0$ ($E \to 1^+$) in the asymptotic limit?
- Is the transition in D(E) continuous or discontinuous?
- Fit the normal diffusive $D(E)$ above $E > 1$ with the power law E^m; what exponent do we get? Is it comparable to Aguer's $m \sim 5/2$?, Nobbe or other?

We start by looking at the MSD(t) obtained numerically. The model is the same as the one described in Sec. 4.3.1; to shed some light in this regime we iterate longer to see the behaviour of the MSD. The MSD(t), for $0.999 < E < 1.003$

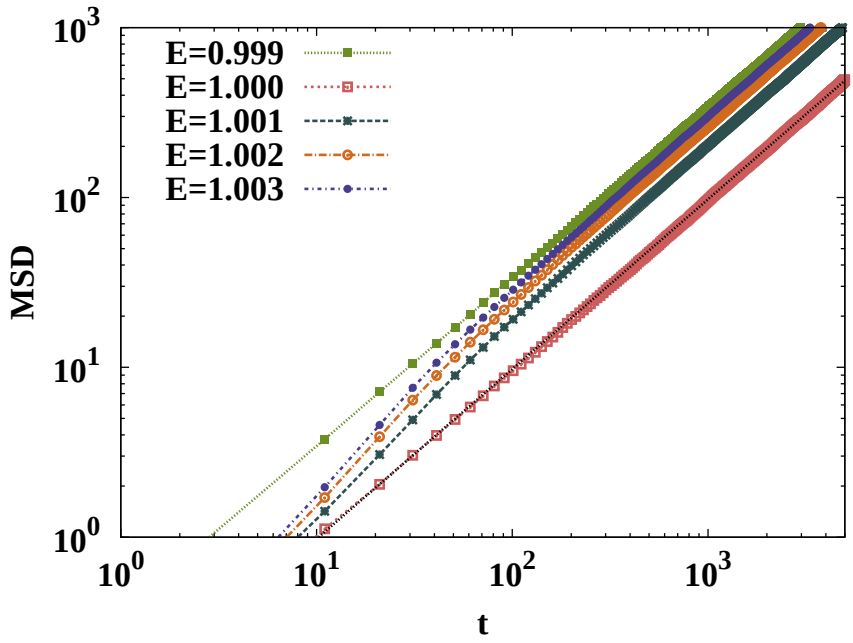

Figure 4.7: MSD in transition zone in the model with high density of scatterers. Input parameters: same as Fig. 4.4.

shows normal diffusion although there are some features that distinguish the MSD at $E < 1$ from the rest. If we look at Fig. 4.7, we can see that there is a transient in the MSD of energies $E = 1.001$, $E = 1.002$, and so on, but it is not present at $E = 1$ or smaller energy. Also note that if we think of the MSD(t) at some specific time and define the value of MSD(t_i, E) as a function of the energy at time t_i, we see that this function drops at $E = 1$ and increases again for $E > 1$. In other words

$$\text{MSD}(t_i, E = 1) < \text{MSD}(t_i, E = 1 + \epsilon),$$

and

$$\text{MSD}(t_i, E = 1 - \epsilon) > \text{MSD}(t_i, E = 1).$$

Note that, as showed in Fig. 4.4, diffusion seems normal in this neighbourhood and there are no islands in phase space.

At $E = 1 + \epsilon$, the available area in configuration space becomes unlimited

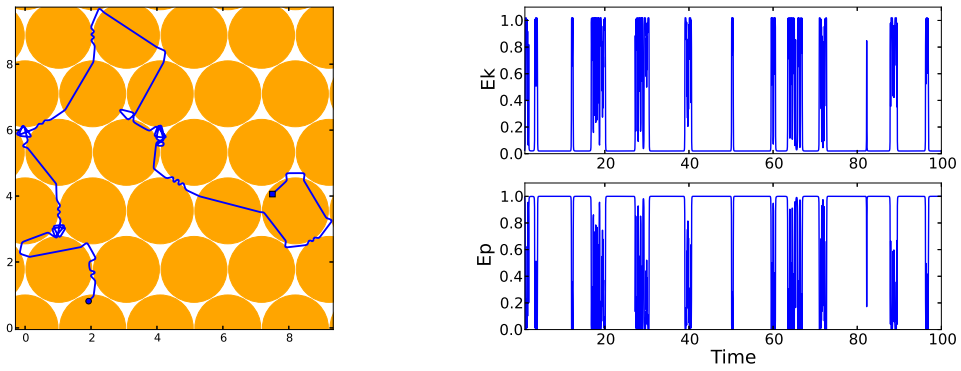

Figure 4.8: Typical trajectory in the transition regime with $E = 1.01$. **Left**: Trajectory in position space. **Right**: Kinetic and potential energy of the particle shown in the left.

and now particles are allow to be everywhere in regions very close to the centre of the scatterers even When reaching this position, the combination is such that particles have very small kinetic energy, not zero, therefore, this causes a sort of semi trapping.

In Fig. 4.8 we can see an example of this process, on the left we see a typical trajectory in configuration space, here the particle travels across the top of the scatterer, it should do it with very small kinetic energy, then when it approaches the end of the scatter, approximately at the boundary of the yellow circle, it will travel faster but at the same time interacting with the potential, performing normal scattering. Note that the particle does not cross the scatterer trough the top, it bounces slowly in the opposite direction (slow scattering). Also, note the pattern in the series of the E_k and E_p in Fig. 4.8. The time series resembles an intermittent process (see Sect. 2.6.1), although we can not make a statement about this at this moment, further analysis is needed to stablish the existence of such a process in this regime.

Random walks with traps of slow motion

By now it is clear that the mechanism that gives raise to $D(E)$ in this interval where $E \to 1^+$ deserves special attention. We will develop a new random walk

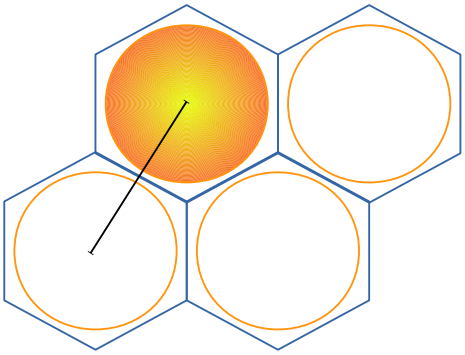

Figure 4.9: Hexagonal unit cell. The circle represent the area where we assume a constant velocity or constant maximum potential. We use this area as a trap. The black line indicates the distance between centre traps.

approximation in this regime inspired by traps of slow motion.

We need to redefine a trap and also compute the average rate at which a particle leaves this trap, τ^{-1}. As we mentioned, when the particles climb over the potential their kinetic energy is very small, thus this creates a semi-trapping mechanism. It is not straightforward to determine exactly the area where this occurs since it would depend on a definition of "slow motion". The potential is radially symmetric at each lattice point, so let us assume that the trapping mechanism takes place on a circle with some radius r_s centred here.

If we look at Fig. 2.8, because of the shape of the potential, we have that as $s_o \to 0$ the wider the top of the potential becomes. And, we would have that $r_\mathrm{s} \to r_o$ as $s_o \to 0$.

Let us take r_s as a first rough approximation. We will consider the circle with radius r_s as the trap. The trap is pictured in Fig. 4.9 as a yellow scatterer with radius $r_\mathrm{s} = r_o = 1$.

In order to calculate the velocity we will assume that inside the trap, or circle, the velocity is constant. If we assume that the potential energy is maxima in this circle, then the kinetic energy is minima, then the velocity is minima, thus $v_\mathrm{min} = \sqrt{2(E - V_\mathrm{max})}$ or $v_\mathrm{min} = \sqrt{2(E-1)}$ if $V_\mathrm{max} = 1$.

The total phase space of the trap is $\Omega = A_\bullet 2\pi v$, where $A_\bullet(r_\mathrm{s})$ is the area of

the circle with radius r_s and v is some constant minimum velocity as explained before.

Then the available phase space where particles leave the trap in time Δt is

$$\omega = L \times 2v^2,$$

where v is a constant velocity and L is the length of the available portion of the trap where particles escape, *i.e.* the length of the circumference with radius r_s.

Altogether, the escape time reads

$$\tau(E, v) = \frac{A_\bullet(r_\mathrm{s})}{2r_\mathrm{s}v_\mathrm{min}}.$$

We can then take $\tau(E)$ and substitute in the random walk approximation $D = l^2/4\tau$, where l is considered to be the distance between to traps or centres of scatters as illustrated in Fig. 4.9 and is given simply by the geometry of the problem $l = 2r_o + w$.

Finally we get

$$D_\mathrm{s}(E, v) = \frac{r_o(2r_o + w)^2}{2A_\bullet(r_\mathrm{s})} v_\mathrm{min}(E). \tag{4.13}$$

In this approximation we see that

$$D_\mathrm{s}(E, v) = \mathrm{const} \times v_\mathrm{min}(E) = \mathrm{const} \times \sqrt{2(E - V_\mathrm{max})},$$

and note that if we choose a constant potential $V = 1$ this expression does not depend on the factor s_o, therefore the closer to the hard limit the better the approximation should be and we get that for $E \to 1^+$

$$D_\mathrm{s}(E) \sim \sqrt{E - 1}. \tag{4.14}$$

Now, let us compare the numerical results with the approximation for $D(E)$ when $E \to 1^+$. In the left panel of Fig. 4.10 we show the diffusion coefficient in the transition regime as well as a fit to the data of the form $D(E) = a(E - 1)^b$. The

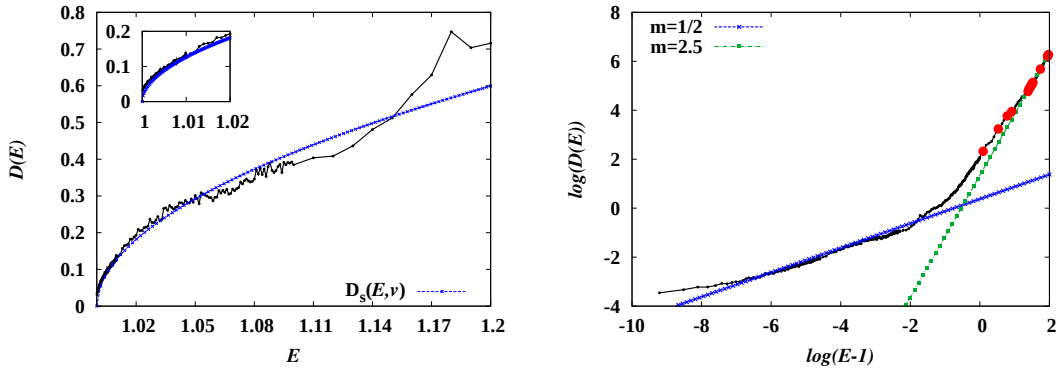

Figure 4.10: Transition regime $E \to 1^+$. Black dotted line: Numerical results as in Fig. 4.4. **Left:** $D(E)$ lin-lin and random walk approximation Eq. (4.13). **Right**: $\log D(E) vs \log(E-1)$. The blue line has a slope 1/2 and the green line has slope 2, the red dots indicate the presence of stable islands in phase space.

starting point for the fitting parameters is from Eq. (4.13) with $r_s = r_o = 1$. With the fitted function $D(E) = a(E-1)^b$ we get an exponent $b = 0.518$ in the energy interval (1.0001, 1.2) matching qualitatively the analytical description in Eq. (4.13).

The approximation we developed here makes assumptions on the radius r_s, and does not match exactly the shape of $D(E)$, on the other hand, it reveals the asymptotic form $\sqrt{E-1}$ as $E \to 1^+$. This means that in this regime the motion of particles is dominated by slow motion in the centre of the scatterers.

To see this more clearly, we plot $\log D(E) vs \log(E-1)$, see right panel of Fig. 4.10. Here, we can see the regime where the data matches the blue line with slope $m = 1/2$, equivalent to the square root in the lin-lin graph, as well as the transition to a different regime where $m = 5/2$, see the green line. Note also that there is a discrepancy in the data with the approximation for small values of $\log(E-1)$, or $E \to 1^+$. This is a sensible regime since we are dealing with energy values close to the unit with many decimal points, which can introduce numerical problems. Moreover, recall that the approximation assumes that the potential, V, and the radius of the potential, r, are constants in the area $A_\bullet$. The model that we use for the simulations sets V as a smooth function of the position, on the other hand in the approximation there is an abrupt jump at r_o. Performing

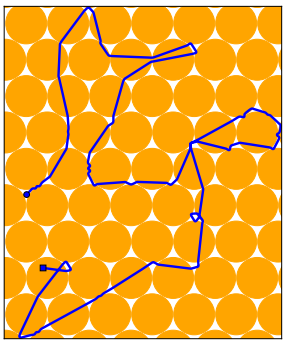

Figure 4.11: Typical trajectory with energy $E = 1.2$ appearing in the model with steep potential and high density of scatterers.

higher precision numerical simulations and modelling $V_{\max}$ as accurate as possible could reduce the difference between the approximation and the data enhanced by the logarithm scale.

When looking at typical trajectories in configuration space we note that for energies in the first zone with $m = 1/2$ the scattering occurs in the zones of small potential, the particle bounces there and then it travels to a trap and travels in the same direction until again it is randomized by the same mechanism (see Fig. 4.8). On the other hand, when particles have $E > 1.2$, a typical trajectory illustrated in Fig. 4.11, particles travel in some given direction until they interact with a scatterer and change its direction once. After changing the direction it travels in the new direction until it gets perturbed again, scattering takes place on a bigger scale.

The form of $D(E)$ comes from a combination of particles that travel with small velocity along the yellow scatterers and randomizes in the middle of the zones with minimum potential energy, and a contribution from particles that travel in straight lines until they get scattered slightly by colliding with a scatter. This last effect is more pronounced as energy is increased.

Physically it means that particles with high energy are less likely to change direction, therefore they travel for longer times before they get scattered. More important than the separation of the scatters, the increment of the energy allows

particles to travel for long times before changing its direction.

Then at $E > 2$ it is not clear what the functional form of $D(E)$ is since we face the appearance of islands in phase space that destroy diffusion. These are marked with red dots in the Fig. 4.10. The islands appear and disappear allowing normal diffusion to exist again for larger energies. In the next section we deal with this energy regime and find the exponent of the curve $D(E)$. For higher energies we will need to provide evidence for the existence of normal diffusion.

4.3.3 High energy regime and law $D(E) \sim E^m$

Our quest is to characterize the diffusion coefficient $D(E)$ at large energies, if there is one. Here we will show numerical results and compare them to Aguer's and Nobbe's theories. Recall that in Aguer's *et. al.* [ADB10] description of large energies, they conclude that for sufficiently large energies

$$D(E) \propto E^{5/2}.$$

First we need to make sure that we deal with an interval in the energy parameter that exhibits normal diffusion.

We analyse the MSD similarly as in Chapter 3. The convergence of the MSD has been tested by extracting the slope, α, of the MSD in different intervals of time. If there is an increment of the α instead of convergence, this would imply no normal diffusion.

The MSD by itself should, in theory, indicate if there is normal diffusion. Unfortunately we have limited computing time and we use a finite number of particles. This means that there is a chance of ignoring crucial initial conditions, or that we do not iterate long enough to see an anomaly. Considering these factors is especially important in this regime, because as the energy parameter is increased to high energies, the particles move faster and consequently travel long distances before changing their direction, meaning that the randomization process takes longer than in the small energy regime.

Given a selection of parameters, if the corresponding phase space contains tiny islands of stability due to quasi ballistic trajectories, it is possible that the ensemble does not catch them due to numerical limitations. The smaller the island, the harder to see its effect by these methods. To avoid mistakes we look at specific regions of the phase space via PSoS. We will try to detect islands of stability in a given interval of energy. Of course, if we find that there are islands of stability due to q-b trajectories in phase space, then our analysis is inconclusive, since this would mean that normal diffusion does not exist. This method only requires to follow some specific orbits for some time, just enough to detect periodicity.

As we will see later, trying to find islands is crucial to compute the diffusion coefficient, since sometimes even when the MSD looks to grow linear with time, in reality we might be in one of the cases where either the ensemble is too small to catch q-b trajectories, or the systems needs to be iterated for longer to see the effects of q-b trajectories. Once we choose a safe interval where we can compute a final curve $D(E)$ we also estimate an error in $D(E)$ from the numeric computed diffusion coefficient. The error we get is from fluctuations of the $MSD(t)$ and it goes beyond the convergence analysis, as will be explained in more detail later.

Finally, we compare Aguer's and Nobbe's theory with numerical results.

MSD at large energies

In Fig. 4.12 we show the MSD for high energies $E > 1$, the black line indicates a slope equal to 1. From this results it seems that the MSD grows linear with time for almost all energies shown. However, as we stated earlier this observation might not be enough to conclude the existence of normal diffusion. If we look at the MSD for $E = 30$, we observe linear growth. It is unclear whether this is only the case for this energy parameter or it continues like that for all $E > 30$. Moreover, we have iterated for a finite time and nothing guarantees that at longer times the trend of linear growth disappears. Computing the MSD for longer times gets almost impossible since we have limited computational time. We observe another element which can help us to deduce normal diffusion, that is the phase space in which we look for islands of stability.

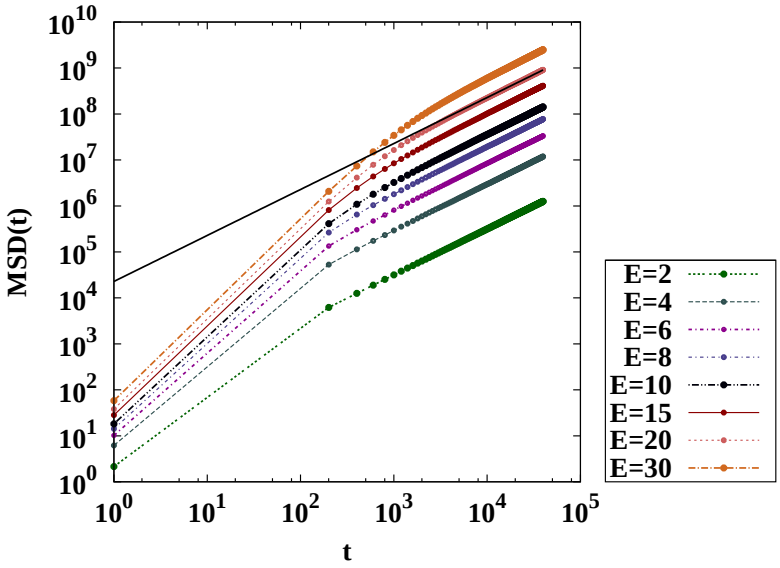

Figure 4.12: Behaviour of the MSD for different energies in high energy regime (model with high density of scatterers). The black line indicates slope 1.

Periodic trajectories and islands in phase space

We mentioned earlier that although we are not interested in the evolution of islands in phase space, we emphasize the need to identify all q-b trajectories and exclude intervals where they exist to calculate safely the diffusion coefficient. When we look at the phase space we find islands that exist for many parameters: some trivial islands that follow main symmetry channels due to the focusing of the potential walls and others that form due to the high energy of the particles.

The structure of the phase space is rich even for small energies. Given that the islands are bigger than certain epsilon, the diagram in Fig. 4.13 indicates the existence of potential islands, some of the points might be representing sticky trajectories. At $E = 5$, we find a peculiar trajectory that emerges from the needle trajectory. Only this time it has enough energy to go to the next scatterer below or above and continues travelling in the same direction. At $E = 5.6$ the island disappears after the bifurcation occurs. The process corresponds to the points in the lower left corner in Fig. 4.13. As we move to higher energies, we find different q-b trajectories at $E = 8$, $E = 10$ $E = 13$, all of them travel just like the

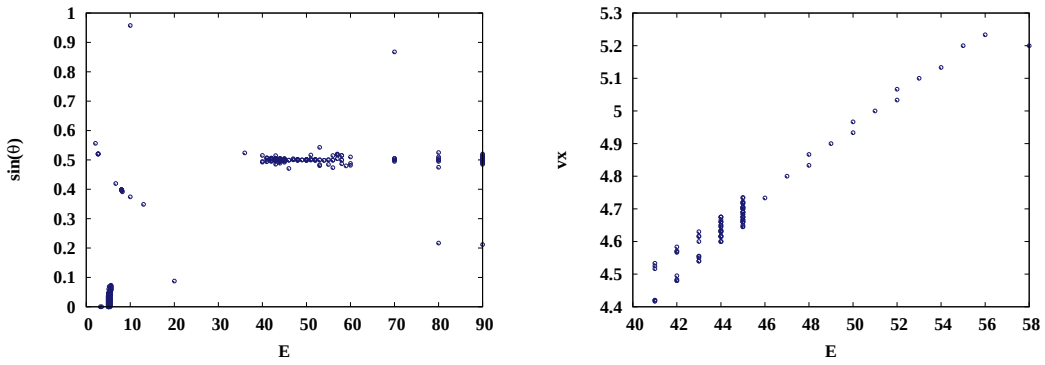

Figure 4.13: Islands in phase space: Model with high density of scatterers and steep potential. Each point represents a potential stable island in phase space along the energy parameter. **Left**: The y-axis indicates the sin of the angle θ of the velocity vector at the moment of exiting the gap. **Right**: The same as in the left (considering the velocity v_x in the y-axis) where we can see a bifurcation (backward).

one we describe with a small perturbation. There is a fixed point formed by the trajectory that crosses just in the middle of the trap and the surrounding initial conditions give rise to trajectories that travel in the same direction and bounce slightly to create islands in phase space with different period. These correspond to the branch of points in the middle left region of the diagram. From the diagram, there is another q-b trajectory at $E = 10$, this is a zig-zag like trajectory with a high order periodicity. In contrast, at $E = 2.7$ and $E = 9.0$ there are q-b islands where the trajectory follows a path in the main symmetry axis (f-f trajectory). The shape of the q-b trajectories gets diverse and it tell us about the kind of jumps that particles are more likely to perform.

At the moment we are just interested in the existence of such trajectories along the energy parameter, such that we can exclude these parameters from the calculation of the diffusion coefficient. From the diagram in Fig. 4.13 we see that there is a gap from $20 < E < 40$ where no islands were found with the methods available. The islands at $E = 40$ go trough a backward bifurcation. The bifurcation occurs form right to left, where the island eventually disappear in the process the stickiness of the orbits is present. But in the other direction, higher energies, regular island are clear. The bifurcation and the corresponding quasi ballistic trajectory are shown in Fig. 4.14. In phase space the island is symmetric

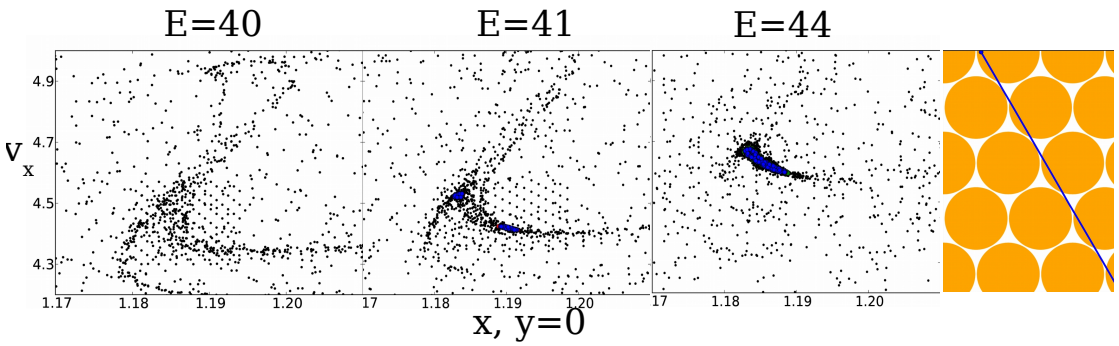

Figure 4.14: Backward bifurcation around $E = 40$. From the left to the right the energy parameter is $E = 40, 41, 44$. The trajectory corresponding to the islands is shown in the right.

and by increasing energy it covers more and more area in the PSoS. We have explored PSoS in energies as large as $E = 90$, the island shown in the figure persists and gets bigger, occupying a big fraction of the phase space. By its shape and evolution in configuration space we conjecture that this orbit exists for all $E > 40$. We select then as an upper bound for the calculation of the diffusion coefficient $E = 40$.

D(E) curve and exponent

To get the curve $D(E)$ we can consider an interval of energies $14 < E < 19$ or $21 < E < 40$, if we ignore the peak at $E = 20$ we can choose $14 < E < 40$.

We are interested in finding a power law for $D(E)$. It is easy to illustrate this by plotting $D(E)$ in $\log - \log$ and finding the slope, which is equivalent to find the exponent. The diffusion coefficient along with an error estimation are shown in Fig. 4.15. The error for each $D(E)$ is represented in bars, the green line indicates a slope $m = 5/2$. We usually obtain the diffusion coefficient as described in Sect. 2.7.2; from the slope α of a linear fit of the MSD in an interval of time, let us say in the interval $(3/4t_{\mathrm{T}}, t_{\mathrm{T}})$, where t_{T} is the total iteration time, and call $D = \alpha/4$. Additionally to this value for the diffusion coefficient we estimate an error for each value of the energy from the fluctuations of the MSD as follows. The MSD of representative energies is shown in Fig. 4.12. First take the slope of

Energy	fit	+/−
$2 < E < 35$	2.524	0.0188
$14 < E < 40$	2.540	0.0186
$21 < E < 35$	2.521	0.0376
$21 < E < 40$	2.545	0.0257

Table 4.1: Exponent m in $D(E) = aE^m$ obtained from fits on different intervals of energies. See text for explanation.

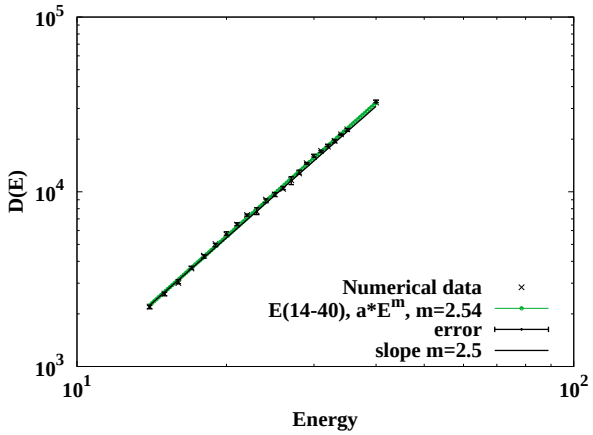

Figure 4.15: Numerical estimated diffusion coefficient as a function of the energy in the model with high density of scatterers and steep potential. Numerical data: same as in Fig. 4.4. Black line has slope $m = 5/2$.

the line formed by the points $(t_i, MSD(t_i))$ and $(t_\mathrm{T}, MSD(t_\mathrm{T}))$. So the slope at each t_i is

$$\alpha_i(t_i) = \frac{MSD(t_\mathrm{T}) - MSD(t_i)}{\Delta t},$$

where t_T is as indicated above the final time and $\Delta t = t_\mathrm{T} - t_i$. Then look at the time series $(t_i, \alpha(t_i))$. For $t_i < t_\mathrm{T}$, there should be an interval of time where the oscillation is small before getting too close to t_T. Now take the highest and smallest value of $\alpha(t_i)$ as an upper and lower bound respectively and call it α_min and α_max. So the error bar comes from $D_\mathrm{min} = \alpha_\mathrm{min}/4$ and $D_\mathrm{max} = \alpha_\mathrm{max}/4$. These values give an indication of how close we are to the exact numerically computed diffusion coefficient.

If we take $D(E_j)$ and fit to a function of the form aE^m in the intervals of energy $(21, 35)$, we get $m = 2.54$. More fits and its exponents, along with an error due to the fitting routing (GNUPLOT), are presented in table 4.1.

Overall, the behaviour seems to be very close to the one predicted by Aguer's theory, where $D(E) \propto E^{5/2}$, but very different from Nobbe's conjecture. By observations of trajectories in configuration space, our model behaves similarly to the dynamics shown in Aguer's model, where particles travel for long times before

changing the direction by a small angle. In contrast, in Nobbe's model particles travel for short distances and change the direction of the path by a large angle. This was noted also in Aguer's paper [ADB10]. We note that in Aguer's numerical results normal diffusion is always the case even for large energies because of the construction of their model, which guarantees randomization.

We have found that our results share many similarities with Harayama and Gaspard (2001) [HG01], where they modelled a particle bouncing with the floor composed of circular scatters. There, the diffusion coefficient shows a non trivial, fractal like, dependence as a function of the energy. They found small stability islands and by introducing weak noise the islands disappear yielding normal diffusion. The weak noise is introduced by randomly changing the outgoing angle after collisions.

The dynamics under a perturbation or weak noise is similar to Aguer's model, in which among all the random variables in their random walk, the angle after collisions is one of them. That is the mechanism that makes normal diffusion in all the parameters of energy that they explore, in this analogy the model we implemented here lacks the perturbation that destroy the islands. We have found that our numerical results agree with Aguer's law $D(E) \sim E^{5/2}$ within the range of parameters where we found normal diffusion and clearly disagree with Nobbe's theory where $D(E) \sim E^{3/2}$. The differences in the dynamics between models might be also due to the different kind of potentials, Nobbe's theory is based on an attractive potential whereas the potential used in Aguer's and this study is repulsive.

4.4 Diffusion in a shallow potential and low density of scatterers

In this section we test the universality of our previous results with respect to parameter variation. For completeness and consistency we will structure the section just as in Sect. 4.3: the study is split in three regimes of energy just as in the

previous case: small energy regime, a transition regime and a high energy regime.

We start by describing the relevant physical parameters in the system that we are using. The softness of the potential is $s_o = 0.05$, which is the same as the one used in model in the model in Chapter 3 but now with fixed separation of scatterers at $w = 0.3$. These parameters yield a shallower version of the model studied in Sect. 4.3, inspiring the title of this section.

With this setting in the small energy regime we will compare the random walk approximations $D_{\mathrm{MZ}}(E)$ and $D_{\mathrm{B}}(E)$ developed before to numerical results by varying the energy parameter, as well as elaborate on the impossibility of observing normal diffusion for larger energies.

4.4.1 Global numerical results - summary of D(E)

We will present results of $D(E)$ separately: small and high energies, now we will give a wide presentation of $D(E)$ in a broad interval (and comment on the transitions regime at $E = 1$). The numerical results are summarized in Fig. 4.16. The functional form of $D(E)$, is not uniform and we can clearly distinguish different regimes.

We start with the small energy regime where we try to approximate the diffusion coefficient via random walk approximations by ignoring the peaks although the mechanism that generates the peaks contributes to the general form. Then, the transition regime where $E \to 1^-$ here gets obscured by islands in phase space and we can not see clearly the trend.

As we move to high energies more q-b trajectories appear and these exist for all $E > E^*$ therefore we can not make a conclusion about diffusion in the high energy regime. We conjecture that islands dominate the phase space as energy increases.

In this section we will elaborate on the following points:

- For $E < 1$, explain the structure of $D(E)$ and indicate if is possible to separate the free flight and the random walk like regime.

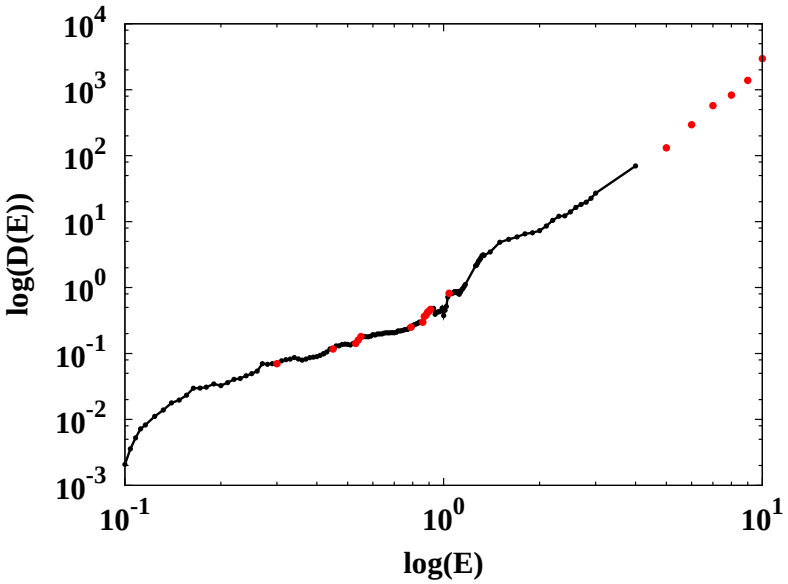

Figure 4.16: Model with shallow potential ($w = 0.3$, $s_o = 0.05$ and $r_o = 1.0$): Numerical results of the diffusion coeffcient $D(E)$ in $\log - \log$. Red dots indicate that we have found a stable island, we lack information for the intervals in-between. These gaps obscure the actual shape of $D(E)$.

- Explain the increment of the $D(E)$ in the regime $0.5 < E < 1$ in terms of periodic orbits.
- Show a numerical exploration where islands are eventually ubiquitous for $E > 1$.

4.4.2 Small energy regime and random walk models

We take our approximations for $D(E)$, equations $D_{\mathrm{MZ}}(E)$ and $D_{\mathrm{B}}(E)$ (Eqs. (4.8) and (4.11)), and compare them to numerical results. The model input parameters are $w = 0.3$, $s_0 = 0.05$ and $r_o = 1.0$ and we use iteration time $t = 5000$ and ensemble size $n = 100000$. Recall that in the Lorentz gas $w = 0.3$ is beyond the random walk regime (see Fig. 2.6), hence Machta and Zwanzig's random walk does not apply there. We emphasise that with these settings we do not expect an exact match of the approximations with the actual form of $D(E)$ but a qualitative one.

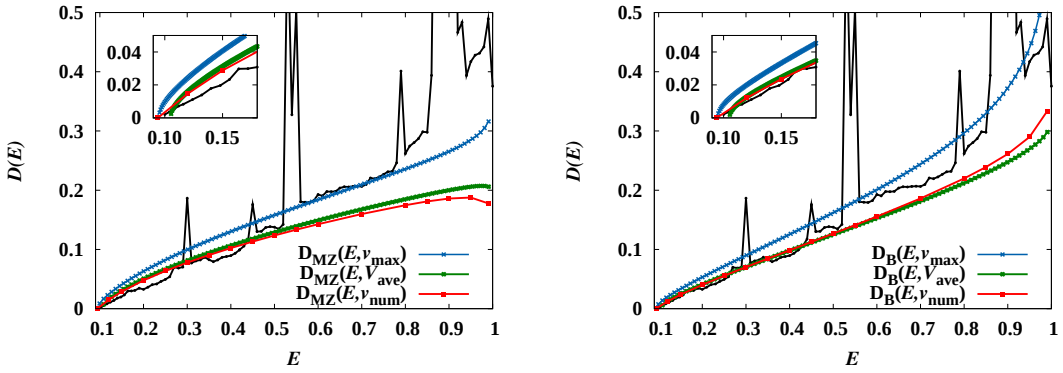

Figure 4.17: Diffusion coefficient as a function of the energy in a model with shallow potential: Numerical data and random walk approximations (input parameters $s_0 = 0.05$, $w = 0.3$, $r_o = 1.0$, ensemble size 100000 and iteration time 5000). **Left:** Machta and Zwanzig approximation $D_{\mathrm{MZ}}(E)$ Eq. (4.8). **Right:** Boltzmann approximation $D_{\mathrm{B}}(E)$ Eq. (4.11). Green lines indicate that an average potential has been used and blue lines a maximum velocity. Red lines indicate a numerical computed average velocity.

In Fig. 4.17 we can see the numerical results and the approximations, $D_{\mathrm{MZ}}(E)$ and $D_{\mathrm{B}}(E)$. From the numerical results we see that this system is more irregular in the sense that we found more peaks along the energy parameter. Observe also that this model seems to have qualitatively different functional forms in three different regimes $E_* < E < 0.5$, $0.5 < E < 0.8$, and $0.8 < E < 1$.

In the left panel of Fig. 4.17 we show D_{MZ}. First we note that $D_{\mathrm{MZ}}(E, V_{\mathrm{ave}})$ with average velocity misses the threshold, though the effect is not as strong as in the case presented in Sect. 4.4. Here, the separation of scatterers is large enough so that the discrepancy between radius, approximated radius and real radius, is very small.

For small energies close to E_*, the approximation with an average numerical velocity seems to match the asymptotic form of $D(E)$ when $E \to E_*$. It has the characteristic of preserving the threshold as well as the shape of $D(E)$ up to $E = 0.4$. $D_{\mathrm{MZ}}(E, v_{\max})$ overestimates diffusion on small energies, but it matches very well the data in $0.55 < E < 0.8$. Does this mean that particles leave the trap preferably with maximum velocity which happens in the middle of the gap? We will put to test this hypothesis by calculating numerically the probability of escaping trough different zones in the exit of the trap.

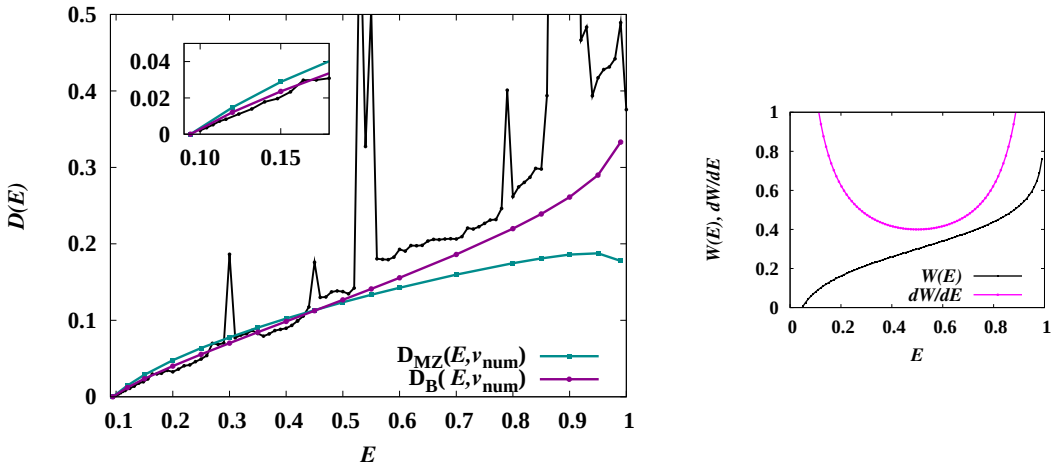

Figure 4.18: Model with shallow potential. **Left**: Black dotted lines: numerical simulations as in Fig. 4.16. Comparison between approximations $D_{\mathrm{MZ}}(E)$ and D_{B}(E) in the small energy regime. Data: same as in Fig. 4.17. **Right:** Gap size $W(E)$ (*c.f.* to Fig. 4.1), and its derivative $dW(E)/dE$.

Now, in the right panel of Fig. 4.17 we can see the approximation $D_{\mathrm{B}}(E)$ with the different velocities. Observe that in general $D_{\mathrm{B}}(E)$ follows $D(E)$ even for high E, $E < 1$. In the inset, we can see that $D_{\mathrm{B}}(E, v_{\mathrm{num}})$ follows very closely the data as $E \to E_*$.

The asymptomatic behaviour of $D_{\mathrm{B}}(E) \to \infty$ as $E \to 1^-$ is understood from the equation (4.11). This is an artificial effect due to the construction of D_{B} in terms of $r(E)$ which is in the denominator of D_B.

To see more clearly the differences between approximations in Fig. 4.18 we compare $D_{\mathrm{MZ}}(E, v_{\mathrm{num}})$ and $D_{\mathrm{B}}(E, v_{\mathrm{num}})$. The point where D_{MZ} deviates from the data is around $E = 0.5$. But in general, $D_{\mathrm{B}}(E)$ is a better representation of the diffusion coefficient, especially for high energies where it follows the trend of the numerical results if we ignore the peaks.

To understand why $D(E)$ seems to have different regimes we look at the gap size $W(E)$. Recall that $W(E) = L - 2r(E)$, so the shape of the potential that is included in $r(E)$ has an effect also on $W(E)$. We can see the shape of $W(E)$ in the right of Fig. 4.18. The change in $W(E)$ is stronger just after $E = 0.5$ which is the turning point and we can see it in the derivative of $W(E)$, $dW(E)/dE$. At this

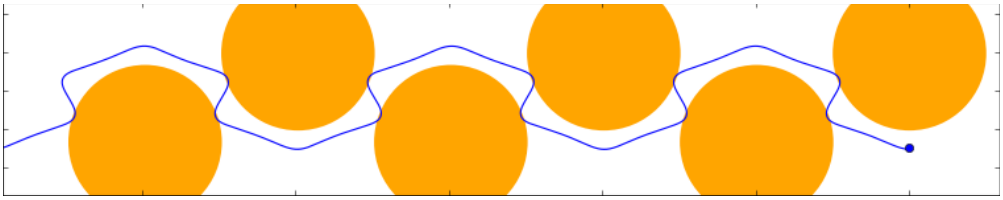

Figure 4.19: Quasi ballistic trajectory at $E = 0.88$ present in the model with shallow potential. The yellow circles have radius 1 and illustrate where the scatterers in the original hard Lorentz gas would be positioned.

critical point not only the particles have more chance to escape but the concavity of $W(E)$ changes, affecting the dynamics and possibly yielding a process where the jumps from traps to traps occur with higher velocity.

This effect might not appear clear in $D(E)$, since at $E = 0.5$ there is a peak which takes us to another factor to consider: there are islands that appear in the surrounding interval, at $E = 0.5$ and $E = 0.88$ consequence of quasi ballistic trajectory. Let us explore in more detail the corresponding trajectories and try to find a relation between them and the type of diffusion in between parameters.

From the analysis in Chap. 3, where $E = 0.5$, we identify a quasi ballistic trajectory at $w = 0.3$, which is also present here. The trajectory and respective island are shown in Fig. 3.10. Then, note also that around $E = 0.88$ there is another q-b trajectory. The shape of this trajectory is shown in Fig. 4.19.

The conjecture, or heuristic argument, is the following, we observed that there is a different regime that starts after a peak due to a quasi ballistic trajectory at $E = 0.5$. From the shape of the trajectory, we observe that it travels trough regions with maximum velocity. After the peak, there are some trajectories that behave likewise for some finite time, sticky trajectories. The trajectories perform correlated jumps between unit cells with similar behaviour which also mean that they travel with maximum velocity for some time before scattering. This process enhances the diffusion coefficient as the MSD gets affected.

Eventually, the stickiness effect should be less, since we observe normal diffusion, but as we approach $E = 0.88$ the shape of the trajectory at this energy is present.

These trajectories travel between traps with velocities v_1 and v_2. The trajectory follows a path $rrll$ in terms of symbol probabilities. It crosses the unit cell in two jumps transversally. Observe that the trajectory travels through zones with small potential in two consecutive jumps in the same direction rr or ll. This accelerates the particle, then it crosses again trough the middle slowing down. If this trajectory inherits its ballistic motion property near its domain we can test it by observing 1 and 2−symbol probabilities as in Chapter 3 Section 3.3.3.

All these factors are related and play a role determining the dynamics of the system. The nature of the dynamics is such that the particle finds it easy to travel fast with this kind of jumps. As a result we observe that in this regime the slope of $D(E)$ increases.

4.4.3 Intermediate energy regime: slow motion

At the beginning of this section we showed a comprehensive scenario of $D(E)$ (see Fig. 4.16). As energy increases we note that the diffusion coefficient exhibits an intricate shape as a function of the energy.

Recall that at $E = 1+\epsilon$ the particles have enough energy to cross the scatterers inducing a slow motion trapping mechanism.

Although this regime is interesting for $E > 1$ here the shape of $D(E)$ is obscured by islands. The separation between scatters here is bigger so the diffusion coefficient is not mainly dictated by traps of slow motion but by randomization between scatterers. And, what we see in this zone are the leftovers of the trapping mechanism. The regime $E > 1$ was studied in detail in section 4.3, where the slow motion trapping is more prominent.

4.4.4 High energy regime and islands in phase space

We are interested in finding a law that can characterize the diffusion coefficient as a function of large energies, not so much in the structure of the phase space.

Nevertheless, understanding what happens in phase space as we move along parameters allow us to choose parameters that yield normal diffusion. Therefore we discuss briefly the evolution and geometry of the island in phase space.

Note that as the energy is increased particles travel, more or less, in the same direction for longer times than at small energies. It makes sense to compute the MSD in times sufficiently large until the dynamics gets randomized allowing to extract a good estimation of the diffusion coefficient. Buts this is not always the case.

The key here is not to iterate for large times because as we will see normal diffusion simply does not exist in some parameters because of the appearance of q-b trajectories. For instance, look at Fig. 4.20. There the MSD of different ensembles with different energies are shown. One could, erroneously, take the slope in something that could look like a linear regime, but the real nature of the dynamics reveals itself at sufficient large times. As is clearly illustrated in the figure, although it might appear that the MSD has reached a linear regime, if we iterate longer we realize that the MSD does not grow linearly in time. For instance

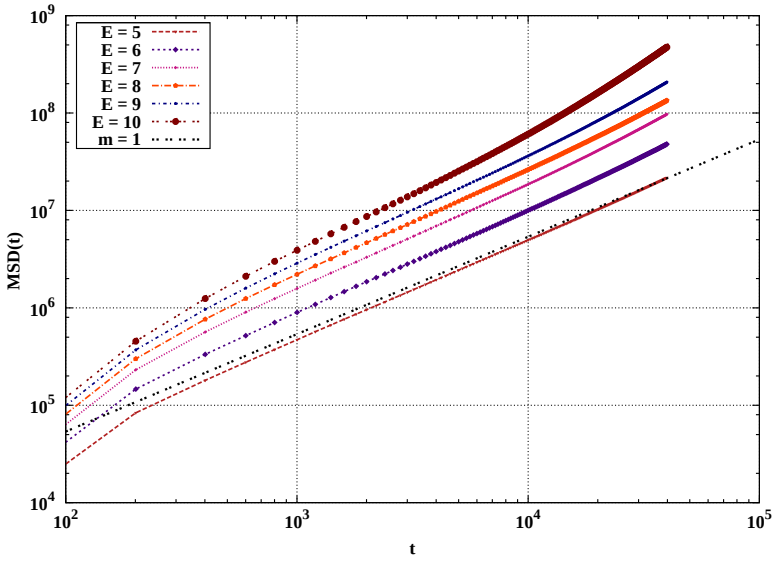

Figure 4.20: Typical MSD at different energies in the model with shallow potential. Observe that the MSD of $E = 10$ is not linear with respect to time but only becomes clear until very large times.

in $E = 10$ where after $t = 10^4$ it is obvious that the MSD grows faster than linear. Therefore normal diffusion does not exist for this parameter.

By now, it is clear that there are islands in phase space that appear and disappear depending on the choice of parameters. Is this the case for any arbitray large energy? We note that as we move to high energies, stable islands get bigger and look like they exist for all larger parameters.

In this model, diffusion ceases to be normal around $E = 5$ due to the appearance of a quasi ballistic trajectory, see Fig. 4.21. This trajectory goes in the direction of a main symmetry axis, it bounces with every scatter in its way. If we follow the path, it first touches tangentially an equipotential line and the next interaction with the scatter is with an equipotential line closer to the maximum but returns symmetrically to the next scatter where, again, it touches tangentially the first equipotential line. The PSoS shows its respective island and stickiness of trajectories around. It is clear that this orbit kills diffusion, even if the ensemble in the simulation does not catch one of this trajectories, the stickiness effect will play a role in the behaviour MSD given enough time.

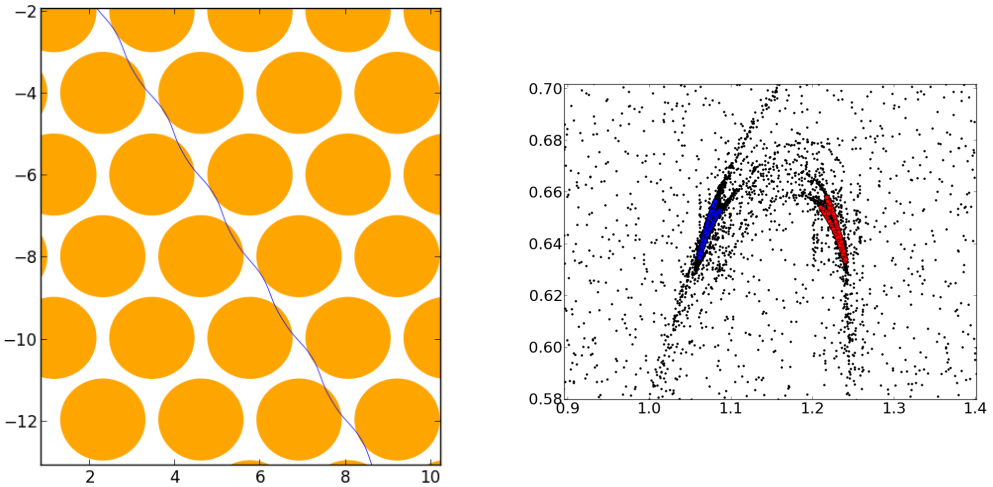

Figure 4.21: Left: Quasi ballistic trajectory appearing in the model with shallow potential, at $E = 5$. The yellow circles have radius 1 and illustrate where the scatterers in the original hard Lorentz gas would be positioned. **Right**: a fraction of the PSoS (trajectory on the left) showing a bifurcation. The y-axis indicates the sin of the angle θ of the velocity vector at the moment of exiting the gap.

Is there a transition for large E where this trajectory is destroyed? The topology of this trajectory is the same as the one founded in the study of $D(w)$ for large w ($w = 0.90$), where we were up to the conjecture that it existed for $w \to \infty$. In other words, what is the onset of the infinite horizon due to this trajectory? We need to work out an argument that guarantees its existence for $E \to \infty$.

In simulations with $E = 10$ we found another island in phase space due to a trajectory that crosses the middle of the gap. It seems to be of the same nature of the trajectory just described in earlier, for $E = 5$ in the previous model. In this case, the island exist for all higher energies.

Then, for even higher energies, about $E = 20$, we found a non trivial trajectory, this one with a higher order symmetry. It touches tangentially one scatterer, then goes over the top of two scatterers and then again, it touches tangentially another scatterer.

We try to capture the essence of the island appearing as we change the energy parameter, see Fig. 4.22.

There each point represents a possible island. We observe that in small energies some islands disappear but at higher energies others exist in a large interval of energy. The islands in the branch in the middle correspond to the same type of trajectory as the one found in Fig. 4.21. As energy increases different islands due to quasi ballistic trajectories coexist. The points at the bottom correspond to the high order period island at $E = 20$ and the points at the top of the diagram correspond to the vertical trajectory.

If our conjecture is correct, this trajectory exists for all energies larger than a critical point ($E \approx 5$) and we can not find a law for normal diffusion. Compare also to Fig. 4.20, long time is required to capture the ballistic nature of the q-b periodic trajectory in the MSD. In contrast to the model presented in Sec. 4.3 here these type of trajectories start to appear at smaller energies.

Since we want to find m in $D(E) \propto E^m$ as $E \to \infty$ the selection of parameters in this model is not ideal. One needs to find a set of parameters that yields normal diffusion in a relatively large interval of energies if possible.

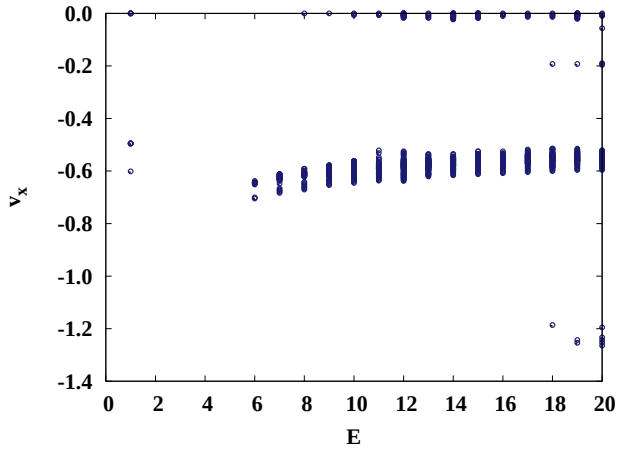

Figure 4.22: Islands in phases space for the model with shallow potential. In this graph: each point represents an island in phase space along the energy parameter. We show the x component of the velocity vector at the moment of exiting the boundary of the unit cell (see Fig.2.1).

In the next section we describe what would happened if we increase the density of scatterers and decrease the smoothness of the potential.

4.5 Existence of islands under variation of parameters

In the same spirit of last section, here we describe the evolution in the energy parameter of a system with the separation of scatterers $w = 0.1$ and softness $s_o = 0.01$ and as usual $r_o = 1$. This systems has a steep potential and high density of scatterers.

We start our analysis by looking at the MSD(t) for different energies, Fig. 4.23. Here, we have used an ensemble size of 40000 particles and iterate up to $t = 40000$. From this figure we can easily conclude that at $E = 2$ there is no normal diffusion, as the MSD grows faster than linear. When we study the phase space we see that this is due to a quasi ballistic trajectory which travels trough a main channel, then it gets destroyed as we move to higher energies. The shape of this trajectory is

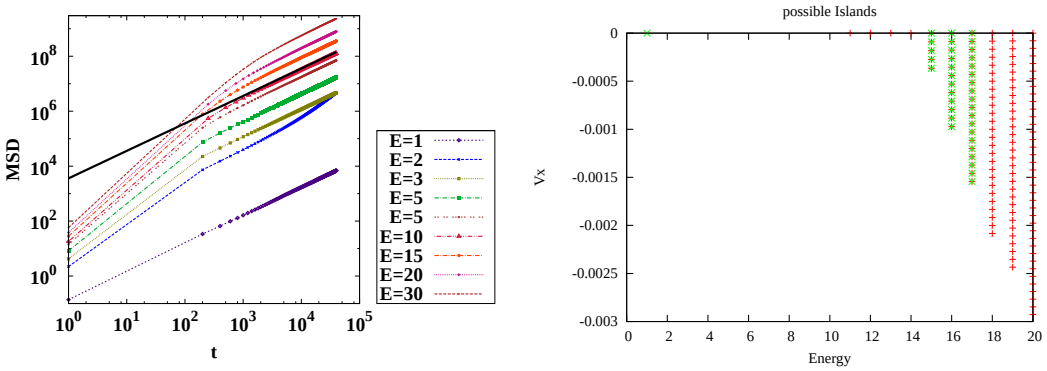

Figure 4.23: Numerical results for the model with $w = 0.10$ and $s_o = 0.01$. **Left**: MSD(t) for different energies, the straight line indicate slope 1. **Right**: Phase space diagram that shows islands of stability for this model.

the same as the one at $E = 0.5$ with $w \sim 0.3$ and $s_o = 0.05$ (see Fig. 3.10).

The rest of the MSD seems to grow linear with time but when inspecting the phase space, there we find quasi ballistic trajectories. At $E = 11$ sticky orbits appear and at $E = 15$ it is numerically possible to detect an island with magnitude $v_x = 0.004$ and $x = 0.006$. The orbit we encounter here is the vertical one, it follows the path illustrated in Fig. 4.24. The islands gets bigger as energy increases. Does it disappear or does it exist for all $E > 15$?

As energy increases, velocity phase space gets more structure as more complicated orbits appear. The period of this orbit increases and is related to a non symmetric scattering of the particle. The mechanism is the same as in the vertical periodic orbit, but with higher period. The particle travels through several scatterers in the same direction until it changes its direction at a specific angle, again it travels the same distance trough the scatterers and so on.

If we track the islands for higher energies, the island evolves and gets bigger as seen in Fig. 4.23. This seems to be an island that exists for all $E > E^*$.

This exercise illustrates the point that, for high energies, even if our ensemble catches crucial orbits we need to iterate for long times to see its contribution in the MSD. In our numerical exploration we came to the conjecture that islands are eventually ubiquitous for $E > 1$ for all parameters w, s_o.

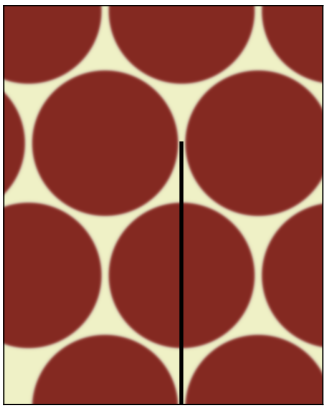

Figure 4.24: Vertical periodic trajectory. This kind of trajectory exists for many values of energy in the model with $w = 0.1$ and softness $s_o = 0.01$.

4.6 Conclusions

Our results indicate that in the energy parameter there are regions where diffusion fails to exists but then we get again normal diffusion as we move in energy parameter. In contrast to Bagchi, Zwanzig and Marchetti's [BZCM85], they conjectured that normal diffusion was only present for $E < V_{\max}$. It might be that the parameters they used are in the normal diffusion regime for all energies, but by smoothing the potential further might yield to a similar scenario as the one we found.

In the first case we presented (steep potential with high density of scatterers):

- For small energies the approximation based on the random walk D_{MZ} predicts the asymptomatic when the energy parameter is close to the threshold. And, D_B dominates for larger interval of energy. Therefore the interval can be regraded as a two different regimes: a random walk regime and a collision less regime.
- Interesting transition regime when $E \to V_{\max}$: this regime is dominated by traps of slow motion. The diffusion coefficient abruptly drops at $E \to 1^-$. This is due the fact that in this regime particles have enough energy to go

over the maximum of the potential but when doing so they have very small kinetic energy. We developed a random walk approximation based on traps of slow motion, near the maxima of the potential, that successfully reveals the asymptotic behaviour when $E \to 1^+$.

- For large energies we learned that the energy dependent diffusion coefficient for large energies with a Fermi potential, when D exists, presents a power law $D(E) \propto E^{5/2}$ in agreement with Aguer's theory. The power law comes from particles following long paths in the same direction before changing direction by a small angle.

From the second model (shallow potential):

- D_{B} is in general a better approximation outperforming D_{MZ} even when $E \to E_*$. Therefore, indicating that motion is dominated by a random walk and free flight along the whole regime.
- In the energy regime where $E \to V_{\max}$ the effect of slow motion trapping is unclear since the separation of scatterers is large enough so that particles can travel between scatters with normal scattering. Therefore we just see a reminiscence of the trapping effect.
- Numerical results suggests that stability islands in phase space are ubiquitous for all $E > 1$ and for all sets of parameters w and s_o. We conjectured that once it exists this special trajectory exists for all energies above.

We suspect that in the system with the soft Lorentz gas the islands obscure the real structure of $D(E)$. The structure we observe in the small energy regime is very irregular. It would be interesting to study the dependence of the diffusion coefficient in the soft Lorentz gas eliminating the islands in which case we should be able to find a large interval of energy.

For those regimes, peaks in $D(w)$ or $D(E)$, where diffusion is not normal the next natural step is to describe it as anomalous diffusion.

Chapter 5

Concluding remarks and outlook

Concluding remarks

In this thesis we studied the deterministic diffusion process taking place in a softened version of the periodic Lorentz gas and we draw the following conclusions:

1. Numerical simulations showed that the diffusion coefficient is an irregular function of control parameters: the separation of the scatterers, the smoothness of the potential, and the total energy of the particle.

   The origin of these irregularities are islands of stability in phase space due to periodic trajectories in configuration space. These periodic trajectories are of quasi ballistic nature in their motion, hence their motion dominates the growth of the MSD, preventing normal diffusion. There is another type of periodic trajectories that suppress the diffusion coefficient, but do not yield sub-diffusion, localized ones. Despite the irregular shape of the diffusion coefficient, when following the islands in phase space along two parameters, separation of the scatters and the softness of the potential, we found that the islands appear in ordered and structured branches. That means that the specific combination of parameters determines the behaviour of the diffusion coefficient.

2. The coarse shape of the diffusion coefficient as a function of the separation of

scatters is well approximated in the limit of high density by a simple random walk argument properly adapted to this soft model. Following these lines, a collision-less flight argument was also developed. For this, the diffusion coefficient is expressed in terms of the escape time between collisions. This is a crude approximation, since collisions do not happen in the presence of a potential field, instead the particle interacts with the potential and bounces. It is only in the limit where the potential is steep that the interaction of the particles with the walls resembles a specular collision. The collision less flight approximation outperforms the random walk approximation in the lower density regime, therefore differentiating a regime dominated by random walk and a second regime dominated by free flight like behaviour. A series of approximations based on the Green Kubo formula were also adapted to this model. These approximations include memory effects between jumps in the simple random walk approximation. Taking into account memory effects improves the approximation of the diffusion coefficient, especially for the low density regime. This implies that the system is not random and higher order correlations are needed to describe the diffusion coefficient. We observed that the correlations are related to the type of jumps between traps, in other words, to the type of periodic trajectories.

3. For the energy dependent diffusion coefficient we studied two different models. From this we learned that the strength and occurrence of the irregularities, as the parameter is varied, depend on the selection of the parameters.

   (a) For small energies, when the energy is less than the maximum of the potential, we defined a gap and the escape time in terms of the energy and tested the Machta and Zwanzig random walk approximation for diffusion, as well as the collision less flight approximation. In all the cases, the collision less flight approximation outperforms the Machta and Zwanzig approximation, except in the limit when the energy parameter approaches the threshold for diffusion.

   (b) We developed a second random walk approximation for the regime where the energy parameter, E, approaches the maximum of the potential, $V_{\max}$. This random walk, motivated by traps of slow motion at the

centre of the scatterers, predicts $D(E) \propto \sqrt{E - V_{\max}}$ when $E \to V_{\max}^{+}$. In this regime, the particles have enough energy, for the first time, to climb over the potential but do so with small kinetic energy, hence their motion is on average slower than for smaller energies. Therefore the diffusion coefficient suffers a sudden drop at $E = V_{\max}$.

(c) For the high energy regime, numerical results suggest that there is an energy for which quasi ballistic trajectories are ubiquitous, making impossible the computation of the diffusion coefficient. We used the model where normal diffusion exists for relatively large energies and we found that $D(E) \propto E^m$ with $m = 5/2$ in agreement with a theoretical approximation in the literature. The motion of the particles at high energies is dominated by long flights with rare small angle deflections in the trajectory of the particle.

Overall, the softened version of the Lorentz gas, turned out to be a very interesting model for the study of deterministic diffusion. Depending on the combination of parameters, the scenario for diffusion can change drastically.

We mentioned earlier (Sect. 2.6.2) experiments with antidot lattices which resemble the dynamics of periodic Lorentz gas. In such structures it is possible to measure magneto transport as a function of a magnetic field *e.g.* [WLR97]. The magnetoresistance exhibits oscillations and a maximum which responded, among other factors, to the lattice period. This behaviour is linked to special orbits of the electrons and can be explained by chaos theory [FGK92, LKP91b].

We thus recognize the importance in understanding the basic mechanism behind the transport properties in such systems. Understanding the behaviour of periodic structures is key to build machinery according to specific technological needs. Studying simple and smart microscopic models can shed some light on the desired response when tuning control parameters.

Outlook: Study of superdiffusion

As noted in Chapters 3 and 4, there are zones along the studied parameters, separation of scatterers, smoothness of the potential and energy of the particle, where normal diffusion fails to exist. This means that the mean square displacement grows faster than linearly in time which takes us to the regime of superdiffusion. In order to explore this situation, first one should characterize numerically the type of superdiffusion. Next, we would like to explore the following:

- Position probability distributions and velocity correlation functions play an important role in determining the dynamics of the system and need to be explored. We find in the literature the works of Cristadoro, Sanders, Gilbert *et. al.* on anomalous diffusion in (infinite-horizon) billiards [CGLS14]. They model the process via Lévy walks. Lévy walks allow particles to travel for a random time, power law distributed, before changing direction. The model takes into account two mechanisms: normal trajectories and propagating trajectories along long distances. The former yields a normal contribution to the MSD whereas the latter give an anomalous contribution to the MSD. These are responsible for superdiffusion phenomena. One would like to determine whether this stochastic model matches our type of superdiffusion.
- Finally, let us recall that the expression in Eq.(2.9) appears to characterise the super diffusive regime in the hard (periodic) Lorentz gas [Ble92, Det12] with infinite horizon. Therefore, one would also like to test such a result in the quasi-ballistic regimes found in our softened version of the Lorentz gas.

Appendix A

A.1 Numerical method: Velocity Verlet

The trajectories of the particles are calculated with the code BILL2D [SLR16], the code implements the velocity Verlet algorithm [AT87, SW99] to solve the Newton's equations of motion. This method is commonly used in molecular dynamics because of good conservation of the energy. Moreover, since the method is symplectic (preserves phase space properties) and time reversible it is ideal when dealing with chaotic motion type problems.

Now, we present a basic deduction of the method. Let $\mathbf{r}(t)$ be the position vector of the particle, $\dot{\mathbf{r}}(x) = \mathbf{v}(x)$ its velocity and $\dot{\mathbf{v}}(x) = \mathbf{a}(x)$ the acceleration. Taylor expansion of $\mathbf{r}(t + \Delta t)$ and $\mathbf{r}(t - \Delta t)$ yields expressions in which 1st and 3rd order terms cancel out; fourth and higher order terms are ignored. This and other basic convenient manipulations with other terms yield the basic steps of the velocity Verlet algorithm as follows:

- $\mathbf{r}(t + \Delta t) = \mathbf{r}(t) + \Delta t \mathbf{v}(t) + \frac{1}{2}\Delta t^2 \mathbf{a}(t)$
- then derive the acceleration $\mathbf{a}(t + \Delta t)$ from the potential (using only the position of the particle $\mathbf{r}(t + \Delta t)$)
- $\mathbf{v}(t + \Delta t) = \mathbf{v}(t) + \frac{1}{2}\Delta t \mathbf{a}(t) + \mathbf{a}(t + \Delta t))$

A.2 Bifurcation Scenario

In Fig. A.1 we present the evolution of a stability island as we varied the w parameter. The PSoS is defined in Section 2.7.3. The input parameters are the same as in the model presented in Chap.3. Starting at $w = 0.3090$ we see a very well defined island and as we move to higher values of w its shape changes slightly until $w \approx 0.312$, after this point the island shows a stable island in the same position and a period 3 bifurcation surrounding it. When we reached $w = 0.3130$ the size of the islands of period 3 decreases and by $w = 0.3135$ we just see the small island and the stickiness and the island in the middle. But the story continues, after $w = 0.3160$ the island bifurcates in to two islands and eventually disappear once again we face the transition to chaotic motion. Note that the variation δw is very small, and despite of this the bifurcation scenario is very complicated.

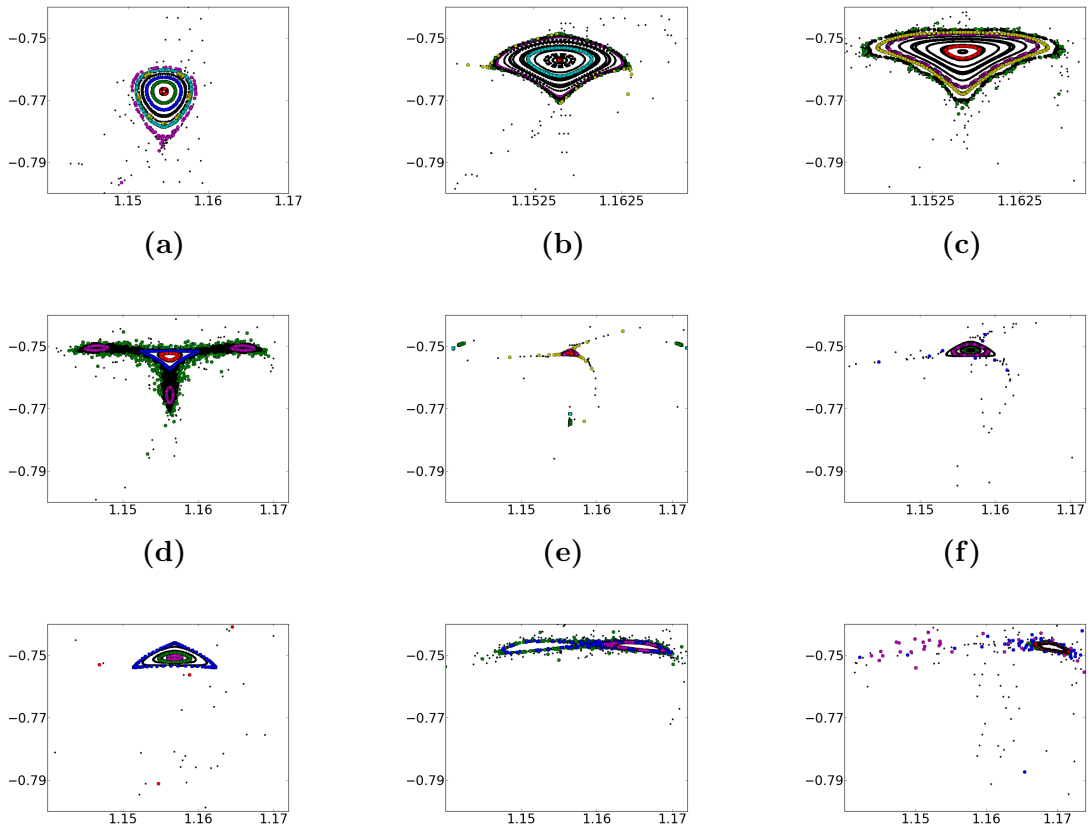

Figure A.1: PSoS and bifurcation scenario around $w = 0.309$. (a) $w = 0.3090$, (b) $w = 0.3110$, (c)$w = 0.3120$, (d) $w = 0.3125$, (e) $w = 0.3130$, (f) $w = 0.3135$, (g) $w = 0.3138$, (h) w=0.3170, and (i) $w = 0.3175$.

A.3 Diagram: islands in parameter space

This is a phase space diagram showing islands of stability, the figures was facilitated by our collaborators (Essa et al.) and were performed with the code BILL2D [SLR16].

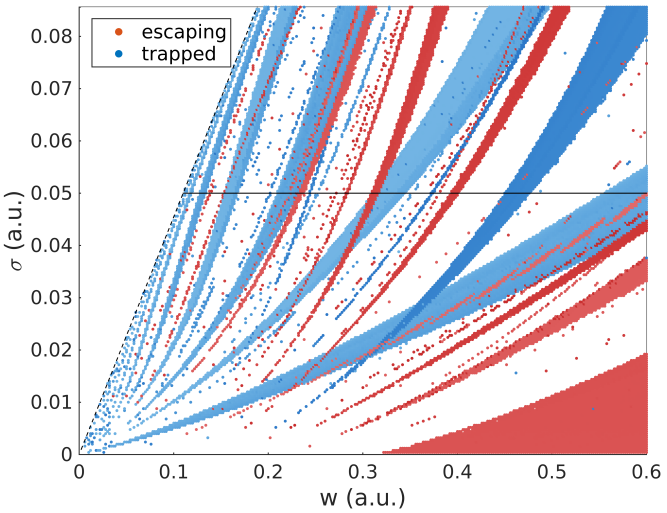

Figure A.2: Phase space diagram: The parameter w is the separation of the scatteres and σ represents the softness of the potential.

A.4 Onset of ballistic infinite horizon

The Fermi potential is defined as

$$V_{\mathrm{F}}(r) = \frac{1}{1 + \exp((r - r_o)/s_o)},$$

where r_o is the radius of the potential and s_o is the smoothness of the potential. The potential is such that $V_{\mathrm{F}}(r_0) = 0.5$ regardless the value of s_o. Just as in the hard Lorentz gas, one wonders about the onset of the infinite horizon in the softened Lorentz gas. Can the onset of the infinite horizon be calculate analytically?

A simple limit analysis indicates that if we want to recover the hard Lorentz gas

$$s_o \to 0 \text{ or } w \to \infty$$

which is what we expect from the construction of the potential.

The potential V_{F} decreases as r goes away from the origin but is never zero, therefore a rigorous free flight scenario is never possible.

Here, we show a trajectory that appears at $w = 0.9$, $s_o = 0.05$, and energy $E = 0.5$, which resembles the free flight trajectory in the Lorentz gas. In Fig. A.3 we can see how the periodic trajectory touches tangentially the equipotential lines as it bounces from scatterer to scatterer. We wonder how this regime compares to the infinite horizon regime in the periodic Lorentz gas? This motivates us to explore the super diffusive coefficient Eq.(2.9) [Ble92] in a future work.

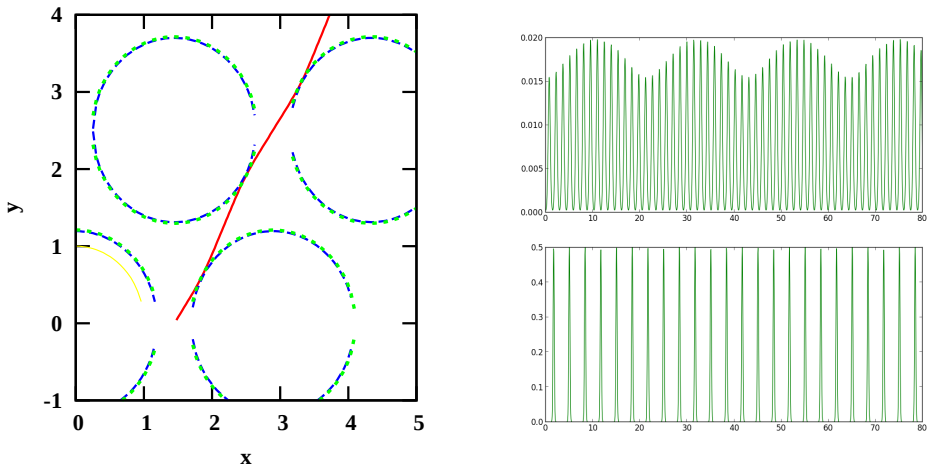

Figure A.3: Left: Quasi-ballistic trajectory touching tangentially equipotential lines of the scatterers as it travels trough a main symmetry axis. Right: Kinetic and potential energy of the trajectory in the left.

Bibliography

[ADB10] Bénédicte Aguer and Stephan De Bievre. On (in) elastic non-dissipative lorentz gases and the (in) stability of classical pulsed and kicked rotors. *Journal of Physics A: Mathematical and Theoretical*, 43(47):474001, 2010.

[AK98] Joachim Asch and Andreas Knauf. Motion in periodic potentials. *Nonlinearity*, 11(1):175, 1998.

[AMK06] Eduardo G. Altmann, Adilson E. Motter, and Holger Kantz. Stickiness in hamiltonian systems: From sharply divided to hierarchical phase space. *Phys. Rev. E*, 73:026207, Feb 2006.

[AT87] MP Allen and DJ Tildesley. *Computer Simulation of Liquids*. Oxford University Press, 1987.

[AT09] Eduardo G Altmann and Tamás Tél. Poincaré recurrences and transient chaos in systems with leaks. *Physical Review E*, 79(1):016204, 2009.

[Bal88] PR Baldwin. Soft billiard systems. *Physica D: Nonlinear Phenomena*, 29(3):321, 1988.

[BBC+13] LA Bunimovich, D Burago, N Chernov, EGD Cohen, CP Dettmann, JR Dorfman, S Ferleger, R Hirschl, A Kononenko, JL Lebowitz, et al. *Hard ball systems and the Lorentz gas*, volume 101. Springer Science & Business Media, 2013.

[BD05] L.A. Bunimovich and C.P. Dettmann. Open circular billiards and the Riemann hypothesis. *Phys. Rev. Lett.*, 94:100201/1–4, 2005.

[BDD+00] LA Bunimovich, SG Dani, RL Dobrushin, MV Jakobson, IP Kornfeld, NB Maslova, Ya B Pesin, J Smillie, Yu M Sukhov, and AM Vershik. *Dynamical systems, ergodic theory and applications*, volume 100. Springer Science & Business Media, 2000.

[BGF+01] ME. Briggs, P. Gaspard, MK. Francis, RV. Calabrese, RW. Gammon, JV. Sengers, and J.R. Dorfman. Experimental evidence for microscopic chaos. *Proceedings of the 5th Experimental Chaos Conference. World Scientific. 2001, Singapore.*, pages 411–26, 2001.

[BGJ96] J.A. Blackburn and N. Grønbech-Jensen. Phase diffusion in a chaotic pendulum. *Phys. Rev. E*, 53:3068–3072, 1996.

[Ble92] P.M. Bleher. Statistical properties of two-dimensional periodic Lorentz gas with infinite horizon. *J. Stat. Phys.*, 66:315–373, 1992.

[BS80] L.A. Bunimovich and Ya.G. Sinai. Markov partitions for dispersed billards. *Commun. Math. Phys.*, 78:247, 1980.

[BS81] L.A. Bunimovich and Ya.G. Sinai. Statistical properties of Lorentz gas with periodic configuration of scatterers. *Commun. Math. Phys.*, 78:479–497, 1981.

[BSC91] L.A. Bunimovich, Ya.G. Sinai, and N.I. Chernov. Statistical properties of two-dimensional hyperbolic billiards. *Russ. Math. Surveys*, 46:47–106, 1991.

[BT04] Péter Bálint and Imre Péter Tóth. Mixing and its rate in soft and hard billiards motivated by the lorentz process. *Physica D: Nonlinear Phenomena*, 187(1):128–135, 2004.

[Bun74] L A Bunimovi. On billiards close to dispersing. *Mathematics of the USSR-Sbornik*, 23(1):45, 1974.

[Bun85] L.A. Bunimovich. Decay of correlations in dynamical systems with chaotic behaviour. *Sov. Phys. JETP*, 62:841–852, 1985.

[Bun01] L.A. Bunimovich. Mushrooms and other billiards with divided phase space. *Chaos*, 11:802–808, 2001.

[BVA12] Leonid A. Bunimovich and Luz V. Vela-Arevalo. Many faces of stickiness in hamiltonian systems. *Chaos: An Interdisciplinary Journal of Nonlinear Science*, 22(2):026103, 2012.

[BZCM85] Biman Bagchi, Robert Zwanzig, and M. Cristina Marchetti. Diffusion in a two-dimensional periodic potential. *Phys. Rev. A*, 31:892–896, Feb 1985.

[CAM+07] P. Cvitanović, R. Artuso, R. Mainieri, G. Tanner, and G. Vattay. *Chaos: Classical and quantum*. Niels Bohr Institute, Copenhagen, 2007. webbook under chaosbook.org.

[CGLS14] Giampaolo Cristadoro, Thomas Gilbert, Marco Lenci, and David P Sanders. Machta-zwanzig regime of anomalous diffusion in infinite-horizon billiards. *Physical Review E*, 90(5):050102, 2014.

[Che94] N.I. Chernov. Statistical properties of the periodic lorentz gas. multidimensional case. *J. Stat. Phys.*, 74:11–53, 1994.

[Che97] N. Chernov. Entropy, lyapunov exponents, and mean free path for billiards. *J. Stat. Phys.*, 88(1-2):1–29, JUL 1997.

[Che99] N.I. Chernov. Decay of correlations and dispersing billiards. *J. Stat. Phys.*, 94:513–556, 1999.

[Chi79] B.V. Chirikov. A universal instability of many-dimensional oscillator systems. *Phys. Rep.*, 52:263–379, 1979.

[CM06] Nikolai Chernov and Roberto Markarian. *Chaotic billiards*. Number 127. American Mathematical Soc., 2006.

[CS84] Boris V Chirikov and Dima L Shepelyansky. Correlation properties of dynamical chaos in hamiltonian systems. *Physica D: Nonlinear Phenomena*, 13(3):395–400, 1984.

[CY00] Nikolai Chernov and Lai-Sang Young. Decay of correlations for lorentz gases and hard balls. In *Hard ball systems and the Lorentz gas*, pages 89–120. Springer, 2000.

[DC99] C.P. Dettmann and E.G.D. Cohen. Microscopic chaos from brownian motion? *Nature*, 401:875–875, 1999.

[DC09] D. I. Dolgopyat and N. I. Chernov. Anomalous current in periodic Lorentz gases with infinite horizon. *Russian Mathematical Surveys*, 64:651–699, August 2009.

[Det00] C.P. Dettmann. The lorentz gas: A paradigm for nonequilibrium steady states. In *Hard-ball systems and the Lorentz gas*, pages 315–366, 2000.

[Det11] C. P. Dettmann. *Recent Advances in Open Billiards with Some Open Problems*, pages 195–218. World Scientific Publishing Co, 2011.

[Det12] C. P. Dettmann. New Horizons in Multidimensional Diffusion: The Lorentz Gas and the Riemann Hypothesis. *Journal of Statistical Physics*, 146:181–204, January 2012.

[Det14] Carl P Dettmann. Diffusion in the lorentz gas. *Communications in Theoretical Physics*, 62(4):521, 2014.

[DG09] C. P. Dettmann and O. Georgiou. Survival probability for the stadium billiard. *Physica D Nonlinear Phenomena*, 238:2395–2403, December 2009.

[DG11a] C. P. Dettmann and O. Georgiou. Open mushrooms: stickiness revisited. *Journal of Physics A Mathematical General*, 44(19):195102, May 2011.

[DG11b] Carl P. Dettmann and Orestis Georgiou. Transmission and reflection in the stadium billiard: Time-dependent asymmetric transport. *Phys. Rev. E*, 83:036212, Mar 2011.

[DG12] C. P. Dettmann and O. Georgiou. Quantifying intermittency in the open drivebelt billiard. *Chaos*, 22(2):026113, June 2012.

[DL91] Victor Donnay and Carlangelo Liverani. Potentials on the two-torus for which the hamiltonian flow is ergodic. *Communications in mathematical physics*, 135(2):267–302, 1991.

[Don99] Victor J. Donnay. Non-ergodicity of two particles interacting via a smooth potential. *Journal of Statistical Physics*, 96(5):1021–1048, 1999.

[Dor99] J.R. Dorfman. *An introduction to chaos in nonequilibrium statistical mechanics*. Cambridge University Press, Cambridge, 1999.

[EM90] D.J. Evans and G.P. Morriss. *Statistical mechanics of nonequilibrium liquids*. Academic Press, London, 1990.

[FGK92] R. Fleischmann, T. Geisel, and R. Ketzmerick. Magnetoresistance due to chaos and nonlinear resonance in lateral surface superlattices. *Phys. Rev. Lett.*, 68:1367–1370, 1992.

[FKCD01] Nir Friedman, Ariel Kaplan, Dina Carasso, and Nir Davidson. Observation of chaotic and regular dynamics in atom-optics billiards. *Physical review letters*, 86(8):1518, 2001.

[FLH+01] A. Fuhrer, S. Lüscher, T. Heinzel, K. Ensslin, W. Wegscheider, and M. Bichler. Transport properties of quantum dots with steep walls. *Phys. Rev. B*, 63:125309, Mar 2001.

[FR84] B. Friedman and Martin R.F. Decay of the velocity autocorrelation function for the periodic Lorentz gas. *Phys. Lett.*, A:23–26, 1984.

[Gas92] P. Gaspard. Diffusion, effusion, and chaotic scattering. *J. Stat. Phys.*, 68:673–747, 1992.

[Gas98] P. Gaspard. *Chaos, scattering, and statistical mechanics*. Cambridge University Press, Cambridge, 1998.

[GBF+99] P. Gaspard, M.E. Briggs, M.K. Francis, J.V. Sengers, R.W. Gammons, J.R. Dorfman, and R.V. Calabrese. Microscopic chaos from brownian motion? – reply. *Nature*, 401:876, 1999.

[GK98] P. Gaspard and R. Klages. Chaotic and fractal properties of deterministic diffusion-reaction processes. *Chaos*, 8:409–423, 1998.

[GK02] J. Groeneveld and R. Klages. Negative and nonlinear response in an exactly solved dynamical model of particle transport. *J. Stat. Phys.*, 109:821–861, 2002.

[GN82] T. Geisel and J. Nierwetberg. Onset of diffusion and universal scaling in chaotic systems. *Phys. Rev. Lett.*, 48:7–10, 1982.

[GN84] T. Geisel and J. Nierwetberg. Intermittent diffusion: A chaotic scenario in unbounded systems. *Phys. Rev. A*, 29:2305–2308, Apr 1984.

[GN90] P. Gaspard and G. Nicolis. Transport properties, Lyapunov exponents, and entropy per unit time. *Phys. Rev. Lett.*, 65:1693–1696, 1990.

[GS99] P. Grassberger and T. Schreiber. Microscopic chaos from brownian motion? *Nature*, 401:875–876, 1999.

[GS09] Thomas Gilbert and David P. Sanders. Persistence effects in deterministic diffusion. *Phys. Rev. E*, 80:041121/1–7, 2009.

[GT83] S. Grossmann and S. Thomae. Shape dependence of correlation times in chaos-induced diffusion. *Phys. Lett. A*, 97:263–267, 1983.

[GT84] T. Geisel and S. Thomae. Anomalous diffusion in intermittent chaotic systems. *Phys. Rev. Lett.*, 52:1936–1939, 1984.

[Gut13] Martin C Gutzwiller. *Chaos in classical and quantum mechanics*, volume 1. Springer Science & Business Media, 2013.

[GWNO90] T. Geisel, J. Wagenhuber, P. Niebauer, and G. Obermair. Chaotic dynamics of ballistic electrons in lateral superlattices and magnetic fields. *Phys. Rev. Lett.*, 64:1581–1584, Mar 1990.

[GZR87] T. Geisel, A. Zacherl, and G. Radons. *Phys. Rev. Lett.*, 59:2503–2507, 1987.

[HG01] T. Harayama and P. Gaspard. Diffusion of particles bouncing on a one-dimensional periodically corrugated floor. *Phys. Rev. E*, 64:036215/1–16, 2001.

[HKG02] T. Harayama, R. Klages, and P. Gaspard. Deterministic diffusion in flower-shaped billiards. *Phys. Rev. E*, 66:026211/1–7, 2002.

[HP08] B. Hasselblatt and Y. Pesin. Hyperbolic dynamics. *Scholarpedia*, 3(6):2208, 2008.

[JBS90] Rodolfo A Jalabert, Harold U Baranger, and A Douglas Stone. Conductance fluctuations in the ballistic regime: A probe of quantum chaos? *Physical Review Letters*, 65(19):2442–2445, 1990.

[Jus14] W. Just. Applied dynamical systems. LTCC Lecture notes, see http://www.maths.qmul.ac.uk/∼wj/, 2014.

[KD95] R. Klages and J.R. Dorfman. Simple maps with fractal diffusion coefficients. *Phys. Rev. Lett.*, 74:387–390, 1995.

[KD97] R. Klages and J.R. Dorfman. Dynamical crossover in deterministic diffusion. *Phys. Rev. E*, 55(2):R1247–R1250, FEB 1997.

[KD99] R. Klages and J.R. Dorfman. Simple deterministic dynamical systems with fractal diffusion coefficients. *Phys. Rev. E*, 59:5361–5383, 1999.

[KD00] R. Klages and C. Dellago. Density-dependent diffusion in the periodic Lorentz gas. *J. Stat. Phys.*, 101:145–159, 2000. see also chao-dyn/9910038 for further details.

[KFAD01] Ariel Kaplan, Nir Friedman, Mikkel Andersen, and Nir Davidson. Observation of islands of stability in soft wall atom-optics billiards. *Physical review letters*, 87(27):274101, 2001.

[KFAD04] Ariel Kaplan, Nir Friedman, Mikkel Andersen, and Nir Davidson. Stable regions and singular trajectories in chaotic soft-wall billiards. *Physica D: Nonlinear Phenomena*, 187(1):136–145, 2004.

[KGDK12] Georgie Knight, Orestis Georgiou, Carl P. Dettmann, and Rainer Klages. Dependence of chaotic diffusion on the size and position of holes. *Chaos: An Interdisciplinary Journal of Nonlinear Science*, 22(2):023132, 2012.

[KK92] Markus Klein and Andreas Knauf. *Classical Planar Scattering by Coulombic Potentials*, volume 13. Springer Science & Business Media, 1992.

[KK02a] R. Klages and N. Korabel. Understanding deterministic diffusion by correlated random walks. *J. Phys. A: Math. Gen.*, 35:4823–4836, 2002.

[KK02b] N. Korabel and R. Klages. Fractal structures of normal and anomalous diffusion in nonlinear nonhyperbolic dynamical systems. *Phys. Rev. Lett.*, 89:214102/1–4, 2002.

[KK04] N. Korabel and R. Klages. Fractality of deterministic diffusion in the nonhyperbolic climbing sine map. *Physica D*, 187:66–88, 2004.

[Kla] Rainer Klages. From deterministic chaos to anomalous diffusion. *Reviews of Nonlinear Dynamics and Complexity, Volume 3*, pages 169–227.

[Kla07] R. Klages. *Microscopic chaos, fractals and transport in nonequilibrium statistical mechanics*, volume 24 of *Advanced Series in Nonlinear Dynamics*. World Scientific, Singapore, 2007.

[Kna87] A. Knauf. Ergodic and topological properties of Coulombic periodic potentials. *Commun. Math. Phys.*, 110:89–112, 1987.

[Leb98] P. Leboeuf. Normal and anomalous diffusion in a deterministic area-preserving map. *Physica D*, 116:8–20, 1998.

[LKP91a] A. Lorke, J.P. Kotthaus, and K. Ploog. Localization in GaAs electron-dots and anti-dots. *Superlattices and Microstructures*, 9(1):103–106, 1991.

[LKP91b] Axel Lorke, Jörg P. Kotthaus, and Klaus Ploog. Magnetotransport in two-dimensional lateral superlattices. *Phys. Rev. B*, 44:3447–3450, Aug 1991.

[LL92] A.J. Lichtenberg and M.A. Lieberman. *Regular and chaotic dynamics*, volume 38 of *Applied Mathematical Sciences*. Springer, New York, 2nd edition, 1992.

[Lor05] H.A. Lorentz. The motion of electrons in metallic bodies. *Proc. Roy. Acad. Amst.*, 7:438–453, 1905.

[Lor63] E.N. Lorenz. Deterministic nonperiodic flow. *J. Atmos. Sci.*, 20:130–141, 1963.

[MZ83] J. Machta and R. Zwanzig. Diffusion in a periodic Lorentz gas. *Phys. Rev. Lett.*, 50:1959–1962, 1983.

[NH04] Katsuhiro Nakamura and Takahisa Harayama. *Quantum chaos and quantum dots*, volume 3. Oxford University Press on Demand, 2004.

[Nob93] B. Nobbe. Klassische bewegung im zweidimensional periodischen coulombpotential. *Studienarbeit, FB Physik der TU Berlin*, 1993.

[Nob95] B. Nobbe. Classical motion in two-dimensional crystals. *J. Stat. Phys.*, 78:1591–1605, 1995.

[Ott02] Edward Ott. *Chaos in Dynamical Systems*. Cambridge University Press, 2 edition, 2002.

[Pea05] K. Pearson. The problem of the random walk. *Nature*, 72:294, 342, 1905.

[PFP+08] Thomas G. Pedersen, Christian Flindt, Jesper Pedersen, Niels Asger Mortensen, Antti-Pekka Jauho, and Kjeld Pedersen. Graphene antidot lattices: Designed defects and spin qubits. *Phys. Rev. Lett.*, 100:136804, Apr 2008.

[Poi85] H. Poincaré. Sur les courbes dfinies par les quations diffrentielles (iii). *Journal de Mathmatiques Pures et Appliques*, 1:167–244, 1885.

[PRN+16] Sami Paavilainen, Matti Ropo, Jouko Nieminen, Jaakko Akola, and Esa Räsänen. Coexisting honeycomb and kagome characteristics in the electronic band structure of molecular graphene. *Nano Letters*, 16(6):3519–3523, 2016. PMID: 27176628.

[PWSB89] L. Pfeiffer, K. W. West, H. L. Stormer, and K. W. Baldwin. Electron mobilities exceeding 10 to the 7th sq cm/V s in modulation-doped GaAs. *Applied Physics Letters*, 55:1888–1890, October 1989.

[Rei65] F. Reif. *Fundamentals of statistical and thermal physics*. McGraw-Hill, Auckland, 1965. see also the amended German translation: Statistische Physik und Theorie der Wärme, 3rd edition, de Gruyter, Berlin, 1987.

[RKT99] Vered Rom-Kedar and Dmitry Turaev. Big islands in dispersing billiard-like potentials. *Physica D: Nonlinear Phenomena*, 130(3):187–210, 1999.

[RKZ99] Vered Rom-Kedar and George Zaslavsky. Islands of accelerator modes and homoclinic tangles. *Chaos: An Interdisciplinary Journal of Nonlinear Science*, 9(3):697–705, 1999.

[RW80] A.B. Rechester and R.B. White. Calculation of turbulent diffusion for the Chirikov-Taylor model. *Phys. Rev. Lett.*, 44:1586–1589, 1980.

[Sin70] Ya.G. Sinai. Dynamical systems with elastic reflections. *Russ. Math. Surv.*, 25:137–189, 1970.

[Sin79] Ya G Sinai. Development of krylovs ideas. afterword to ns krylovs works on the foundations of statistical physics, see reference [k (1979)], 1979.

[Sin00] Ya.G. Sinai, editor. *Dynamical systems, ergodic theory and applications*. Encyclopaedia of mathematical sciences. Springer, Berlin, 2nd edition, 2000.

[Sin68] Ya.G. Sinai. Markov partitions and C-diffeomorphisms. *Funktsional'nyi analiz i Ego Prilozheniya*, 2:64–89, 68.

[SLR16] Janne Solanpää, PJJ Luukko, and Esa Räsänen. Bill2d a software package for classical two-dimensional hamiltonian systems. *Computer Physics Communications*, 199:133–138, 2016.

[Str94] S. H. Strogatz. *Nonlinear Dynamics and Chaos: With Applications to Physics, Biology, Chemistry, and Engineering*. Studies in nonlinearity. Addison Wesley, Reading, MA, 1994.

[SV07] D. Szász and T. Varjú. Limit Laws and Recurrence for the Planar Lorentz Process with Infinite Horizon. *Journal of Statistical Physics*, 129:59–80, October 2007.

[SW99] Q Spreiter and M Walter. Classical molecular dynamics simulation with the velocity verlet algorithm at strong external magnetic fields. *Journal of Computational Physics*, 152(1):102 – 119, 1999.

[Sza00] D. Szasz, editor. *Hard-ball systems and the Lorentz gas*, volume 101 of *Encyclopedia of mathematical sciences*. Springer, Berlin, 2000.

[TKY+91] J. Takahara, T. Kakuta, T. Yamashiro, Y. Takagaki, T. Shiokawa, K. Gamo, S. Namba, S. Takaoka, and K. Murase. Ballistic Electron Transport on Periodic and Quasi-Periodic Triangular Lattices of Scatterers. *Japanese Journal of Applied Physics*, 30:3250, November 1991.

[TRK98] Dmitry Turaev and Vered Rom-Kedar. Elliptic islands appearing in near-ergodic flows. *Nonlinearity*, 11(3):575, 1998.

[WGNO92] J. Wagenhuber, T. Geisel, P. Niebauer, and G. Obermair. Chaos and anomalous diffusion of ballistic electrons in lateral surface superlattices. *Phys. Rev. B*, 45:4372–4383, Feb 1992.

[WKP89] R. W. Winkler, J. P. Kotthaus, and K. Ploog. Landau band conductivity in a two-dimensional electron system modulated by an artificial one-dimensional superlattice potential. *Phys. Rev. Lett.*, 62:1177–1180, Mar 1989.

[WLR97] D. Weiss, G. Lutjering, and K. Richter. Chaotic electron motion in macroscopic and mesoscopic antidot lattices. *Chaos, Solitons and Fractals*, 8(7-8):1337–1357, JUL-AUG 1997.

[Woj85] Maciej Wojtkowski. Invariant families of cones and lyapunov exponents. *Ergodic Theory and Dynamical Systems*, 5(1):145–161, 1985.

[WRM+91] D. Weiss, M. L. Roukes, A. Menschig, P. Grambow, K. von Klitzing, and G. Weimann. Electron pinball and commensurate orbits in a periodic array of scatterers. *Phys. Rev. Lett.*, 66:2790–2793, May 1991.

[You98] Lai-Sang Young. Statistical properties of dynamical systems with some hyperbolicity. *Annals of Mathematics*, 147(3):585–650, 1998.

[YTT+91] T. Yamashiro, J. Takahara, Y. Takagaki, K. Gamo, S. Namba, S. Takaoka, and K. Murase. Commensurate classical orbits on triangular lattices of anti-dots. *Solid state communications*, 79(11):885–887, 1991.

[YZ10] Jinghua Yang and Hong Zhao. Anomalous diffusion among two-dimensional scatterers. *Journal of Statistical Mechanics: Theory and Experiment*, 2010(12):L12001, 2010.

[Zas02] G.M. Zaslavsky. Chaos, fractional kinetics, and anomalous transport. *Phys. Rep.*, 371:461–580, 2002.

[ZGNR86] A. Zacherl, T. Geisel, J. Nierwetberg, and G. Radons. Power spectra for anomalous diffusion in the extended sinai billiard. *Phys. Lett.*, 114A:317–321, 1986.